Co-funded by the
Erasmus+ Programme
of the European Union

The Role of Urban Vegetation in Urban Heat Island (UHI) Mitigation and Outdoor Thermal Comfort Improvement

Case Study of Tampere, Finland

Yasmin Satin Atienza

A thesis submitted for the Joint programme of
Master in Urban Climate & Sustainability

August 2023

Author	Publication type	Completion year
Atienza, Yasmin Satin	Thesis	2023
	Number of pages: 99	
Supervisor I	**Supervisor II**	
Dr. Eeva Aarrevaara	Prof. Rohinton Emmanuel	

Title

The role of urban vegetation in urban heat island (UHI) mitigation and outdoor thermal comfort improvement: Case Study of Tampere, Finland

Degree: Master in Urban Climate & Sustainability

Abstract

Nowadays, cities face continuous exposure to the effects of urban heat island (UHI), a phenomenon where urban areas experience higher temperatures than rural areas (Oke et al., 2017). In Tampere, Finland, it is projected that by 2035, the number of hot days will increase by approximately 64%, and that more than 60% of the city's population will be living in warmer urban zones (Sitowise, 2022b). In this regard, it is essential to consider UHI mitigation strategies which relates in an urban planning perspective to promote a climate-resilient development. In Tampere, urban vegetation, particularly trees, has been prioritised as a key measure for climate change mitigation and adaptation.

The main aim of this research is to assess the influence of urban vegetation on land surface temperature (LST) and outdoor thermal comfort (OTC) at both the city scale and block scale levels respectively. The study employed remote sensing and statistical methods for the city scale analysis which involves the correlation of LST and Normalised Difference Vegetation Index (NDVI), and the distribution of LST across different urban densities represented by Local Climate Zones (LCZ). The research utilised ENVI-met for the block scale analysis which includes the simulation of four (4) developed scenarios: BC (existing), C1 (no vegetation), C2 (greening) and C3 (building height increase) on both critical cold winter and hot summer days.

The results of the city scale analysis show that LST and NDVI has a moderate inverse (r=-0.55, -0.59) correlation during summers, and has a weak direct (r=0.18, 0.25) correlation during winters. Generally, the LST-LCZ distribution shows that built type LCZs with lesser pervious surface generates higher LSTs than the land cover types. In Tampere's city centre, LCZ 2 consistently has the highest LSTs, while LCZ G has the lowest for both seasons. The results shows that this distribution is more consistent in summer than in winter following the rank order: LCZ 2 > 8 > E > 5 > 6 > 9 > D > B > A > G. Lastly, the simulation results assessed through air temperature (T_{air}), mean radiant temperature (MRT), and physiological equivalent temperature (PET), revealed that the presence and addition of vegetation, specifically deciduous trees (C2), brings a significant OTC improvement in both seasons. Moreover, the results exhibits that the absence of vegetation (C1) which leads to the increase in impervious surface cover resulted to an inverse effect, bringing more discomfort to users. Results also show that in C3, increasing the building height (h=23 mts.) brings insignificant effect especially to open spaces. Overall, the city can leverage these findings to inform its urban planning decisions, prioritize greening interventions, and create urban environments that enhance the well-being and comfort of its residents while mitigating the effects of UHI brought about by climate change.

Keywords

Urban heat island, Urban vegetation, outdoor thermal comfort

Originality statement. I hereby declare that this master's dissertation is my own original work, does not contain other people's work without this being stated, cited, and referenced, has not been submitted elsewhere in fulfilment of the requirements of this or any other award.	**Signature** Yasmin Satin Atienza

TABLE OF CONTENTS

ACKNOWLEDGMENT

I would like to express my sincere gratitude to my supervisors, Dr. Eeva Aarrevaara and Professor Rohinton Emmanuel, for their guidance, support, and patience throughout my thesis journey and during the entire MURCS program.

I extend my heartfelt thanks to the City of Tampere planners for their valuable contributions, and assistance, which have been instrumental in shaping this research.

To Lorena, Dechen, Mai, Joe, Navo, Eli, the entire MUrCS Cohort 4, Alexandra, and to all the lecturers and staff - I am grateful for the camaraderie, friendship, and remarkable experiences we shared during this program. Thank you for making the past two years memorable.

I would like to express my deepest appreciation to Diana for being my constant companion throughout this journey. To Aira, for introducing me to this program.

To Krystine, Carl, and Hazel - your encouragement, despite the distance, have been a source of strength for me. I honestly couldn't ask for a better trio.

I am deeply thankful to my partner, Geronimo, for being my pillar of support, providing unwavering encouragement, and reminding me to enjoy the journey this time.

To my family - your love and belief in me have been my driving force and inspiration. Thank you for always being there for me and for pushing me to go after the things that I want in life.

And lastly, to God - for giving me the strength, courage, and determination to pursue this program and for guiding me every step of the way.

Maraming salamat sa inyo!

LIST OF FIGURES

LIST OF TABLES

ABBREVIATIONS

BC	Base Case (Existing Scenario)
C1	Case 1 (No Vegetation Scenario)
C2	Case 2 (Greening Scenario)
C3	Case 3 (Building Height Increase Scenario)
GIS	Geographic Information System
IPCC	Intergovernmental Panel on Climate Change
ISA	Impervious Surface Area
LCZ	Local Climate Zones
LST	Land Surface Temperature
LULC	Land Use and Land Cover
MRT	Mean Radiant Temperature
NDBI	Normalised Difference Built-up Index
NDVI	Normalised Difference Vegetation Index
OLI	Operational Land Imager
OTC	Outdoor Thermal Comfort
PET	Physiological Equivalent Temperature
RH	Relative Humidity
T_{air}	Air Temperature
TIRS	Thermal Infrared Sensor
UBL	Urban Boundary Layer
UCL	Urban Canopy Layer
UHI	Urban Heat Island
USGS	United States Geological Survey
WUDAPT	World Urban Database and Access Portal Tools

CHAPTER 1: INTRODUCTION

1.1 Rationale

In an urban setting, IPCC (2023) highlighted that extreme hot temperatures, air pollution, and malfunction of key infrastructures have intensified and worsened in cities due to climate change. Cities, currently housing half of the global population (United Nations Human Settlements Programme, 2022), face continuous exposure to the effects of urban heat island (UHI), a phenomenon where urban areas experience higher temperatures than rural areas (Oke *et al.*, 2017). This has led to a range of detrimental effects including decreased thermal comfort, increased heat-related morbidity and mortality, deteriorated air quality, increased cooling energy use, and unforeseen economic and societal costs (Saaroni *et al.*, 2018; Acosta *et al.*, 2021; Brozovsky, Gaitani and Gustavsen, 2021). Notably, northern European cities are deemed to be more vulnerable to this phenomenon as they are less adapted to it than their southern counterparts (Ward *et al.*, 2016; Ruuhela *et al.*, 2017). In cold climate cities like Finland, it was estimated that high daily temperatures and prolonged heatwaves can be associated with the rise of mortality cases, significantly affecting the elderly (Kollanus, Tiittanen and Lanki, 2021). For instance, based on a UHI study conducted in Tampere, Finland, it is projected that by 2035, the number of hot days will increase by approximately 64%, and more than 60% of the population will be living in warmer urban zones (Sitowise, 2022b).

In this regard, it is essential to consider UHI mitigation strategies which relates in an urban planning perspective to promote a climate-resilient urban development (Acosta *et al.*, 2021; IPCC, 2023). Urban green infrastructure (UGI) plays a crucial role in reducing the UHI effect, with urban vegetation deemed to be one of the most recommended method to cope up with overheating in cities and improving thermal comfort (Balany *et al.*, 2020; Gatto *et al.*, 2020). The role of urban vegetation in UHI mitigation has been extensively explored in a global scale, however, studying UHI and its effects still depends on the local conditions of the area (Oke *et al.*, 2017). Tampere's Climate Change Adaptation and Preparation Plan (2022) aligns with a sustainable vision that recognizes the significance of UGI, including urban trees, as a key solution

to create a more resilient city (Sitowise, 2022a). Although the UHI study for the Tampere's master plan recommends additional greening measures (Sitowise, 2022b), it is still necessary to analyse the effects of these interventions on the thermal environment, to identify the most effective approach and provide a holistic solution to urban heating challenges in the city centre. A comprehensive understanding of the local context will be essential in crafting effective strategies to combat the UHI effect and create a more climate-sensitive urban landscape in Tampere.

1.2 Aims and Objectives

The primary objective of this research is to evaluate the influence of urban vegetation on land surface temperature (LST) and outdoor thermal comfort (OTC) at both the city scale and block scale levels respectively in Tampere, Finland. Specifically, this study aims to:

1. Evaluate the relationship between LST and vegetation represented by Normalised Difference Vegetation Index (NDVI) in summer and winter seasons,
2. Assess the spatial distribution of LST across different Local Climate Zones (LCZ) in the city centre,
3. Explore the effect of deciduous trees in pedestrian thermal comfort based on simulated scenarios, and
4. Support the urban planning decisions regarding the benefits of urban vegetation, specifically urban trees in curbing heat islands and OTC improvement in summer and winter seasons.

1.3 Outline of Methodology

The research utilises a multi-method approach with both qualitative and quantitative components. The methodology starts with literature review and data collection, then followed by the city scale analysis of the surface temperature and vegetation using remote sensing techniques. During this phase, LST, NDVI, and LCZ

maps were retrieved and processed using GIS methods. Statistical methods were then employed to analyse the correlation of LST and NDVI, and the distribution of LST in different urban densities represented by LCZs. Through a site selection process guided by the data analysis, as well as the policies and future master plan of the city of Tampere, the research narrowed down to a block scale analysis, where a focus area is identified within the inner-city centre. During this phase, ENVI-met software was used to model and simulate four different scenarios to analyse the effects of these interventions in the microclimate and OTC using air temperature (T_{air}), mean radiant temperature (MRT) and physiological equivalent temperature (PET) as indicators.

1.4 Dissertation Outline

The dissertation unfolds into 6 chapters, each focusing on specific aspects of the research topic. The chapters are structured as follows:

Chapter 1 serves as the overview of the study. It introduces the research problem, the main aim and objectives, and a brief description of the methodology that will be employed in the research.

Chapter 2 encompasses the comprehensive reviews of previous works and topics related to urban vegetation, UHI, and OTC, particularly studies done in cold climate cities. It explores the city's plans, projects, and adaptation measures, and identifies the knowledge gap that the research aims to contribute on.

Chapter 3 discusses the methodology and approach employed to achieve the objectives of the research, outlining the structure, datasets, data collection, as well as the technical tools and software utilised in the study.

Chapter 4 outlines the data collected and provides interpretations of the findings, including visual representations to enhance the presentation and understanding of the results.

Chapter 5 discusses the main contributions of the study and discusses how the research outcomes align with the existing studies.

Chapter 6 concludes the research by summarizing the key findings and their implications, acknowledges limitations or constraints encountered during the research process, and provides with recommendations for future studies.

CHAPTER 2: REVIEW OF RELATED LITERATURE

2.1 Urban Heat Island

Urban heat island (UHI) is a localized climatic phenomenon referring to the apparent tendency of urban region to experience warmer temperatures than their neighbouring rural areas (Zhang, Odeh and Han, 2009; Grimmond, Ward and Kotthaus, 2015; Oke *et al.*, 2017; Saaroni *et al.*, 2018; Abdulateef and A. S. Al-Alwan, 2022). UHI can be categorised into four types: urban boundary layer (UHI_{UBL}), urban canopy layer (UHI_{UCL}), surface (Uhu_{ru}), and subsurface (UHI_{sub}) (Fig. 2.1). Each type responds to various scales and exhibits unique temporal and spatial patterns (Oke *et al.*, 2017; Bechtel *et al.*, 2019). From these types, the most explored lines of research are mainly focused on UHI_{surf} and UHI_{UCL} (Bechtel *et al.*, 2019; Acosta *et al.*, 2021).

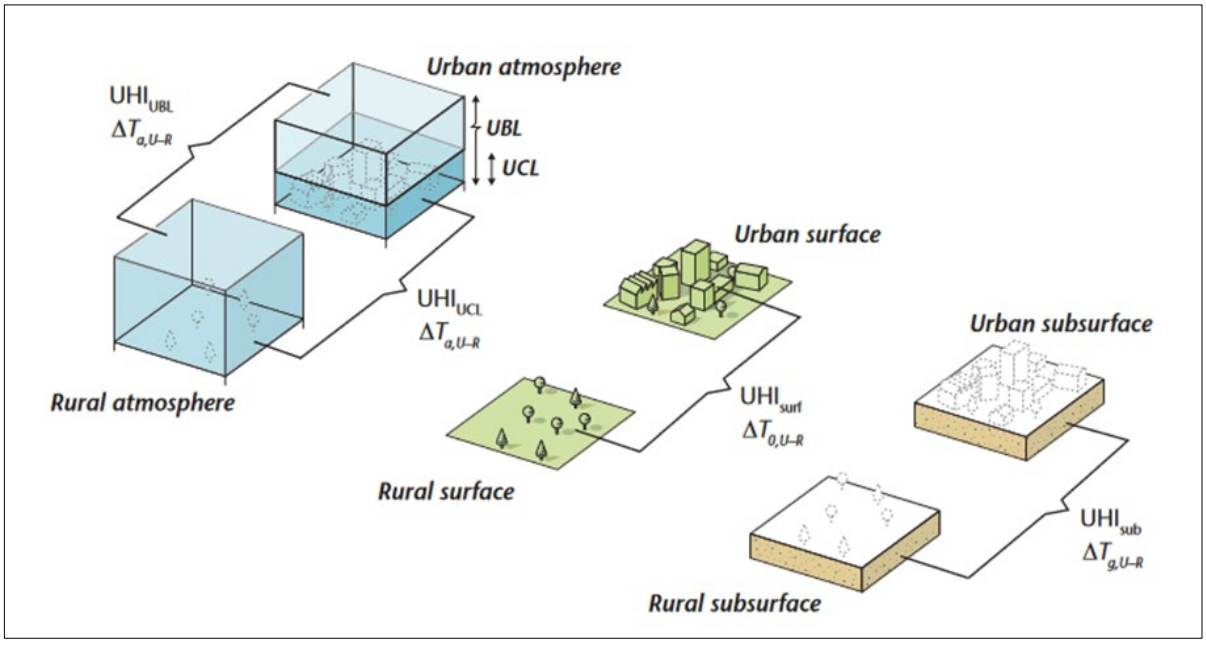

Figure 2.1 Temperature difference of the four types of UHI: urban boundary layer (UHI_{UBL}), urban canopy layer (UHI_{UCL}), surface (UHI_{surf}), and subsurface (UHI_{sub}) (Oke et al., 2017, Urban Climates, p.199)

UHI_{surf} refers to the differences in temperature of the outdoor atmosphere with the dry surfaces and the equivalent rural air to ground surfaces. Its intensity varies seasonally as it is sensitive to the surface cover of the rural surroundings, and several studies show that it is more prevalent during the daytime and summer months (Oke

et al., 2017; Tesfamariam, Govindu and Uncha, 2023). It is commonly assessed through remotely sensed land surface temperature (LST), which has gained common interest due to its availability and practicality especially for analysis done in a citywide, regional or global scale (Yuan and Bauer, 2007; Zhang, Odeh and Han, 2009; Acosta *et al.*, 2021; Marando *et al.*, 2022; Tesfamariam, Govindu and Uncha, 2023; Ullah *et al.*, 2023).

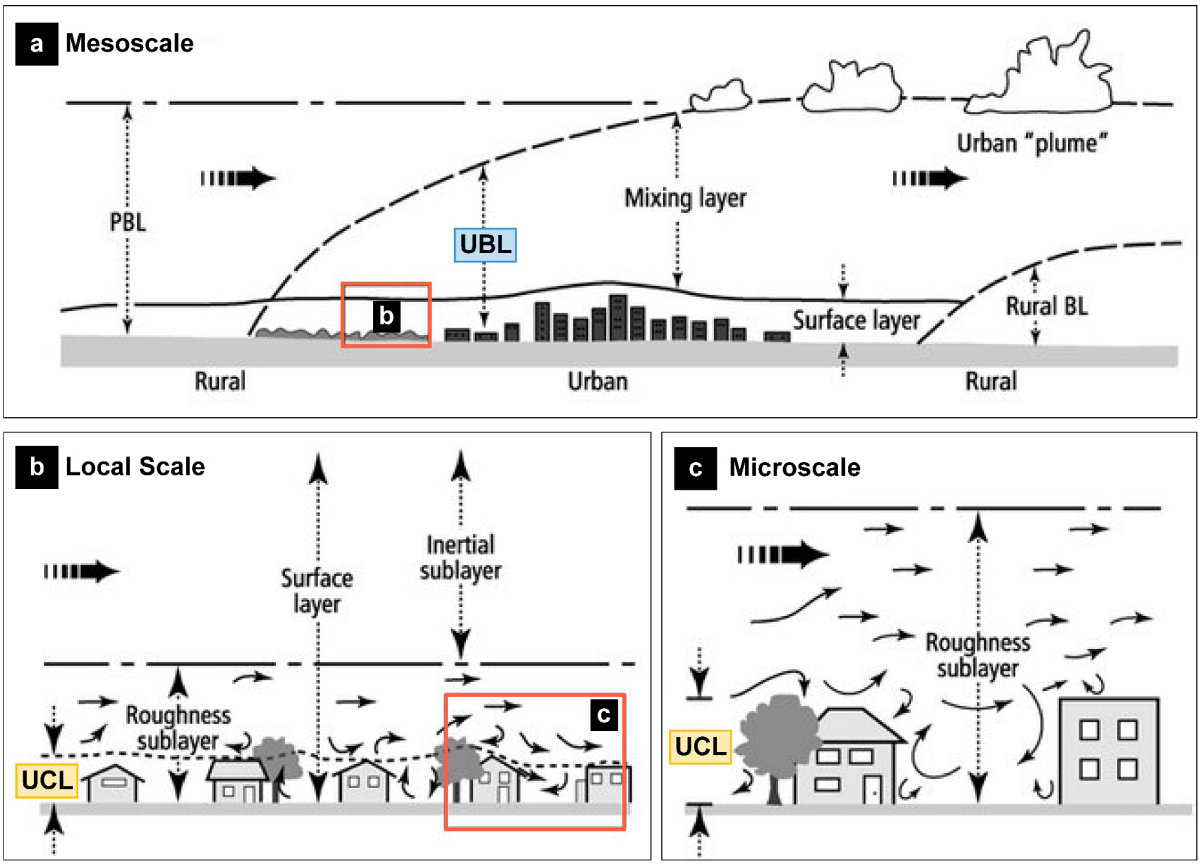

Figure 2.2 Key spatial scales of the urban atmosphere (Grimmond, Ward and Kotthaus, 2015)

UHI_{UCL}, on the other hand, indicates the change between the air temperature in the UCL, the exterior UCL, and the corresponding height in the countryside near-surface layer (Fig. 2.2) (Oke *et al.*, 2017). Studies on UHI_{UCL} generally requires a direct or field measurement at about 1.25 - 2 m above the ground, and is usually strong under clear skies, with its peak lasting several hours after sunset. Humans directly experience the effects of temperature in this layer which could be a detrimental factor to human thermal comfort, health, and functions during heatwave occurrences (World Meteorological Organization, 2023).

2.1.1 Land Surface Temperature (LST), Normalised Difference Vegetation Index (NDVI), and Local Climate Zones (LCZ)

According to Bechtel *et al.* (2019), previous studies on UHI_{UCL} and UHI_{surf} has been hindered due to the lack of framework to interpret the results consistently, thus submitting the researchers to use different land use and land cover (LULC) frameworks for interpretation. Additionally, the difference between 'urban' and 'rural' is insufficient to provide an accurate representation of complexity and range of local climate (Das and Das, 2020; Choudhury, Das and Das, 2021). In this regard, a new LULC classification called the Local Climate Zones (LCZ) was created as a standardized manual of local landscape types to understand the urban morphological pattern and UHI relationship (Stewart and Oke, 2012; Das and Das, 2020). The relationship between LST and LCZ has long been explored in various UHI studies specifically for assisting urban planning and climate management (Zhang, Odeh and Han, 2009; Bechtel *et al.*, 2019; Das and Das, 2020; Choudhury, Das and Das, 2021; Del Pozo *et al.*, 2021; Aslam and Rana, 2022; Zhou *et al.*, 2022), and improving thermal comfort in urban environments. As LST is influenced by both physical and dynamic variables which modify the microclimate of the urban areas, studies claimed that LCZ mapping can lead to the understanding of the urban fabric's influence on the spatial variation of UHI_{surf} (Stewart and Oke, 2012; Aslam and Rana, 2022; Feng and Liu, 2022; Zhou *et al.*, 2022).

UHI is mainly caused by the replacement of vegetated areas with impervious surfaces due to urbanisation (Zhang, Odeh and Han, 2009; Welegedara, Agrawal and Lotfi, 2023). Due to this, several studies analysed the relationship of LST with different land cover indices, which includes the Normalised Difference Vegetation Index (NDVI) (Zhang, Odeh and Han, 2009; Kaplan, Avdan and Avdan, 2018; Naserikia *et al.*, 2022). As NDVI refers to the composition of greenery in an area, its relationship with LST has been explored to understand the effects of the presence of vegetation cover in surface temperature (Al-Saadi, Jaber and Al-Jiboori, 2020; Choudhury, Das and Das, 2021; Emmanuel *et al.*, 2023). Several studies claimed that generally, there is a negative relationship between the two variables indicating the decreasing trend of LST as the vegetation density increases (Yuan and Bauer, 2007; Zhang, Odeh and Han, 2009; Sresto *et al.*, 2022; Tesfamariam, Govindu and Uncha, 2023; Ullah *et al.*, 2023). In

cold climate cities, however, studies show that the correlation is dependent on seasons (Sun and Kafatos, 2007; Naserikia *et al.*, 2022) , and that there is a positive correlation in winter, and negative in summer (Sun and Kafatos, 2007).

2.2. Urban Vegetation as a UHI Mitigation Measure in Cold Climate Cities

In the concept of UHI, 'mitigation' is defined as the modifications or interventions in the physical environment to reduce the amount or extent of UHI, which includes adding vegetation cover. Meanwhile 'adaptation' is regarded as the adjustment to lessen the risks and harm caused by UHI, such as the response to thermal discomfort (Solecki *et al.*, 2005; Gago *et al.*, 2013; Saaroni *et al.*, 2018). According to Saaroni *et al*. (2018), vegetation has become a major tool in UHI mitigation and has become a common topic of research across Europe due to the recent increase in heatwaves and growing interest in UHI phenomenon. Moreover, this strategy is in line with the European Commission's program to develop nature-based solutions to address socio-ecological challenges brought by climate change (Venter, Krog and Barton, 2020).

In cold climate cities, UHI can lead to excessive heat and higher air polution, thus exposing humans, especially the elderly and chronically ill, to heat related health risks and stress (Suomi, 2018; Venter, Krog and Barton, 2020; Drebs, Suomi and Mäkelä, 2023). Studies reveal that increasing vegetation cover in densely built areas, adding more urban forests, and safeguarding trees during growth and redevelopment can reduce UHI effects in the summers while still reaping benefits during the winter (Welegedara, Agrawal and Lotfi, 2023). Several studies on LST show that areas with the highest temperature are in the commercial or industrial areas with lesser vegetation, while water bodies and areas with green cover such as forests and urban parks have the lowest (Brozovsky, Gaitani and Gustavsen, 2021; Sitowise, 2022b; Welegedara, Agrawal and Lotfi, 2023). In Stockholm, Sweden, it was observed that there is an air temperature difference of 0.5–0.8°C to 2°C maximum between a built-up area and a park (Jansson, Jansson and Gustafsson, 2007). In Oslo, Norway, the maintenance, and restoration of tree cover is essential to the ecosystem service of urban heat reduction (Venter, Krog and Barton, 2020). In Edmonton, Canada, it was

revealed that replacement of vegetation cover by impervious surfaces has caused a significant temperature increase in the city area over the past decades (Welegedara, Agrawal and Lotfi, 2023). Moreover, urban vegetation influences UHI_{UCL} behaviour as it can provide shade that lessens radiant temperature and UHI_{UCL} intensities by about 0.5 °C – 4.0 °C (World Meteorological Organization, 2023).

2.2.1. Outdoor Thermal Comfort (OTC) for Pedestrians

Human thermal comfort is defined as a condition of mind which states satisfaction with the immediate environment. It depends on human activities, clothing, and environmental elements which includes air temperature, wind speed, air velocity, and radiation. Radiation is significantly related to mean radiant temperature (MRT), which displays the short- and longwave radiation absorbed at the human body's outer surface (Oke *et al.*, 2017). Achieving optimal thermal comfort involves both physiological and psychological adaptation processes (Li, Sun and Chen, 2023), and covers a range of variables, (Potchter *et al.*, 2018; Ahmadpour *et al.*, 2021), which makes it essential to be considered specially in the local adaptation strategies.

In urban planning, outdoor thermal comfort (OTC) is considered as one of the key variables which affects the liveability and functionality of the cities' pedestrian and public spaces (Potchter *et al.*, 2018; Nie *et al.*, 2022) and failure to achieve the desired user thermal comfort level would lead to the neglect of these spaces (Ahmadpour *et al.*, 2021). Since thermal comfort depends on the balance between the human body and the environment (Potchter *et al.*, 2018), several indices have been used to measure it. One of the most dominantly used indices is the physiological equivalent temperature (PET) (Potchter *et al.*, 2018; Yang *et al.*, 2018; Nie *et al.*, 2022), or 'the air temperature at which, in a typical indoor setting (without wind and solar radiation), the heat budget of the human body is balanced with the same core and skin temperature as under the complex outdoor conditions to be assessed' (Höppe, 1999, p.71). It has been extensively applied and modified in both cold and hot climate zones to classify thermal perception as it shows the human body's heat balance (Potchter *et al.*, 2018; Nie *et al.*, 2022). Moreover, it has been considered preferable than other

indices because its unit (°C) is more comprehensible for urban and regional planners (Matzarakis, Mayer and Iziomon, 1999).

2.2.2. Urban Trees for OTC Improvement

According to (Saaroni *et al.*, 2018), several studies show that there is only a relatively small difference between the number of thermal comfort studies done in 'warm' and 'cold' countries, indicating a growing interest in the field even in cold climate cities. In Lahti, Finland, the vegetation at a pedestrian level led to a thermal comfort improvement in summer (Gatto *et al.*, 2020). Through comparison of the three Swedish cities, Lindberg et al. (2014) concluded that shading from both vegetation and buildings brings a significant decrease in MRT, however, it was recommended to create a diverse outdoor urban space, as extensive areas of shadows are not usually favoured in high-latitude cities (Zhang, Odeh and Han, 2009; Perini, Chokhachian and Auer, 2018; Balany *et al.*, 2020). During cold periods in Ezurum, Turkey, it was found out that increasing the percentage of deciduous trees and grass led to outdoor thermal comfort improvement (Afshar *et al.*, 2018).

In a microclimate setting, the advantages and cooling capacity of urban vegetation depends on its location, size, and type. In this regard, trees have been consistently considered as one of the most studied types and most versatile form of urban vegetation, especially in OTC research (Zhang, Odeh and Han, 2009; Perini, Chokhachian and Auer, 2018; Balany *et al.*, 2020). Generally, tree consistently improve thermal comfort through shading and reduction of direct solar radiation, as well as increase relative humidity through evapotranspiration (Balany *et al.*, 2020; Yilmaz *et al.*, 2021). However, this could have an inverse effect in high latitude cities during winter, thus the importance of tree species should be taken into consideration (Afshar *et al.*, 2018; Saaroni *et al.*, 2018; Gatto *et al.*, 2020; Yilmaz *et al.*, 2021).

Several studies revealed that in cold climate cities, deciduous trees are considered more favourable than evergreen trees because of its seasonal characteristics. It increases thermal comfort through shading which provides cooling during summers, and relatively warms the area through allowing solar radiation to pass

through during winters (Oke *et al.*, 2017; Afshar *et al.*, 2018; Perini, Chokhachian and Auer, 2018; Yilmaz *et al.*, 2021). According to Oke *et al*. (2017), 10-30% and 50-80% of solar radiation is transmitted by deciduous trees during summers and winters respectively. Meanwhile, evergreen trees casts permanent shadows, thus lowering the temperature in winter, which is critical in cold cities (Afshar *et al.*, 2018). While trees have several benefits, studies claimed that combining the different types of green elements such as the trees, grass and shrubs has more significant effect in air temperature reduction and thermal comfort (Oke *et al.*, 2017; Wang *et al.*, 2019; Balany *et al.*, 2020; Marando *et al.*, 2022). In microclimate analysis, Balany *et al*. (2020) stated that vegetation is one of the most complicated elements and most of the software do not consider this complexity. With this, ENVI-met is regarded as a comprehensive microclimate model that takes various urban complexity factors, such as different types of vegetation, building materials, and roadways, into account. It has also been accepted as one of the most reliable software for plant-surface-air interaction, thermal comfort studies and urban outdoor scenario simulations which could help immensely in urban planning.

2.3. Climate Change Adaptation Actions in Tampere, Finland

Tampere, the third largest city in southwestern Finland, is known to be one of the fastest developing urban areas in the country. For years, the city has been engaged in progressive mitigation and adaptation actions to manage the adverse effects of climate change. According to the Tampere's Climate Change Preparation and Adaptation Plan (2022), heatwaves and droughts are considered as significant climate risks in the city. In line with these, the city also highlights the importance of green infrastructure as one of the priority themes for adaptation measures (Fig. 2.3). As hot periods become longer and more pronounced, several risks and vulnerabilities related to heat include health hazards, decreased work efficiency, increased discomfort, increase in cooling building demands, increased need for irrigation, and impacts on biodiversity (Sitowise, 2022a).

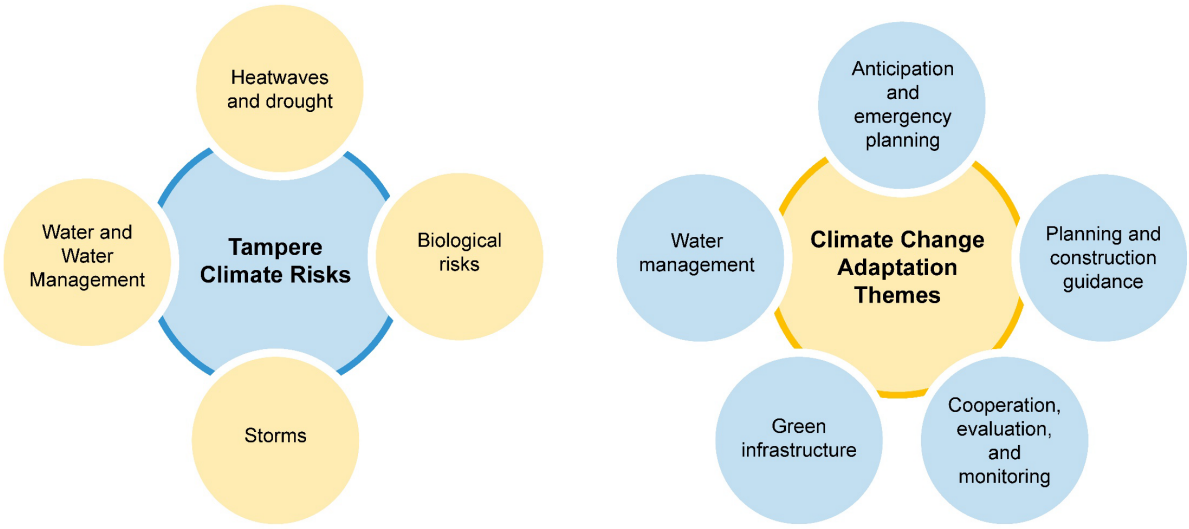

Figure 2.3 Tampere's climate risks and climate change adaptation themes (Adapted from Sitowise, 2022a)

According to the plan, the area most prone to these is identified within the dense city centre area, where a portion of the elderly population resides. In a comprehensive UHI study done by Sitowise for the city centre in 2022, the report highlights that the intensity of UHI effect is reduced due to the proximity of lakes, and can be mitigated through the presence of forests and green areas (Sitowise, 2022b).

2.3.1. Tampere's commitment to urban trees

Climate change adaptation measures have been recognized in numerous policy and program contexts in Tampere, one of which is the 'Carbon Neutral Tampere 2030' Roadmap (2020). According to the roadmap (Fig. 2.4), the city aims to reduce its greenhouse gas (GHG) emissions to 80% compared from 1990 and reach an emission reduction of 73% by 2030. It has 305 measures overall, which are divided into seven themes: urban planning, transport system, construction, energy, consumption, urban nature, and climate work coordination and monitoring (City of Tampere, 2020a).

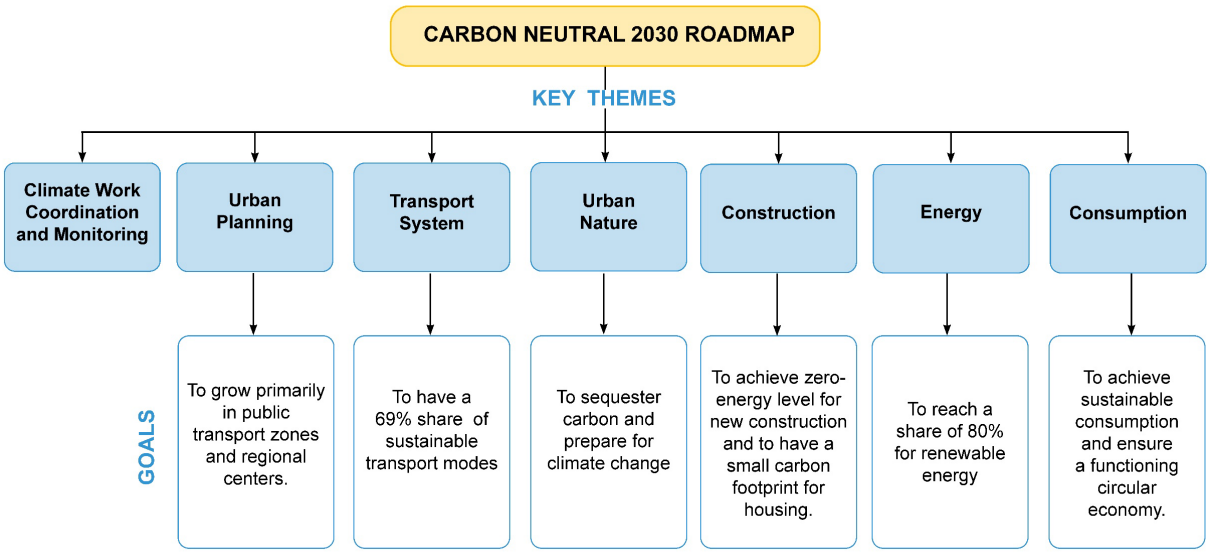

Figure 2.4 Carbon Neutral 2030 Roadmap (adapted from City of Tampere, 2020a)

In line with the *'urban nature'* theme, the city has renewed its focus on trees in the city centre through its Urban Tree Policy in 2020. It evaluates trees based on various factors, such as climate considerations, cultural significance, diversity of tree species, design, maintenance, and the monetary value and advantages of owning trees. The primary objective of the urban tree alignment is to enhance the diversity of tree species planted in urban areas and ensure the long-term survival and well-being of urban trees amidst changing climate conditions. The report states that together with other types of vegetation, urban trees form the backbone of the landscape and green network in the city (City of Tampere, 2020b).

In terms of species, it has been reported that the street trees are mainly composed of linden (66%), maples (19%), birches (7%) and conifers (3%) (City of Tampere, 2020). In 2019, the city participated in an I-Tree assessment to calculate the characteristics and advantages of trees in specific sites. An initial evaluation of 1,810 trees was carried out to assess the structure, functioning, and value of the urban forest in using the I-Tree Eco model developed by the U.S. Forest Service, Northern Research Station (City of Tampere, 2019). The summarized benefits of the trees in these parks are provided in Table 2.1.

Table 2.1 Summary of I-tree Eco Analysis (City of Tampere, 2019)

Summary of I-tree Eco Analysis	
Number of Trees	1,810
Tree Cover	39.50%
Most Common Species	*Betula pendula, Acer platanoides, Pinus sylvestris*
Percentage of trees less than 6" (15.2 cm) diameter:	11.90%
Pollution Removal	602 kilograms/year (€13,4 thousand/year)
Carbon Storage	1,206 thousand metric tons (€194 thousand)
Oxygen Production	36,49 metric tons/year
Avoided Runoff	2,157 thousand cubic meters/year (€4,1 thousand/year)
Structural Values	€3,96 million

2.4. Gaps on Research

In Tampere, urban vegetation, particularly trees, has been prioritized as a key measure for climate change mitigation and adaptation. This approach is outlined in various key documents, including the Climate Change Adaptation and Preparation Plan (2022), Carbon Neutral Tampere 2030, Urban Tree Policy (2020), I-tree Eco Analysis (2019), and the Phase Master Plan of the Inner-city Centre (2021-2025). While the UHI study (Sitowise, 2022b) conducted for the city centre represents a step forward in analysing heat islands and devising strategies for mitigation and adaptation which includes urban vegetation, there remains a need to understand how vegetation can effectively regulate the microclimate and enhance OTC. The report also highlighted the importance of considering both summer and winter time thermal comfort, considering the city's seasonal variations. To address these issues, this study aims to provide valuable guidance for urban planning decisions by analysing the city centre at both city and block scale levels through remote sensing and microclimate modelling and simulation methods. By conducting this analysis, the study aims to contribute to the enhancement of urban environments, through providing a support to a climate-resilient planning that is also conducive to the well-being of city residents.

CHAPTER 3: METHODOLOGY

3.1 Research Approach and Framework

The research employs a comprehensive multi-method approach, including both qualitative and quantitative components. The qualitative aspect involves conducting a thorough literature review to establish a foundation, exploring relevant case studies, data sources, urban plans, and policies related to city and the research topic. On the other hand, the quantitative approach involves utilising GIS methods, ENVI-met modelling and simulation for data collection, and statistical analysis to analyse and interpret the data collected. By following a macro to micro scale pattern, starting with the city analysis through GIS methods and then narrowing down to a specific focus area for ENVI-met simulation, the research captures a comprehensive understanding of the research topic at different scales. Figure 3.1 illustrates an overview of the research structure.

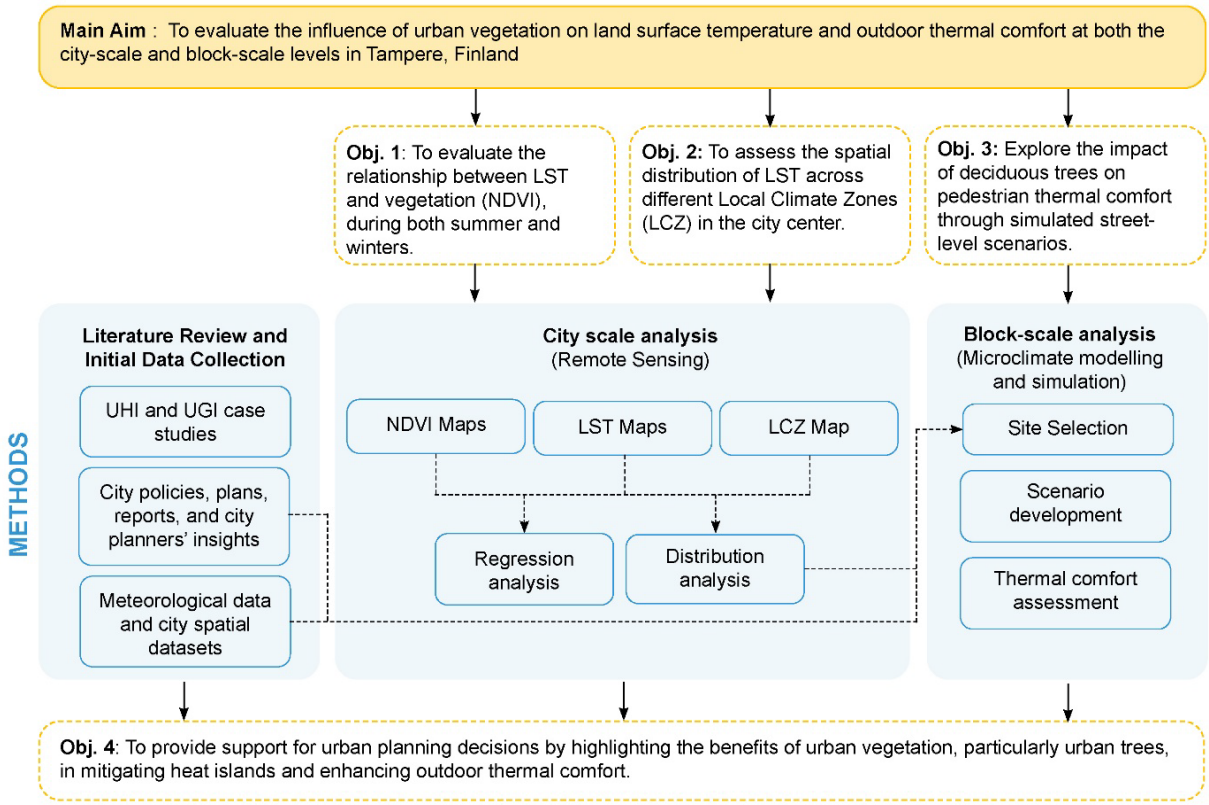

Figure 3.1 Overview of the research structure

3.2 Overview of the Study Area

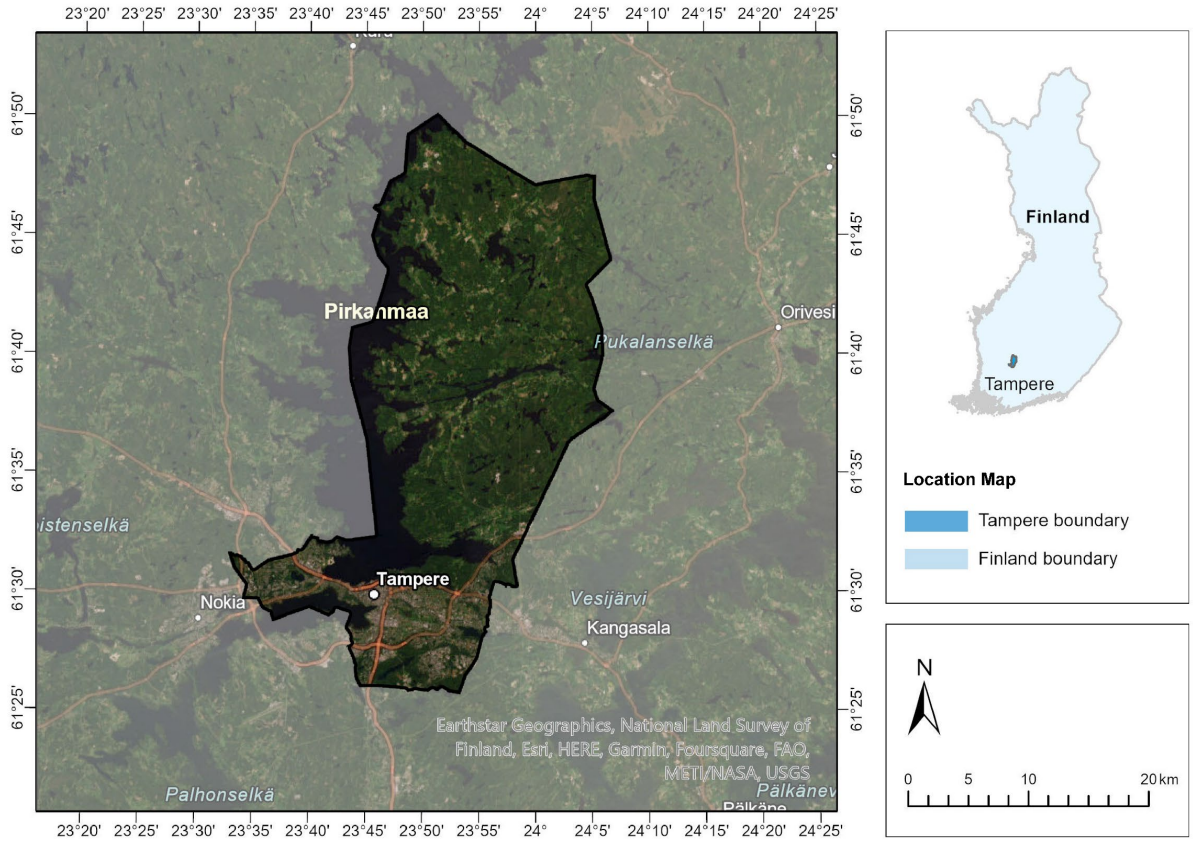

Figure 3.2 Map of Tampere, Finland

Tampere (61°29′53″N; 23°45′36″E) is located in southwestern Finland (Fig. 3.2) and covers an area of 689.6 sq.km. - with 24% of which is water area. The northern part of the region houses a variety of landscapes and forests while the more urbanised areas are in the southern part. The city centre (Fig 3.3) is located between two lakes - Lake Näsijärvi (north) and Lake Pyhäjärvi (south) - and has a footprint of about a quarter of the whole region land area (City of Tampere, 2022a). Belonging to Köppen-Geiger climate classification subtype *'Dfb'*, the city experiences a humid continental climate characterised by severe cold winters, absence of dry seasons, warm summers, and strong seasonality. During the 30-year period 1991-2020, Tampere has an annual average temperature of 5.2°C with February being the coldest (-2.5°C to -9.1°C) and July being the warmest (12.2°C to 22.5°C). Throughout the years, the lowest measured temperature was -31.7 °C (2003) and the highest was 32°C (2010). It has an average annual rainfall of 583 mm, with March as the driest month (29 mm) and July as the wettest (74 mm) (Jokinen *et al.*, 2021).

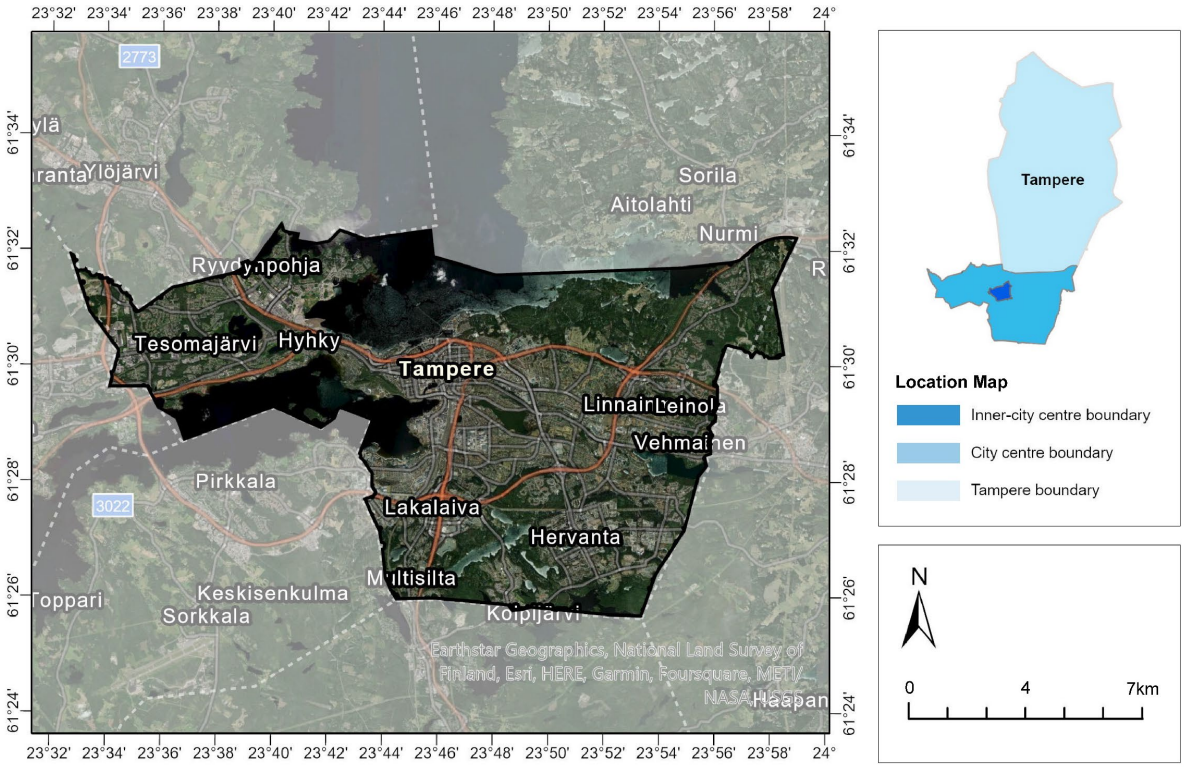

Map of City Centre with design area boundaries

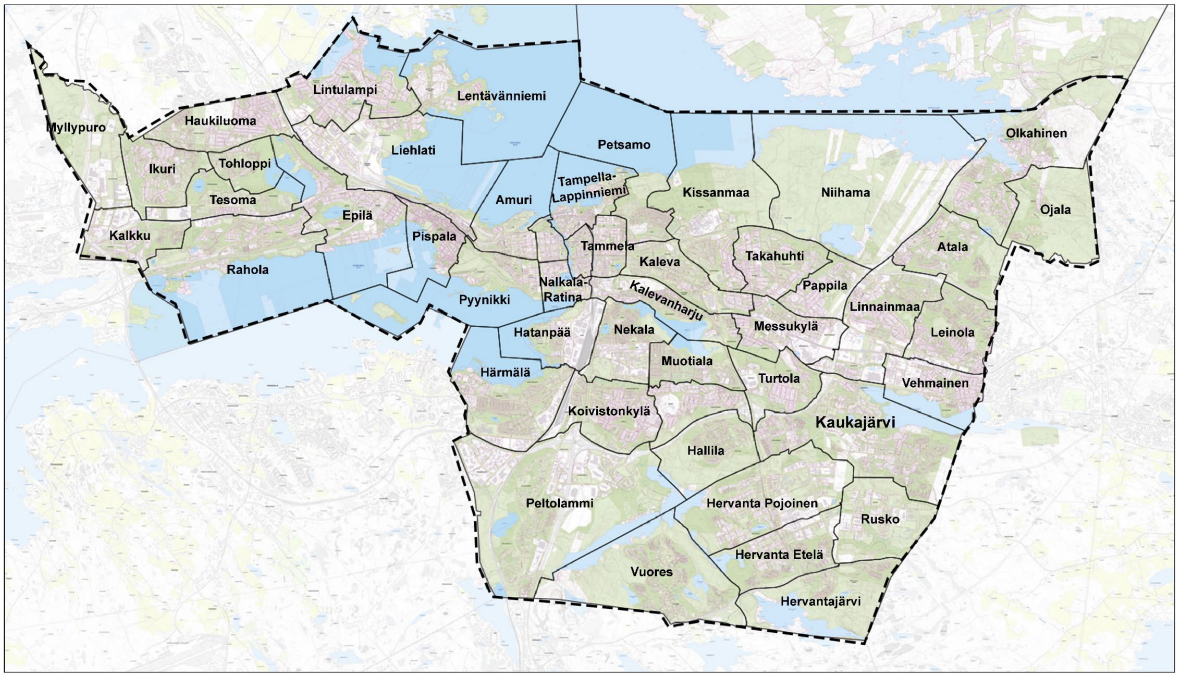

Figure 3.3 Map of Tampere City Centre with design area boundaries

Tampere has 250,353 inhabitants, with a population density of 474.4 pesons/sq.km by the end of 2022. The population is mostly dominated by people under the age of 40 and has an annual growth rate of 1.4% which equates to 3,000-

4,000 new residents per year. In the inner-city centre, there is a population increase of about 6.2% from 2017-2022, with the age group of 30-45 having the highest increase of 12% (City of Tampere, 2022a).

3.3 Data Collection and Processing

The data used in this research include Landsat 8 OLI/TIRS images with 30m resolution for the years 2018 and 2022 obtained from the USGS Explorer, and the city LCZ map with the resolution of 100m obtained from the WUDAPT website. To analyse the urban fabric, various shapefiles were collected from the municipality which include datasets such as the city boundary map, land cover, surface material cover, urban trees, and buildings. These spatial data and images were processed using the GIS–based remote sensing software ArcGIS Pro 2.8. All images were clipped to fit the city centre boundary map (Fig. 3.3) and resampled from 30m to 100m for a uniform resolution. Table 3.1 presents the list of data used in this research.

Table 3.1 Summary of data used in the study

Data	Data Source	Format	Application
Landsat 8 OLI/TIRS satellite images	USGS Explorer	Raster file	LST and NDVI maps retrieval; Spatial and Statistical Analysis
European LCZ Map	WUDAPT website	Raster file	Tampere LCZ map extraction; Spatial and Statistical Analysis
City Building Data	City of Tampere	Shape file	Spatial Analysis; ENVI-met
Urban Street Trees	City of Tampere	Shape file	Spatial Analysis; ENVI-met
Surface Cover	City of Tampere	Shape file	Spatial Analysis; ENVI-met
Urban Green Dev. Areas	City of Tampere	Shape file	Spatial Analysis
Tampere LST Heat Zones	City of Tampere	Shape file	Spatial Analysis
Meteorological Data	Finnish Meteorological Institute	MS Excel	ENVI-met simulation input

3.3.1 LCZ Map Retrieval

LCZ provides a systematic framework for understanding the local climate and has been considered as one of the research baselines in representing the urban fabric and UHI relationship. It has 17 standard classes (Fig. 3.4) that can be distinguished by structural and land cover characteristics influencing the atmospheric temperature at a screen height of 1-2 m above the ground. The classes include ten built types (LCZ 1-10) and seven land cover types (A-G), with all being identified by various properties (Stewart and Oke, 2012; Das and Das, 2020) as seen in Appendix A.

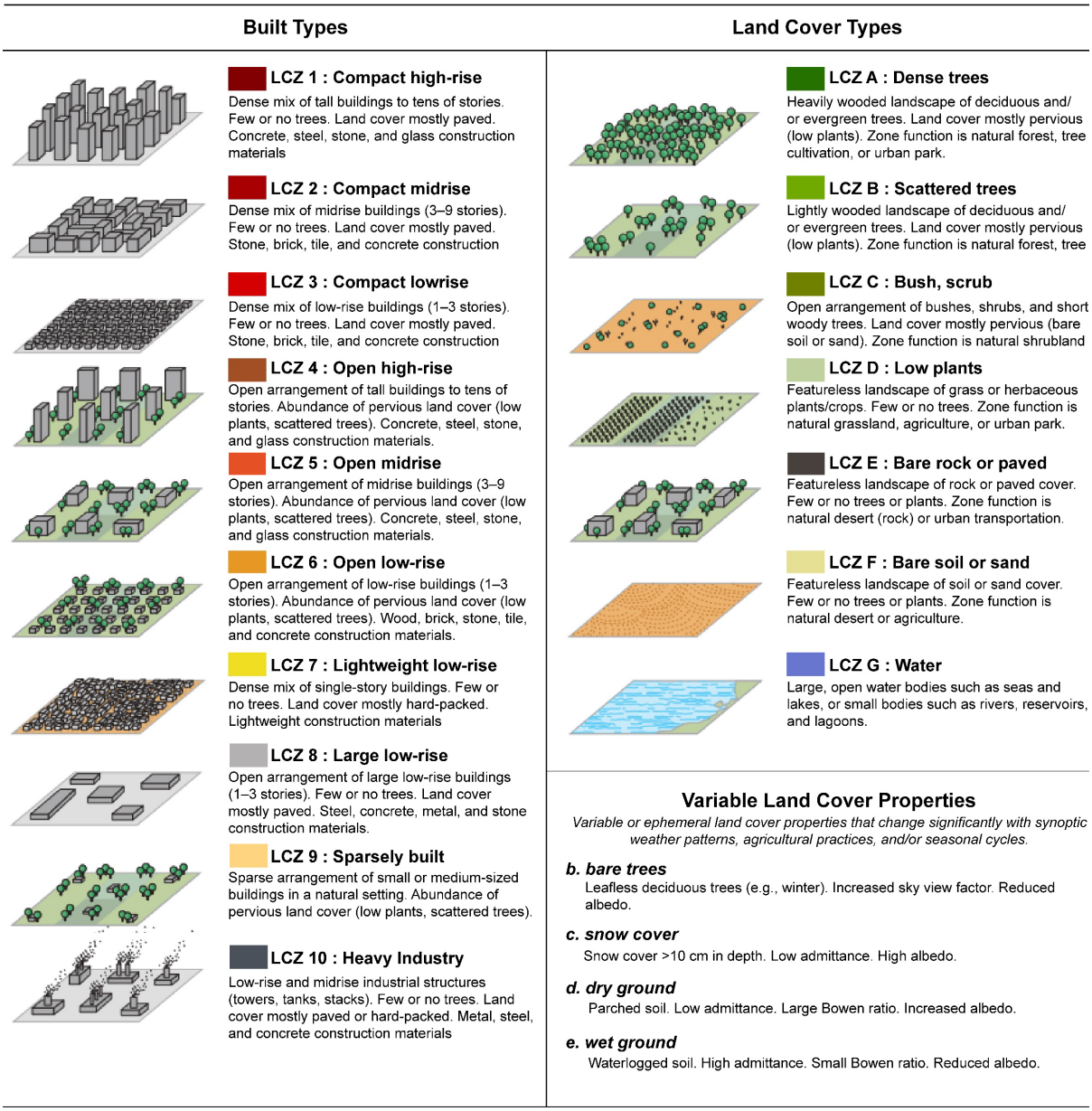

Figure 3.4 LCZ classes with description (adapted from Stewart and Oke, 2012)

In this study, the city LCZ map was clipped from the *'European LCZ Map'* created by Demuzere et al. (2019) which was available in the WUDAPT website. WUDAPT provides basic and consistent description of urban morphology of different cities and has delivered available maps or datasets for multiple studies for different purposes (Aslam and Rana, 2022). In this regard, this map was used as the experiments have >70% overall accuracy scores which is within the acceptable minimum accuracy of 50% to pass the WUDAPT quality control (Demuzere *et al.*, 2019).

3.3.2 LST and NDVI retrieval

In urban studies, LST is regarded as a vital parameter in determining UHI and it is mostly affected by the seasons, time, population, and land cover. Landsat 8 OLI/TIRS Collection 2-Level 1 images were obtained in two different seasons for the years 2018 and 2022, with February and July as representative months for winter and summer seasons respectively. Images with less than 10% of cloud cover were used to minimize the brightening and darkening impacts of clouds and its shadows within the study area (Zhu and Woodcock, 2012). Table 3.2 presents the metadata of the acquired Landsat-8 images used for the study.

Table 3.2 Acquired Landsat 8 images metadata

Date Acquired	Time	Cloud Cover (%)	Sun Elevation (°)	Sun Azimuth (°)
2018 Feb 24	9:41:22	0.33	18.14	164.44
2018 July 18	9:40:48	6.75	48.47	161.08
2022 Feb 28	9:35:28	0.04	19.66	164.47
2022 July 21	9:41:42	2.91	47.93	161.35

Figure 3.5 gives an overview of the LST retrieval process. As seen in Appendix B, remotely sensed LST entails an array of procedure, including the calculation of TIRS band 10 to spectral radiance, followed by its conversion to at-satellite brightness temperature. After this, NDVI was calculated using thermal image bands 4 and 5 to

get the proportion of vegetation and then the land surface emissivity. Lastly, the emissivity corrected LST was calculated (Avdan and Jovanovska, 2016; Emmanuel *et al.*, 2023).

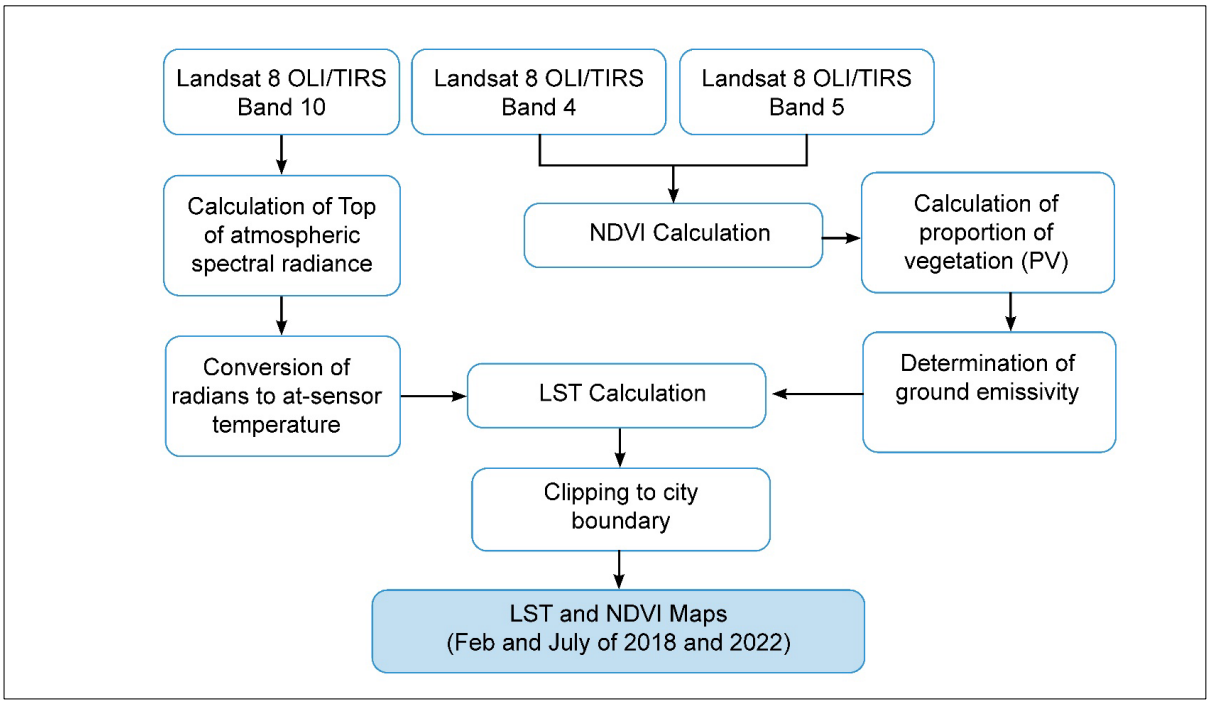

Figure 3.5 LST and NDVI calculation process (adapted from Avdan and Jovanovska, 2016; Emmanuel et al., 2023)

3.3.3 Statistical Methods

A sample with 1,395 generated points was used to analyse the correlation between LST and NDVI, where points located in water bodies were omitted, following the methods of previous studies (Yuan and Bauer, 2007; Ullah *et al.*, 2023). Using MS Excel for the data points, a simple line regression analysis was used to determine the correlation between the two variables from February and July.

3.4 Microclimate Modelling and Simulation

In this section, the analysis narrowed down to the block-level ENVI-met simulation of the focus area within Tampere's inner-city centre (Fig 3.6).

3.4.1 Identification of Focus Area

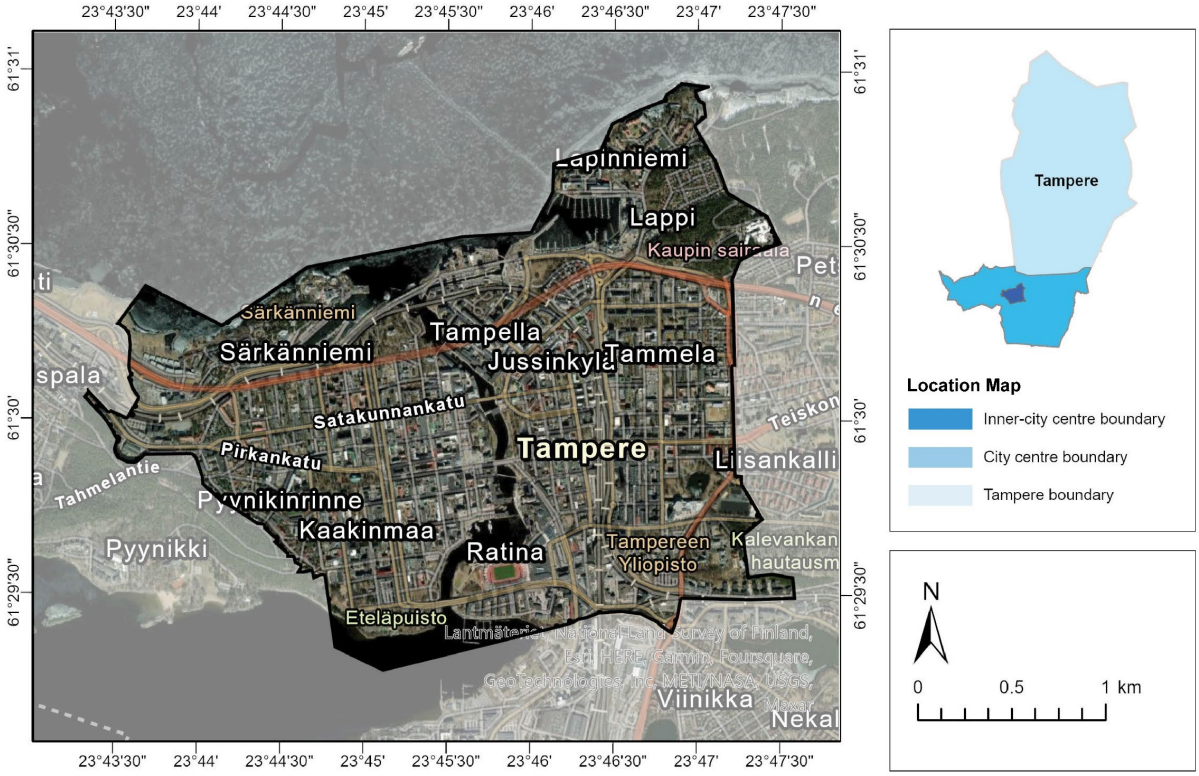

Figure 3.6 Map of Tampere Inner-City Centre

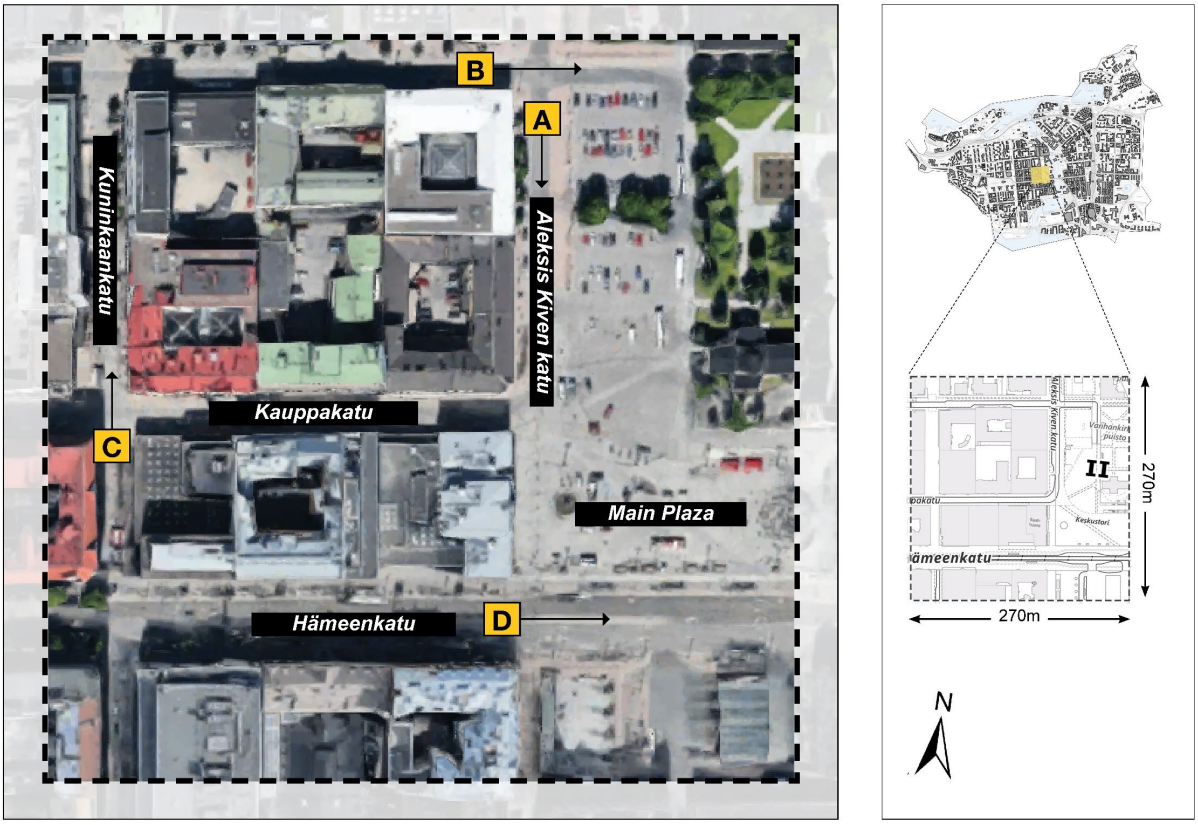

Figure 3.7 Focus area for microclimate modelling and simulation (adapted from Google Maps, 2023)

a View of Aleksis Kiven katu Street

b View of Open Parking Space

c View of Kuninkaankatu Street

d View of Hämeenkatu Street

Figure 3.8 Street view images within the focus area (Google Maps, 2023)

Figures 3.7 and 3.8 displays the focus area (Google Maps, 2023), a 270m x 270m site in the inner-city centre which includes Keskustori or the main plaza, Hämeenkatu (main street), Kuninkaankatu, Kauppakatu and Aleksis Kiven katu streets - all planned to be pedestrian axes in the future for OTC analysis. Belonging in the LCZ 2 compact midrise classification, the urban morphology of the district can be characterised having mid-rise buildings. The surface cover is mostly compromised of granite pavement (single stones) for the main streets, cobblestones for the main plaza, and concrete pavement and asphalt for roads. The streets are lined with mostly deciduous trees, with *Tilia x vulgaris* and *Acer platanoides* being the most common species.

3.4.2 ENVI-met Modelling and Simulation

In this study, ENVI-met ver. 5.0 was used for both modelling, simulation, and analysis of the outcomes. ENVI-met is a comprehensive 3-dimensional microclimate model that takes various urban complexity factors and was chosen for this study as it is one of the most accepted software for plant-surface-air interaction, thermal comfort studies and urban outdoor scenario simulations which could help immensely in urban planning (Duarte *et al.*, 2015; Balany *et al.*, 2020; Gatto *et al.*, 2020).

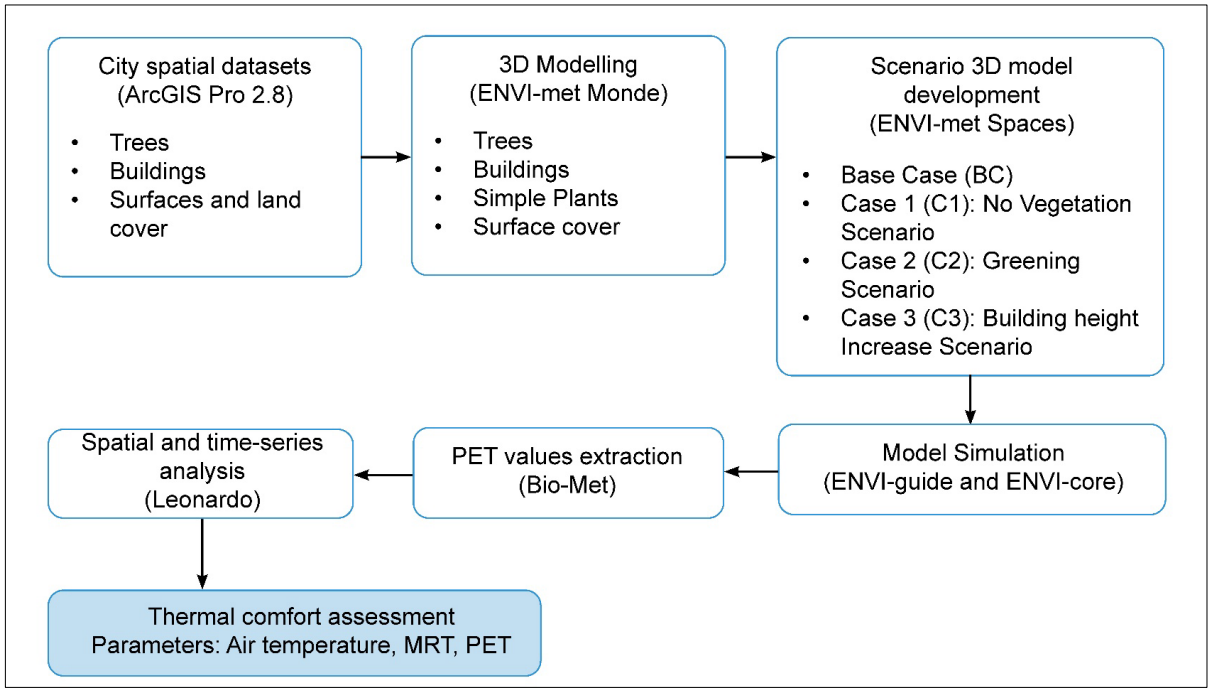

Figure 3.9 ENVI-met workflow

Figure 3.9 illustrates the model and simulation workflow using ENVI-met. Firstly, vector shapefiles were processed in ArcGIS Pro 2.8 and converted into 3D using ENVI-met Monde. Secondly, shapefiles are translated into four different scenarios which were guided by a site selection process using the ENVI-met Spaces, followed by using ENVI-core to simulate the model using the meteorological data, then Bio-met for PET value extraction using the default body parameters. Finally, results were analysed and extracted through Leonardo for a more comprehensive thermal comfort assessment. In this study, four scenarios were developed using ENVI-met (Fig. 3.10):

a. Base Case (BC) exhibits the current scenario with the existing trees, buildings, and surface cover, where buildings cover up to 35% of the area, impervious surfaces at 55%, and vegetation or pervious surface of 10% (Fig 3.10a).

b. Case 1 (C1) displays the no vegetation scenario where all trees and vegetation are removed. In this scenario only buildings (60%) and impervious surface (40%) make up the land cover area (Fig 3.10b).

c. Case 2 (C2) displays the addition of more deciduous trees, following the existing trees and spacing from the current scenario. Vegetation is increased to 25% with two rows of *Tilia* were added along the Hämeenkatu main street while a row of *Acer platanoides* were added for Kuninkaankatu, Kauppakatu and Aleksis Kiven katu streets. *Tilia* and grass cover were added on open spaces where the open parking and bus stop parking were (Fig 3.10c).

d. Lastly, Case 3 (C3) exhibits the increase of building height up to 23 meters, with the same land cover percentage as the existing scenario (Fig 3.10d).

For the vegetation, the leaf area density (LAD) settings were changed to *'seasonal'* using Albero, a part of ENVI-met software, to analyse the effects of deciduous trees as they shed their foliage in winter. This research employed a simple forcing simulation where basic meteorological parameters (Table 3.3) are used to analyse the models on both critical cold and hot days. The meteorological input data were extracted in 10m high Tampella observation station (61°30'04"N 23°45'53."E) from

Finnish Meteorological Institute (FMI) website. In Finland, FMI has recorded that June 2021 has the warmest temperature in the country's history since 1937, and in Tampere, it was recorded that June 22 was the hottest day of that year (Finnish Meteorological Institute, 2021). In this regard, the study used June 22 for the summer and January 15 - the coldest day of the same year - as the date for winter simulation for all scenarios.

Table 3.3 ENVI-met parameters used in the study

Parameter	Description	Value	
Computational domain and grid	Model Dimension	135 x 135 x 30	
	Grid Cells *(dx,dy,dz)*	2 x 2 x 2	
	Nesting grids	10	
Surfaces and Materials	Building walls	Default Wall - moderate insulation	
	Building roofs	Default Wall - moderate insulation	
	Soil type		
	Main Street	Granit Pavement (single stones)	
	Sidewalks / Minor Streets	Concrete Pavement Gray)	
	Open Parking / Roads	Asphalt Road	
Vegetation *(See Fig. 3.10 for vegetation placement)*	Trees	*Tilia; Acer platanoides; Malus domestica, Prunus padus*	
	Grass cover	Grass cover (50cm average dense)	
General Settings		**Winter**	**Summer**
	Simulation Date and Time	January 15, 2021	June 21, 2021
	Start Time (HH:MM)	19:00	19:00
	Total Simulation Time	30hrs	30hrs
Meteorological data (Simple Forcing)	Time of Max. Air Temperature	23:00 -9.9° C	14:00 33° C
	Time of Min. Air Temperature	2:00 -21° C	23:00 19.2° C
	Time of Min. Rel. Humidity	0:00 75% RH	14:00 27% RH
	Time of Max. Rel. Humidity	21:00 89% RH	23:00 90% RH
	Wind speed	4.5 m/s	2.7m/s
	Wind direction	202.5°	202.5 °
Bio-Met (body parameters)	Age (y); Weight (kg); Gender	35 y; 75kg; Male	
	Body Position	Standing	
	Walking speed (m/s)	1.34 m/s	
	Clothing parameters (clo.)	1 (clo.)	0.5 (clo.)

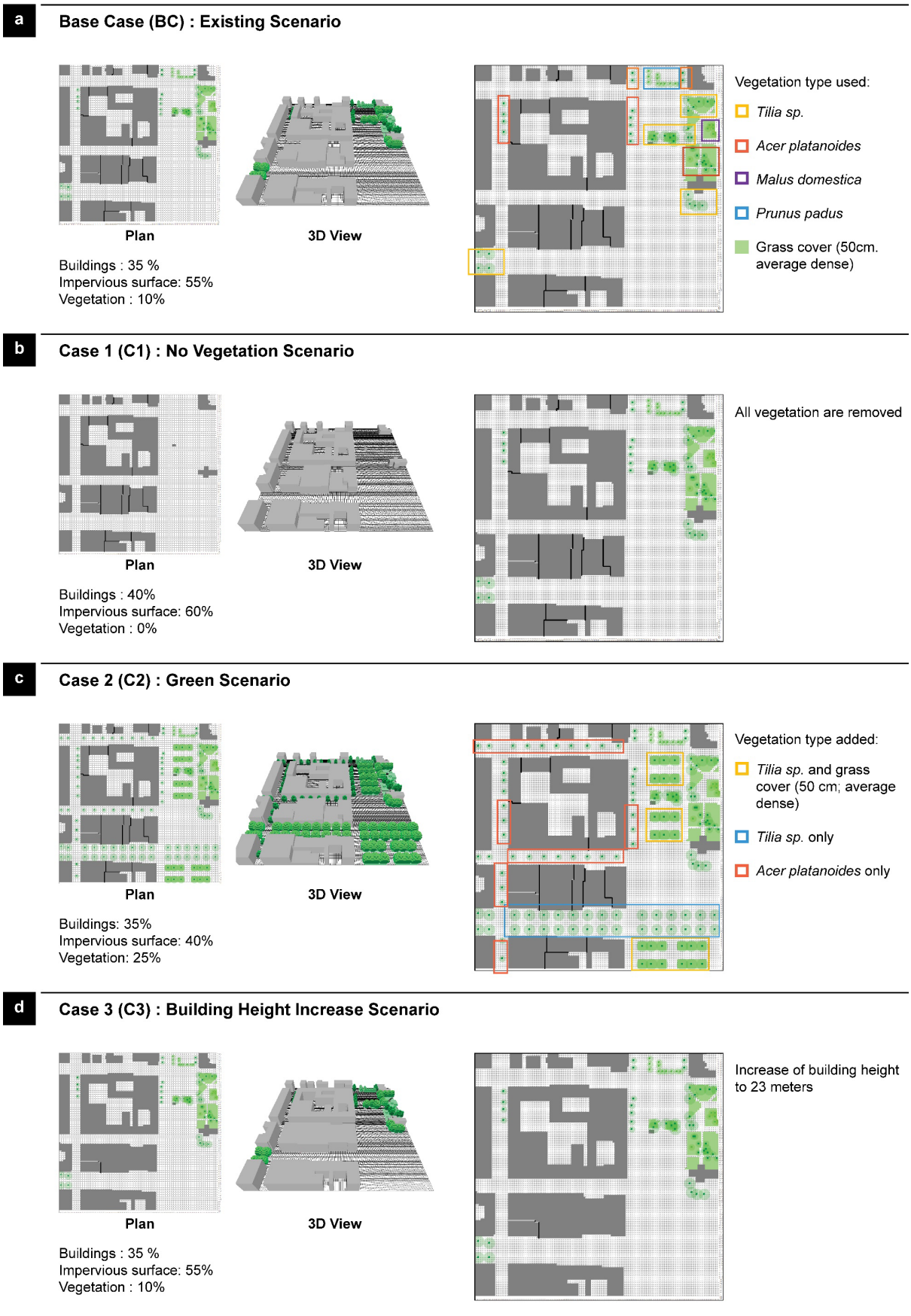

Figure 3.10 Four (4) ENVI-met model scenarios with description

3.4.3 Assessment Parameters

Using ENVI-met, results were then analysed based on three parameters: air temperature (T_{air}), mean radiant temperature (MRT) and physiological equivalent temperature (PET), to provide a comprehensive thermal comfort analysis. In this study, T_{air} is used as it is considered as one of the main micro-meteorological parameters (relative humidity, wind speed, and solar radiation) used to determine thermal perception (Gatto *et al.*, 2020). MRT is used as a parameter to understand the influence of shadow patterns brought by trees and buildings to the spatial variation (Lindberg *et al.*, 2014; Duarte *et al.*, 2015; Gatto *et al.*, 2020). It is defined as ' the uniform temperature of an imaginary enclosure (or environment) in which the radiant heat transfer from the human body is equal to the radiant heat transfer in the actual nonuniform enclosure' (Li, 2016), and in comparison, to T_{air}, it exhibits large spatial distinctions over shorter distances (Lindberg *et al.*, 2014). It also has a strong influence on thermal comfort indices such as PET (Li, 2016).

Table 3.4 PET range (Matzarakis, Mayer and Iziomon, 1999)

PET	Thermal Perception	Physiological Stress Grade
<4	Very Cold	Extreme cold stress
4.1 - 8.0	Cold	Strong cold stress
8.1 - 13.0	Cool	Moderate cold stress
13.1 - 18.0	Slightly Cool	Slight cold stress
18.1 - 23.0	Comfortable	No thermal stress
23.1 - 29.0	Slightly warm	Slight heat stress
29.1 - 35.0	Warn	Moderate heat stress
35.1 - 41.0	Hot	Strong heat stress
>41.0	Very Hot	Extreme heat stress

PET values displays a range of thermal perception and physiological stress grade (Table 3.4) , and was adopted to further analyse OTC, as this index considers the effect of radiative fluxes on body heat balance (Zhang, Odeh and Han, 2009; Duarte *et al.*, 2015; Morakinyo *et al.*, 2017). For this study, the simulated microclimate data from ENVI-met were obtained and imported to Bio-Met using the default parameters for a standardised person (Table 3.3).

CHAPTER 4: RESULTS

This chapter, structured into three sections, presents the quantitative findings of the study. First exhibits the results of the LST-NDVI analysis, followed by the city centre's LCZ map and distribution of LST across different LCZ classes. The last section displays the results of the microclimate simulation using air temperature (T_{air}), mean radiant temperature (MRT) and physiologically equivalent temperature (PET), as parameters for thermal comfort analysis.

4.1 Seasonal and Spatial Variations of LST and NDVI

In winter (Fig. 4.1 a,b), it can be observed that the temperature difference, which ranges from -12.50°C to -28.50 °C, is less pronounced as Tampere experiences cold temperatures and is mostly blanketed by snow cover during this season. Meanwhile, ranging from 6.00°C to 38.00°C, both summer results (Fig. 4.1 c,d), show profound surface temperature contrasts, as high LSTs are observed in the built-up areas across the city, while relatively cooler areas are seen in parks and forests. It also shows that during this season, waterbodies are clearly defined having the lowest LST values.

In the case of NDVI (Fig. 4.2), a distinct variation in the results can be observed between winter (Fig. 4.2 a,b) and summer (Fig. 4.2 c,d). Generally, NDVI values ranges from -1 to 1 and can be classified to (a) non-vegetation with values from -1 to 0.199, representing sand, barren rock, water or snow, (b) low vegetation with values ranging from 0.2 to 0.5, indicating sparse vegetations such as grasslands and shrubs, and (c) high vegetation or dense vegetation with values from 0.501 to 1.0 (Remote Sensing Phenology, 2018; Hashim, Abd Latif and Adnan, 2019). In this study, generally low NDVI values are observed during winter as the maximum value (0.25) representing sparse vegetation can only be seen in the northeastern and southern parts of the city centre. During summer however, a higher maximum value is observed (0.55) as dense vegetation is evident in several portions of the city while low values can be clearly observed in water bodies.

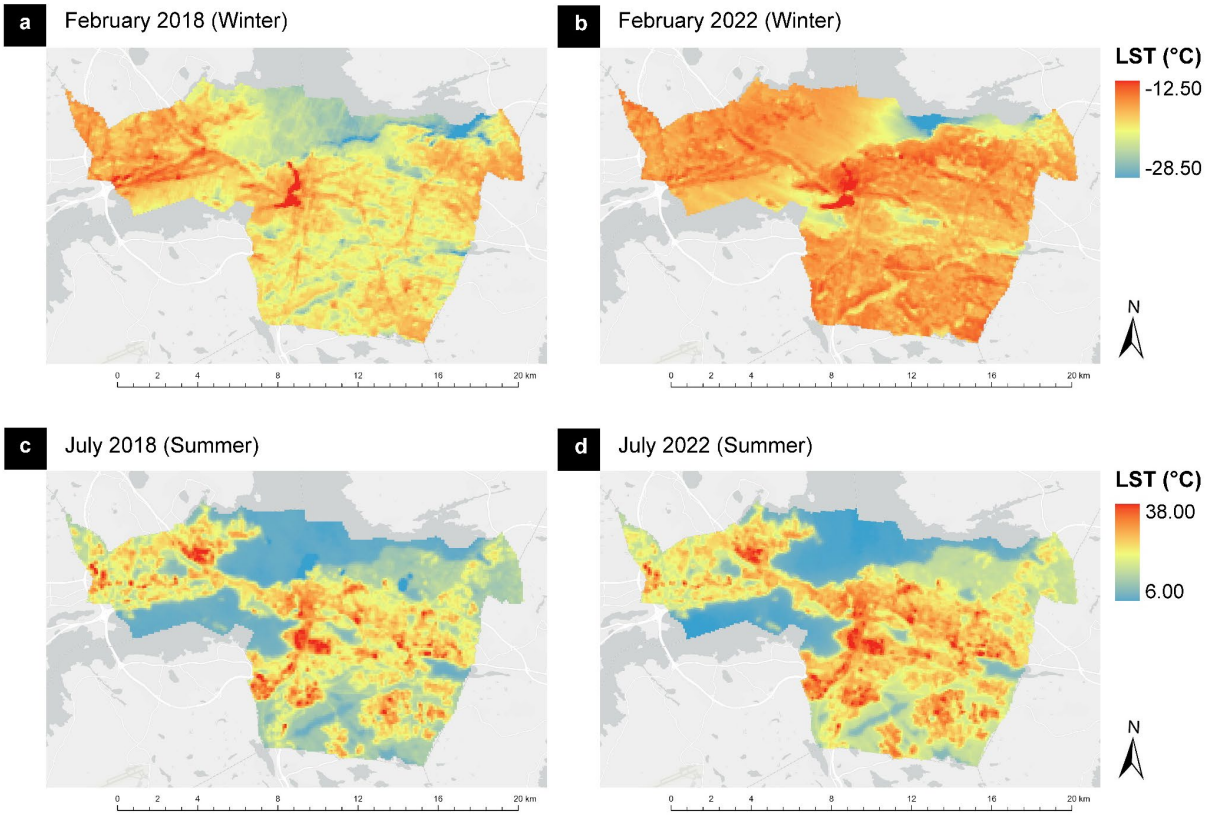

Figure 4.1 LST maps of Tampere city centre: (a,b) winters (c,d) summers

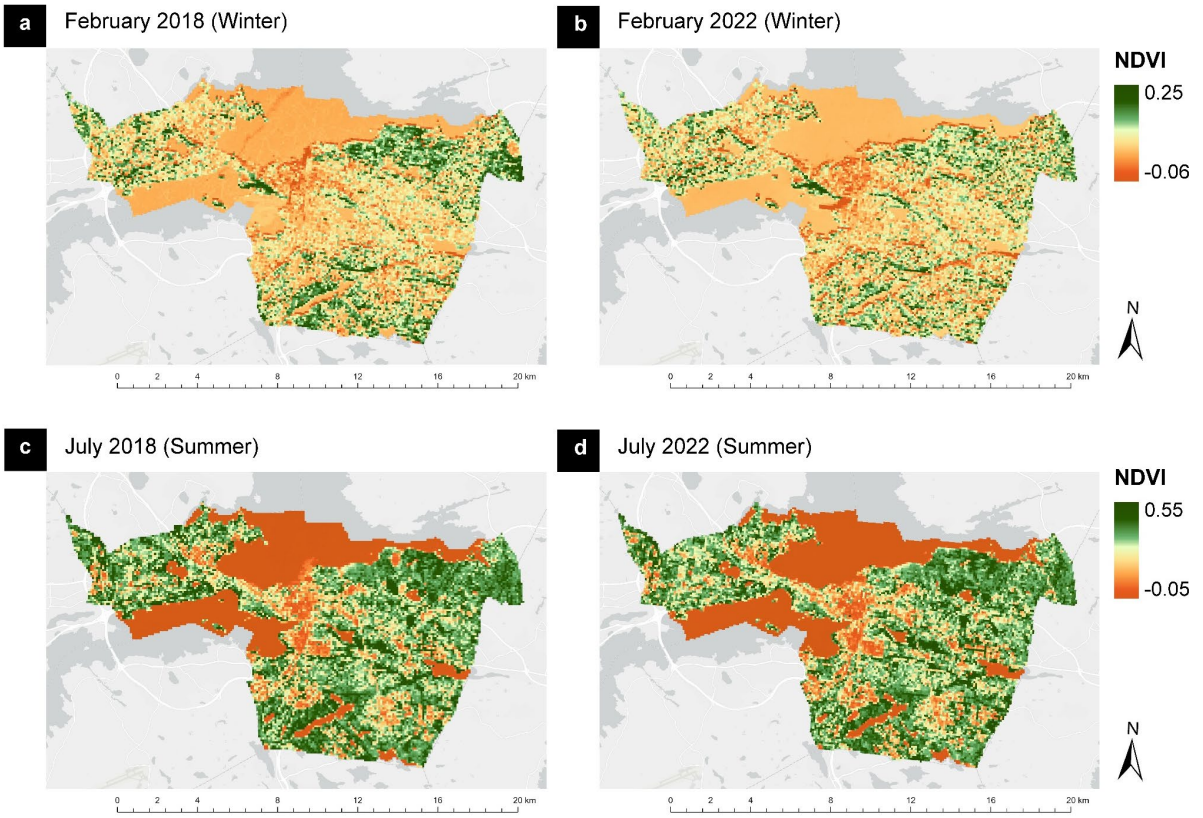

Figure 4.2 NDVI maps of Tampere city centre: (a,b) winters (c,d) summers

Results show that LST-NDVI relationship varies across different seasons. In winters (Fig. 4.3 a,b), when the city experiences extreme cold temperatures, it is observed that LST and NDVI has a weak positive correlation with r = 0.18 for February 2018 and r = 0.25 for February 2022. Having p-values of <0.05 suggests that the relationship is statistically significant, however, the relatively low r^2 values show that variables other than NDVI have stronger influence on LST during winters.

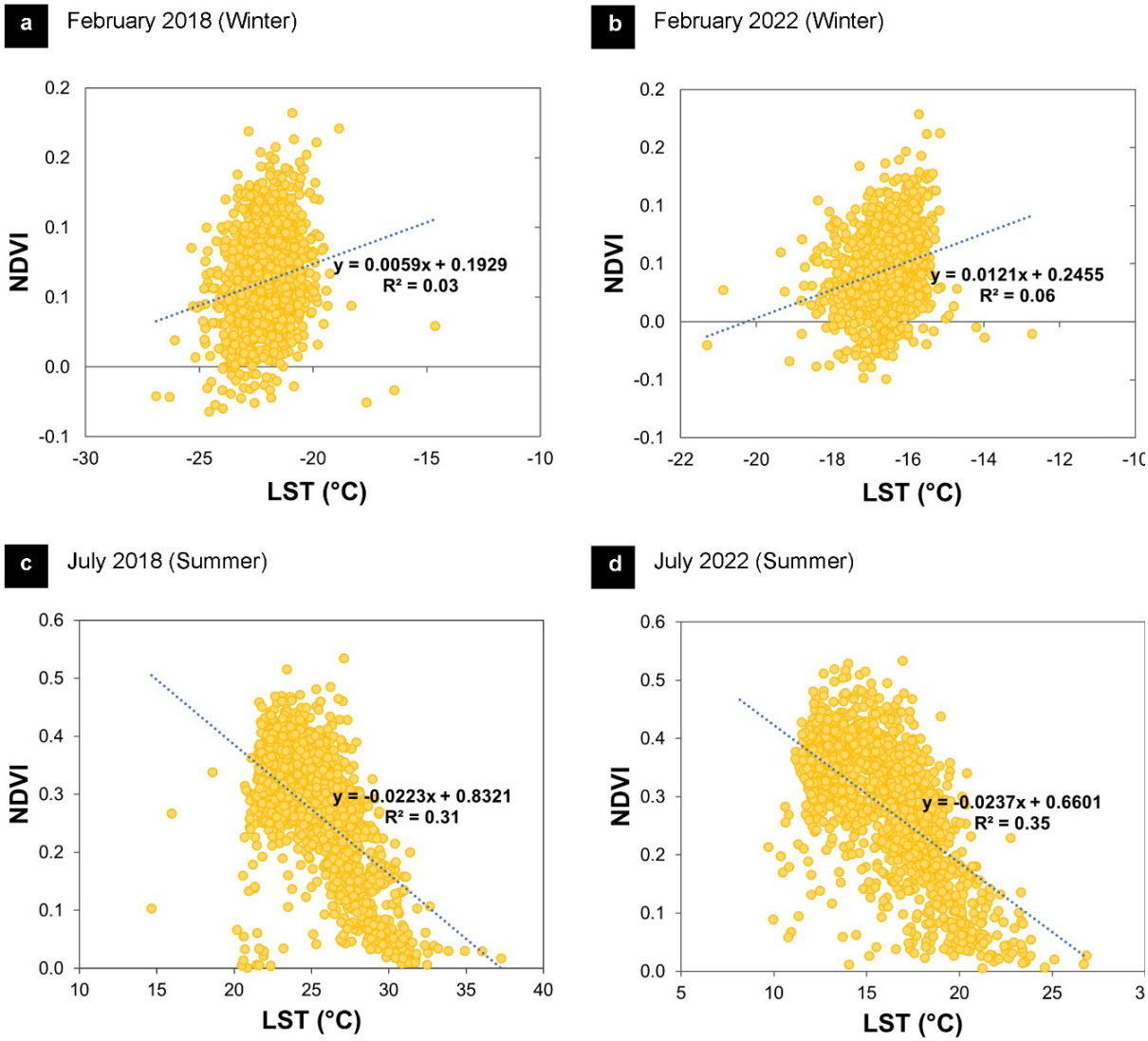

Figure 4.3 LST and NDVI scatterplots: (a,b) winters (c,d) summers

During summers (Fig. 4.3 c,d), LST and NDVI have a statistically significant ($p<0.05$) moderate negative correlation with r = -0.55 for July 2018 and r = -0.59 for July 2022. This indicates that higher vegetation health or density represented by NDVI leads to a decrease in LST.

4.2 Tampere City Centre Local Climate Zone (LCZ) Map

In this study, results show that five out of ten built up LCZs (LCZ 2, 5, 6, 8, 9) and five out of seven land cover LCZs (LCZ A, B, D, E, G) were recognized in the extracted map of Tampere's city centre (Fig. 4.4). About 67% of the extracted data is accounted to the land cover types while the remaining 33% is for the built types. Overall, Fig. 4.5 shows that LCZ A is the most dominant LCZ land cover type, covering 32% of the area, while LCZ E (1.1 sq.km.) has the smallest. In terms of built types, LCZ 6 (19.1 sq.km.) is the most dominant at 11%, while LCZ 2 (1.2 sq.km.) has the smallest area at 1%.

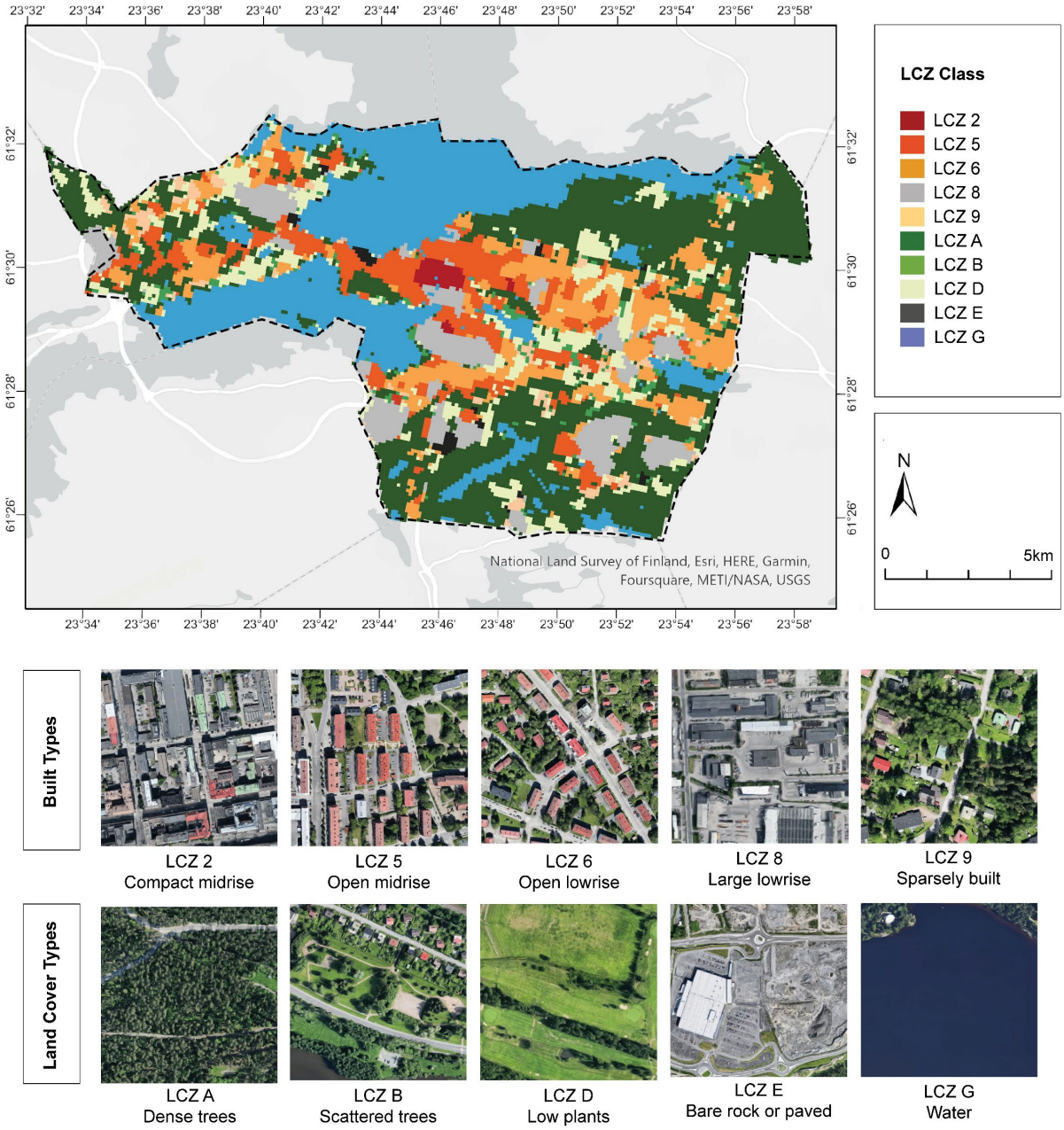

Figure 4.4 Tampere city centre LCZ map (adapted from Demuzere et.al, 2019) and classification images (Google Earth, 2023)

4.2.1 LST Distribution across LCZ Classes

Table 4.1 displays the average LST values across the LCZs in summer and winter season for both years. Results show that for both built and land cover types, LCZs 2 and G have the highest and lowest mean LST for both seasons respectively. LCZ 2 (compact midrise) recorded high LST values with 29.3°C (2018) and 19.8°C (2022) for summers and -20.4°C (2018) and -15.4°C (2022) for winters.

Table 4.1 Descriptive statistics of winter and summer LST values across LCZs

LCZ TYPES	WINTER LST						SUMMER LST					
	February 2018			February 2022			July 2018			July 2022		
	Min	Max	Mean	Min	Max	Mean	Min	Max	Mean	Min	Max	Mean
LCZ 2	-22.1	-16.4	-20.4	-16.4	-14.0	-15.4	25.3	31.8	29.3	15.1	21.9	19.8
LCZ 5	-24.5	-19.4	-21.8	-18.0	-15.1	-16.5	22.4	31.7	27.2	13.5	23.4	17.8
LCZ 6	-24.7	-19.7	-22.1	-18.4	-15.7	-16.7	22.6	30.0	26.5	12.8	24.6	17.1
LCZ 8	-24.3	-14.6	-21.8	-18.0	-12.7	-16.5	20.8	37.3	29.1	11.6	26.8	19.8
LCZ 9	-23.8	-19.8	-22.1	-17.8	-15.9	-16.7	22.1	30.2	26.1	12.0	19.2	16.5
LCZ A	-26.9	-19.5	-22.2	-21.3	-15.2	-16.5	18.6	30.8	23.3	8.2	25.2	13.8
LCZ B	-25.0	-19.7	-22.3	-18.4	-15.9	-17.0	21.5	27.8	24.8	11.2	19.3	15.1
LCZ D	-26.3	-18.8	-22.3	-19.3	-15.7	-16.8	14.7	29.4	25.4	10.0	21.7	15.8
LCZ E	-24.0	-20.6	-22.1	-17.3	-15.7	-16.6	22.0	30.6	27.8	12.1	21.8	18.3
LCZ G	-27.3	-11.5	-23.3	-22.9	-11.9	-17.5	12.4	26.4	20.1	6.4	16.5	8.3

Conversely, LCZ G which represents water bodies exhibited the lowest with -23.3°C (2018) and -17.5°C (2022) for summers and 20.1°C (2018) and 8.3 °C (2022) for winters. This may be attributed to the evaporative cooling process and water's higher heat capacity. Arranged from highest to lowest, Figure 4.6 exhibits the LST values distribution and variation among different LCZs. Results show that during winters (Fig 4.6 a,b), the rank of the average values differs for both years, with only about half of the types (LCZ 2, 6, B, D, and G) being in the same rank order. Meanwhile, the average LSTs of LCZs during the summers (Fig 4.6 c,d), consistently followed the rank order: LCZ 2 > LCZ8 > LCZ E > LCZ 5 > LCZ 6 > LCZ 9 > LCZ D > LCZ B > LCZ A > LCZ G.

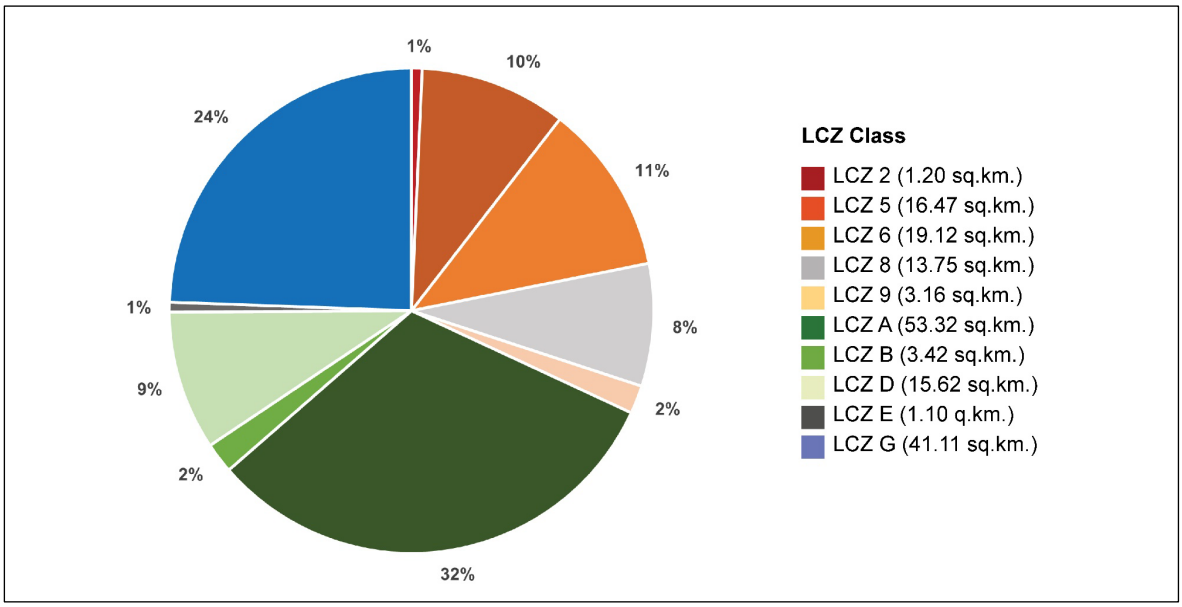

Figure 4.6 LCZ land cover percentage (%)

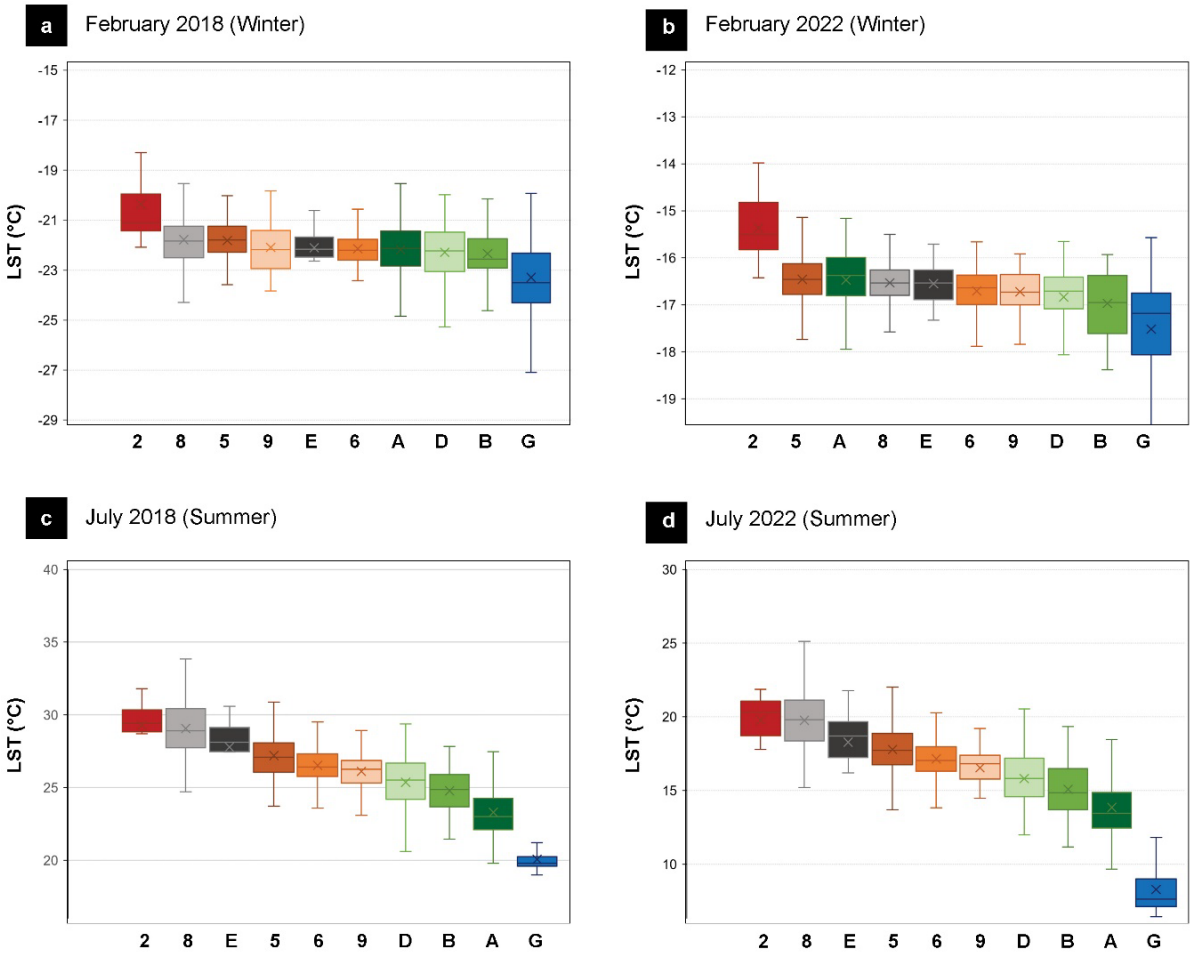

Figure 4.5 LST-LCZ box whisker plots

In the box plots, the line inside the box represents the interquartile range (IQR), spanning from the first quartile (Q1) and third quartile (Q3) of the data. The line inside the box is the median LST, while the whiskers outside the box represents the minimum and maximum values of the data excluding the outliers

4.3 ENVI-met Simulation Results and OTC Analysis

For the ENVI-met simulation analysis, outdoor thermal comfort (OTC) was assessed using different methods. First, a 24-hr analysis was done for the mean T_{air}, MRT, and PET values of all receptors to examine how the different scenarios behave. Secondly, scenarios (C1, C2, C3) are analysed across the six receptors (Fig. 4.7): Points A, B, C for streets and Points D, E, F for open spaces based on their average difference from the existing scenario (BC). Lastly, Leonardo was used for the spatial analysis and visualisation of simulation results. The average, minimum, and maximum data of each variable were extracted at 14:00 at the pedestrian level (1.4 m) for both critical cold winter day (January 15, 2021) and hot summer day (June 22, 2021).

Figure 4.7 ENVI-met models showing the six (6) receptors

4.3.1 Air Temperature (T_{air})

Figures 4.8 and 4.9 show the average time behaviour of T_{air} in all receptors for both winter and summer days, while Appendix C displays the detailed graphs of each receptor. On average, T_{air} reaches its lowest point between 6:00-8:00, then gradually increase to reach its peak at 23:00 during winters (Fig. 4.8).

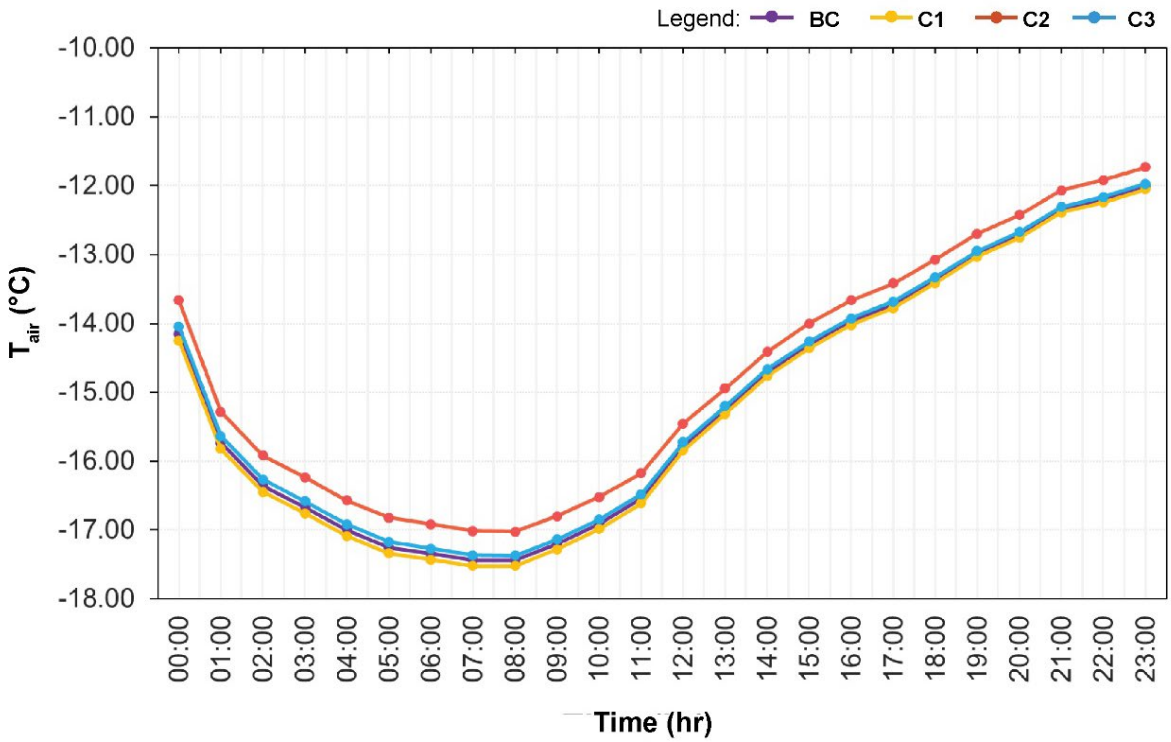

Figure 4.8 Mean T_{air} of the four (4) scenarios at 1.4m on a critical cold winter day

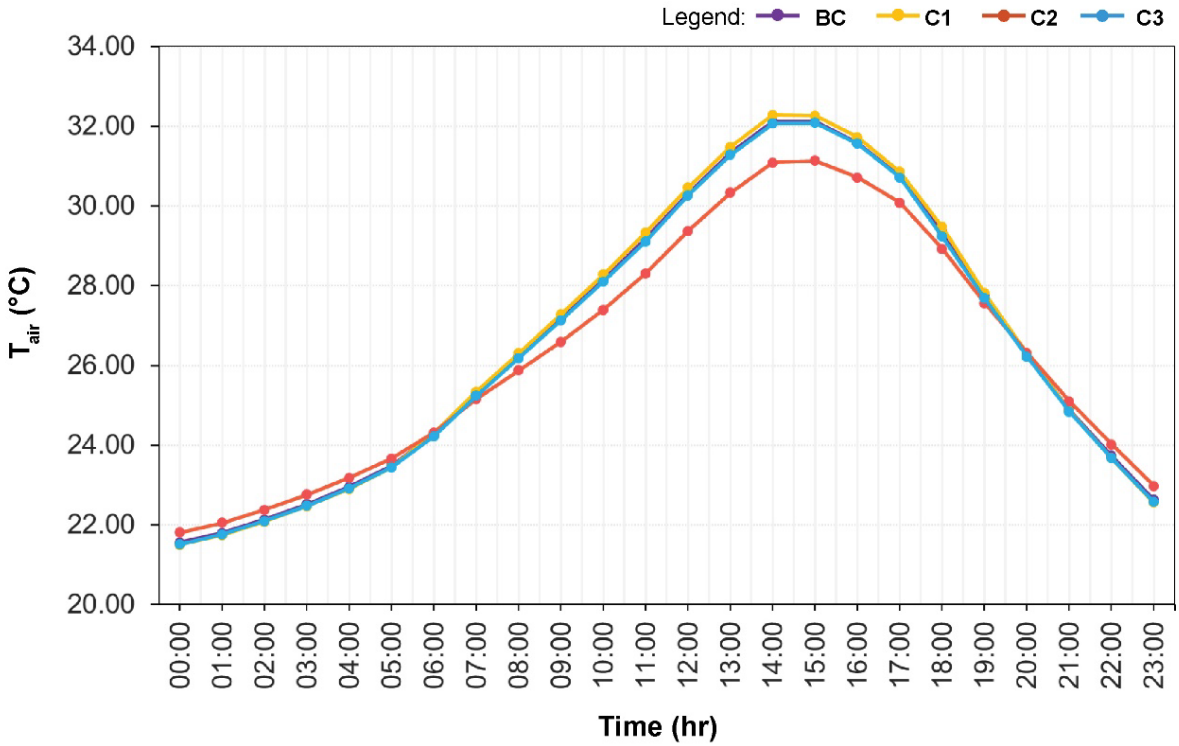

Figure 4.9 Mean T_{air} of the four (4) scenarios at 1.4m on a critical hot summer day

In contrast, during the summer (Fig. 4.9), T_{air} behaviour exhibits a gradual increase, reaching its peak between 13:00-15:00 before it decreases. In both seasons, it can be observed that there is little variation of T_{air} across all scenarios, however, C2 exhibits a more distinct outcome. In winter, it can be observed that it brought an increase all throughout the day, while in summer, it mitigates T_{air} from 7:00 to 19:00, then slightly reversing this effect at night-time between 20:00-6:00.

Table 4.2 presents the difference of all scenarios from BC in both critical cold (winter) and hot (summer) days. In comparison with the existing scenario (BC), C1 brings a further decrease in T_{air} while both C2 and C3 displays increase during winters. Notably, increasing the vegetation at C2 scenario brings a more pronounced effect than increasing the building height at C3, as seen in the mean T_{air} rise of 0.40 °C in streets and 0.32 °C in open spaces. Conversely, in summer, the results are reversed. C1 leads to a warmer T_{air} across all receptors while both C2 and C3 scenarios resulted to a cooler T_{air}. Again, the effect of C2 is more noticeable as it brings an average reduction in T_{air} of 0.20 °C in streets and 0.34 °C in open spaces.

Table 4.2 T_{air} difference from existing scenario (BC) in streets and open spaces

where positive (+) values = increase, and negative (-) values = decrease

Receptors		**T_{air} difference from BC in winter (°C)**			**T_{air} difference from BC in summer (°C)**		
		C1	**C2**	**C3**	**C1**	**C2**	**C3**
STREETS	Point A	-0.09	0.38	-0.04	0.07	-0.08	-0.05
	Point B	0.02	0.51	0.07	0.06	-0.36	-0.07
	Point C	-0.07	0.30	0.18	0.05	-0.15	-0.11
	Average	**-0.05**	**0.40**	**0.07**	**0.06**	**-0.20**	**-0.07**
OPEN SPACES	Point D	-0.03	0.24	0.02	0.05	-0.49	-0.02
	Point E	-0.03	0.52	0.05	0.03	-0.29	-0.03
	Point F	-0.20	0.20	0.08	0.03	-0.24	-0.02
	Average	**-0.09**	**0.32**	**0.05**	**0.04**	**-0.34**	**-0.02**

Spatially at 14:00 (Fig. 4.10), both seasons display that cooler areas are found within the building courtyards, extending to streets where the building shadows are cast, while open spaces exhibit a relatively warmer T_{air}. In winter (Fig. 4.10a), it can be observed that there is a small variation between BC, C1, and C3 in streets and

open spaces which indicates that the removal of vegetation (C1) and building height increase (C3) bring insignificant effect to the existing scenario. On the other hand, adding vegetation (C2) in streets and open spaces significantly warms the areas as seen in the increase in value range. Moreover, the effect of the added trees along the Hämeenkatu street also extends the warmer T_{air} to the main plaza, where no trees are added.

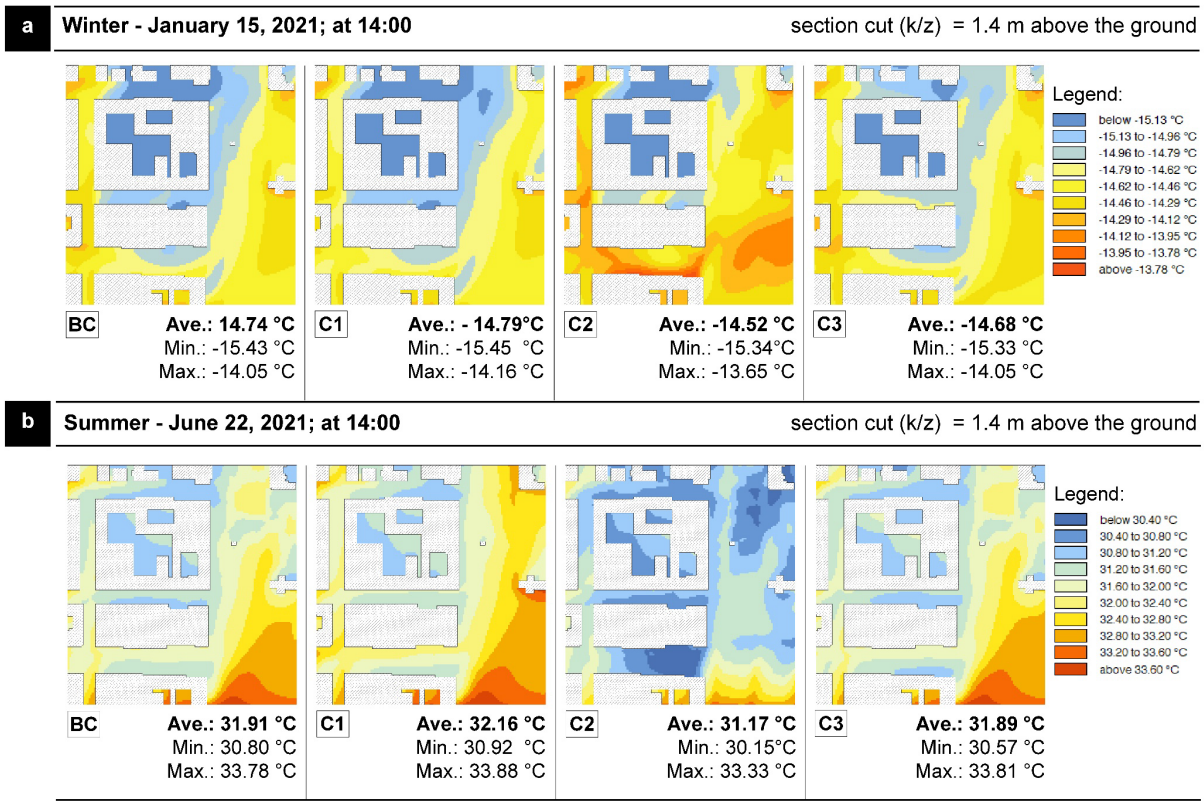

Figure 4.10 T_{air} simulation result on a (a) critical cold winter day, and (b) critical hot summer day

In the summer (Fig. 4.10b), C2 had a noticeable impact on cooling, as evidenced by the expansion of cooler areas. Furthermore, when comparing BC with C3, the difference in the range of values is negligible, indicating that the increase of building height had minimal to no effect on T_{air} during this time.

4.3.2 Mean Radiant Temperature (MRT)

As T_{air} resulted to a slight variation, the analysis is further extended to MRT to understand how the surfaces, specifically shading brought by trees and buildings

affect OTC at each receptor (Appendix D). In comparison with the behaviour of T_{air}, mean MRT (Fig. 4.11) displays more temperature variation across all the scenarios.

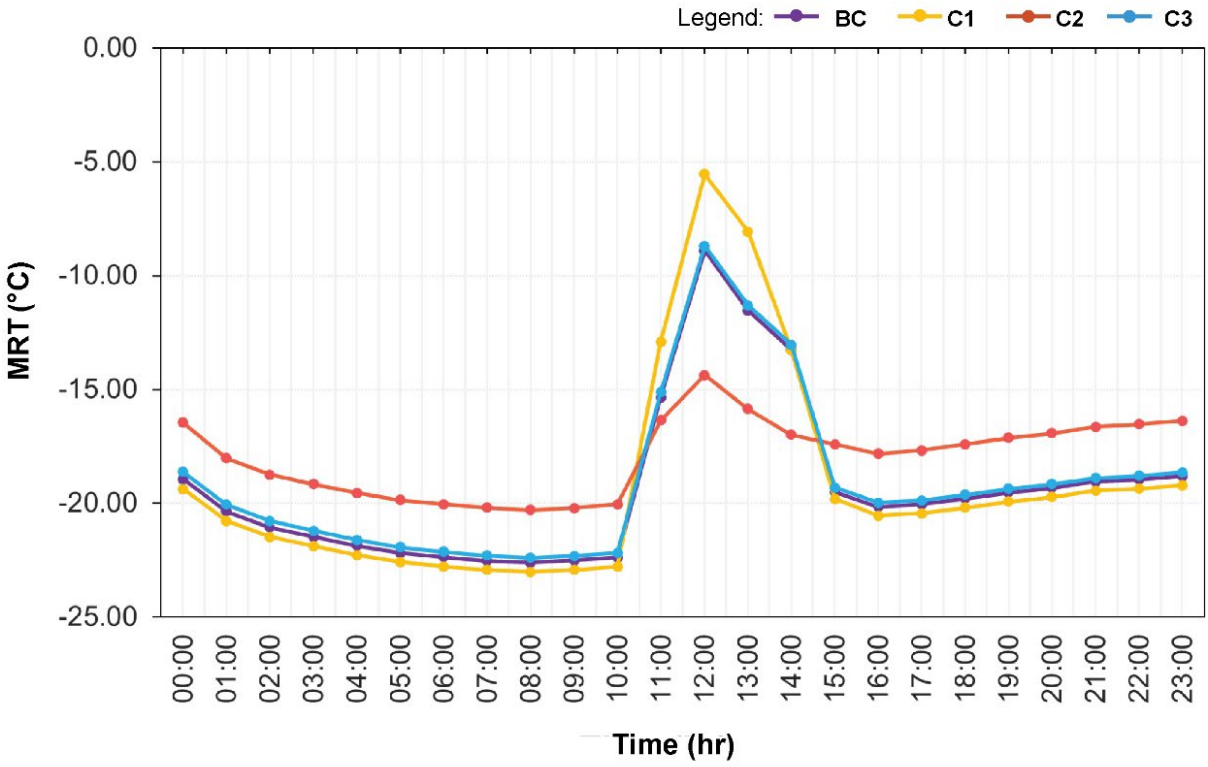

Figure 4.11 Mean MRT of the four (4) scenarios at 1.4m on a critical cold winter day

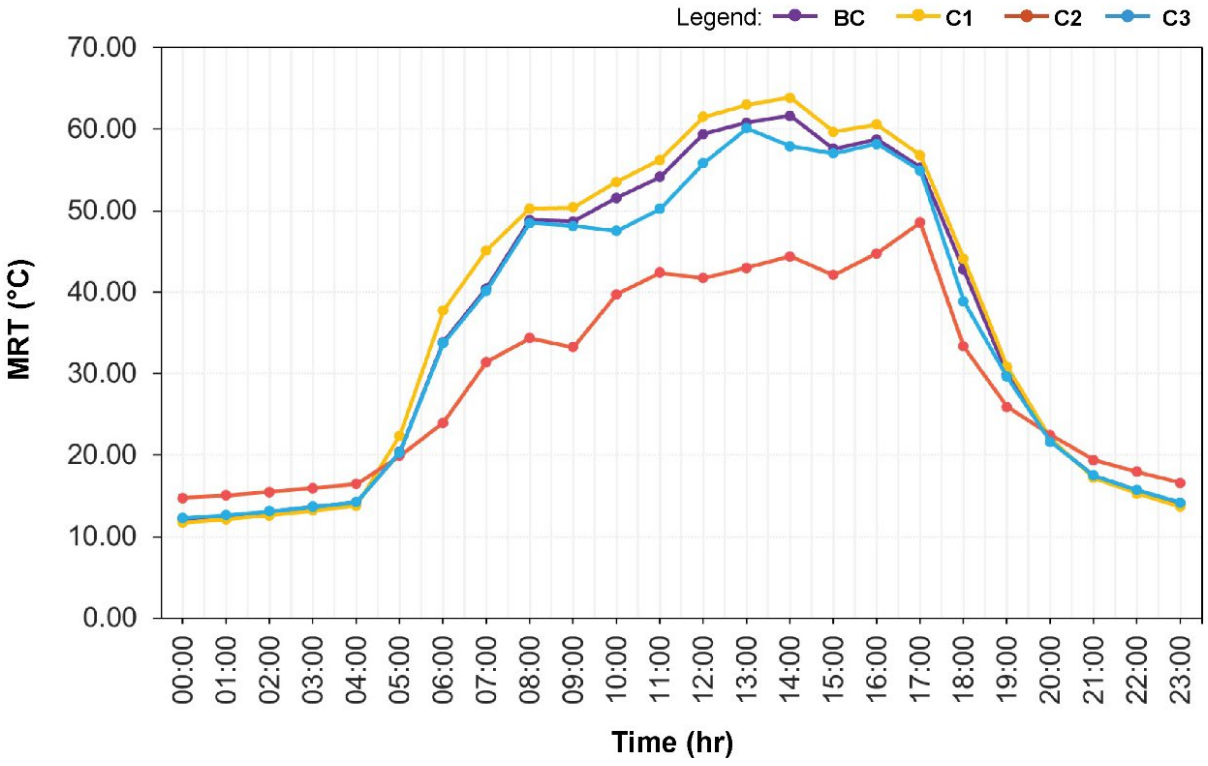

Figure 4.12 Mean MRT of the four (4) scenarios at 1.4m on a critical hot summer day

In winter, C2 generally has the highest values throughout the day except between 11:00-15:00 where it has the lowest. On the other hand, C3 displays the lowest MRT, except peaking drastically between 11:00-14:00. It can also be observed that the building height increase (C3) has a small effect on the existing scenario during this season as seen in the overlap on the graph. The mean MRT difference from the existing scenario (BC) also follows the same trend with T_{air} seen in Figure 4.12. In summer, C2 generally improves MRT as it has the lowest value between 5:00-19:00 while negating this effect during the night-time. Despite variations in BC, C1, and C3, all scenarios exhibit a consistent trend, which contrasts with C2. Across all receptors, C1 generally decreases MRT during winter, while increases it during summer. Meanwhile both C2 and C3 brings an inverse effect. However, the values at the receptors show that C2 brings more improvement in OTC than C3.

As seen in Table 4.3, in winter, C2 warms the streets by about 1.58 °C and the open spaces by 1.12 °C. Meanwhile, in summer, its effect is more pronounced as it cools the streets by 6.69 °C which is about 5 times cooler than C3's 1.42 °C. Moreover, the increase of vegetation (C2) cools the open spaces by about 11 times higher at 6.18 °C than the increase of building height (C3) at 0.57 °C. This effect may be attributed to the limited impact of building shadows on open spaces due to the location, highlighting the advantages of having flexibility in tree placement.

Table 4.3 MRT difference from existing scenario (BC) in streets and open spaces

where positive (+) values = increase, and negative (-) values = decrease

Receptors		MRT difference from BC in winter (°C)			MRT difference from BC in summer (°C)		
		C1	**C2**	**C3**	**C1**	**C2**	**C3**
STREETS	Point A	-0.16	0.50	0.32	1.13	-4.09	-1.07
	Point B	-0.12	2.92	0.33	0.92	-11.51	-2.59
	Point C	-0.10	1.32	0.33	1.90	-4.48	-0.59
	Average	**-0.13**	**1.58**	**0.32**	**1.31**	**-6.69**	**-1.42**
OPEN SPACES	Point D	-0.14	2.13	0.06	2.57	-9.03	-0.24
	Point E	-0.28	-1.90	0.13	0.75	-1.36	-1.14
	Point F	1.11	3.15	0.14	0.77	-8.15	-0.32
	Average	**0.23**	**1.12**	**0.11**	**1.36**	**-6.18**	**-0.57**

Compared to T_{air}, MRT demonstrates a substantial temperature difference in all the scenarios as seen in the spatial analysis (Fig. 4.13) as MRT is primarily influenced by building and tree shading (Duarte *et al.*, 2015). At 14:00 in winter (Fig. 4.13a), the long shadows casted by buildings and trees resulted to more areas with lower MRT, with the shading brought by trees giving a slightly warmer effect as seen in C2. In the graph (Fig. 4.11) and in the spatial average values (Fig. 4.13), this further decrease in MRT at this time in C2 could be attributed to the added cooler areas brought by tree shadows, which is evident in the main plaza. During the summer (Fig.4.13b), coolest areas are clearly observed where the vegetation and the shadows are present. Warm areas remain in open spaces, courtyards, and parts of the streets where there are limited shade sources.

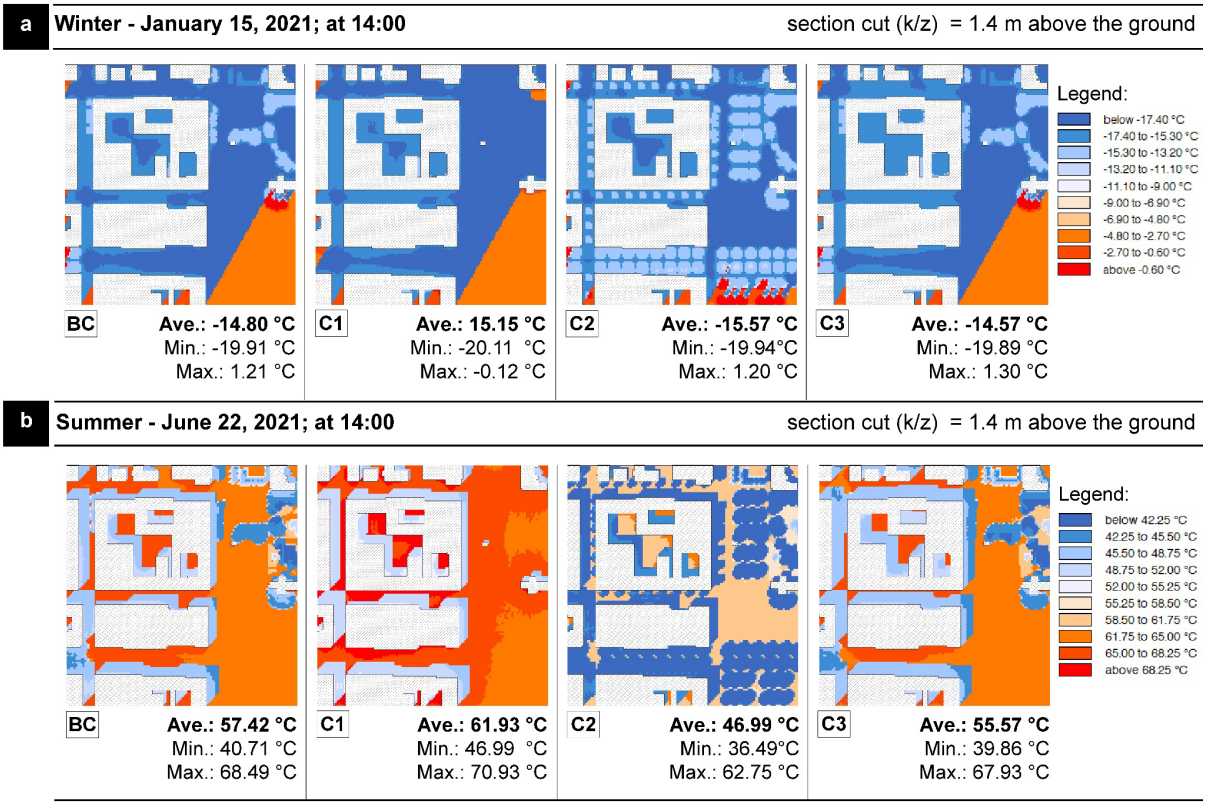

Figure 4.13 MRT simulation result on a (a) critical cold winter day, and (b) critical hot summer day

4.3.3 Physiological Equivalent Temperature (PET)

The scenarios are further evaluated using the PET thermal comfort index, which corresponds to thermal perception and stress levels. Overall, the 24-hr PET values of each receptor for both days which is noted in Appendix E, as well as the average

values in Figures 4.13 and 4.14, resulted to C2 being the best scenario for OTC improvement, while the absence of vegetation in C1 as the worst. In winter (Fig. 4.14), the average PET values follow the same trend, and all are in the *'very cold'* range where users experience *'extreme cold stress'*. The existing scenario experiences the coldest between 7:00-8:00, and the warmest between 12:00-14:00. However, it is evident that C2 brings OTC improvement during winter as seen in the PET increase all throughout the day, while C1 generally brings further PET decrease. It can be observed that C3 shows only a slight to no variation from BC.

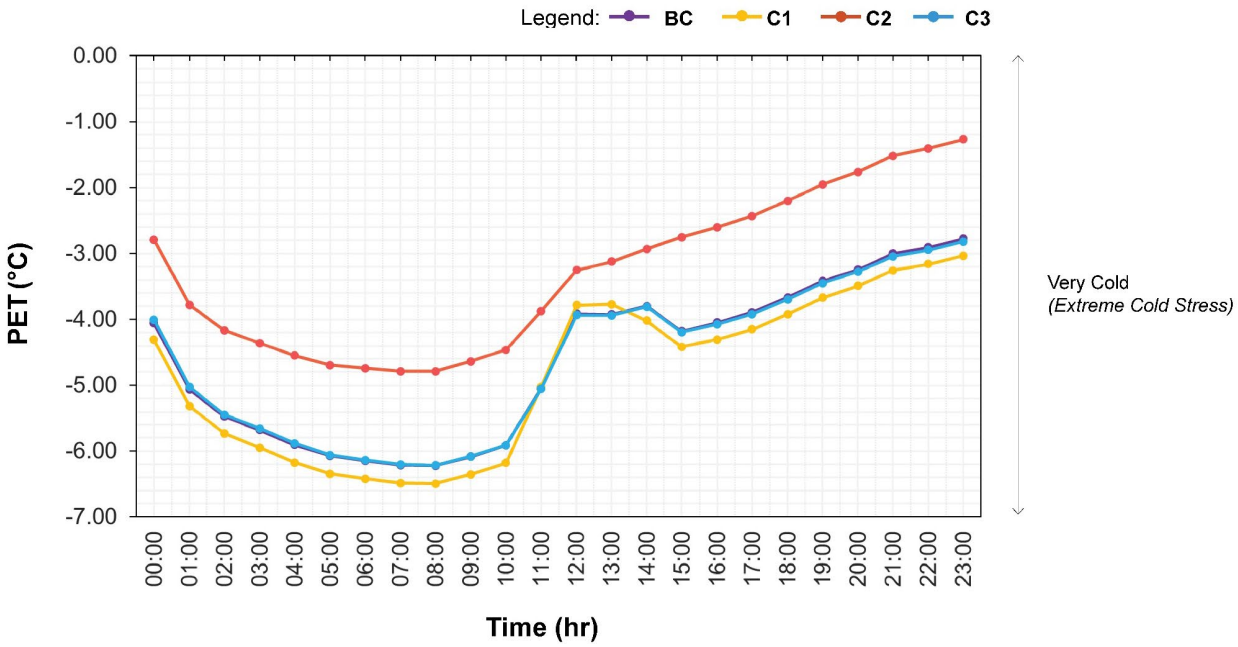

Figure 4.14 Mean PET of the four (4) scenarios on a critical cold winter day

In summer (Fig. 4.15), the results show more variation in thermal perception, ranging from *'slightly cool'* to *'very hot'*. On a hot summer day, the existing scenario (BC) experiences *'strong heat stress'* starting at 8:00, and then gradually increasing to *'extreme heat stress'* from 10:00 to 17:00. This pattern bears a close resemblance with C3 and C1, indicating that the present vegetation cover in the area situation brings the same physiological stress as when the vegetation is removed or when the building height is increased. In Table 4.4 and Appendices F-G, it can be observed that on average, C1 decreases the *'comfortable'* range where *'no thermal stress'* can be felt by 2 hours. Meanwhile, C3 remains to have a minimal effect from BC, only lessening the *'very hot'* range by 1 hour. Remarkably, it can be clearly observed that C2 improves OTC as it has the lowest PET values especially during the peak hours where

users generally experience *'strong heat stress'*. It also extends the *'comfortable'* range by 3 hours and lessens the *'extreme heat stress'* and *'slight cold stress'* by 7 hours and 3 hours respectively.

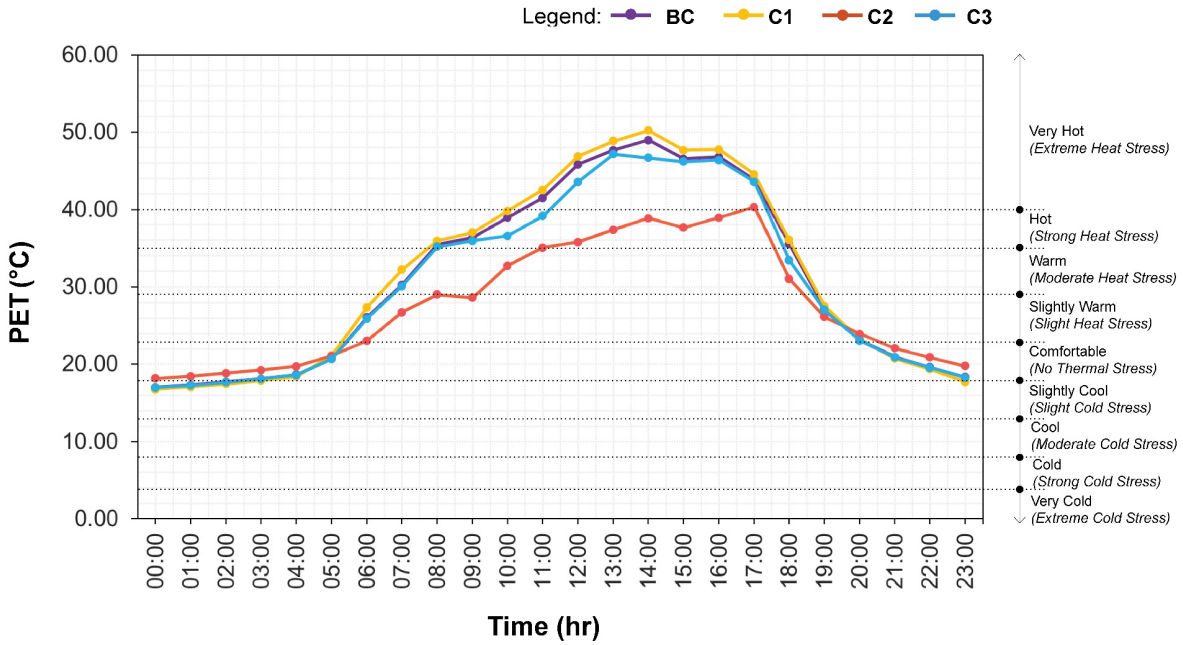

Figure 4.15 Mean PET of the four (4) scenarios on a critical hot summer day

Table 4.4 Distribution of hours in relation to PET Thermal Perception and Physiological Stress Grade

Thermal Perception	Stress Grade	No. of Hours (June 22, 2021)			
		BC	C1	C2	C3
Slightly Cool	Slight Cold Stress	3	5	0	3
Comfortable	**No Thermal Stress**	**6**	**4**	**9**	**6**
Slightly Warm	Slight Heat Stress	3	3	5	4
Warm	Moderate Heat Stress	1	1	3	1
Hot	Strong Heat Stress	4	4	7	4
Very Hot	Extreme Heat Stress	7	7	0	6

Spatially, at 14:00 (Fig. 4.16), PET shows more contrast in summer than in winter. During winter, warmer areas are mostly situated inside the courtyards and in areas near buildings and trees while cooler areas are shown in open spaces. It could also be observed that the open spaces and main plaza is within a slightly warmer range (-2.50°C to -1.00°C) compared to the other scenarios. In summer, clear

contrasts are shown between the hot and cool zones. Shading by buildings and trees represent the cool areas, while high PET values can be observed inside the courtyards and open spaces. It shows a huge improvement in streets and open spaces covered by tree canopy shadows.

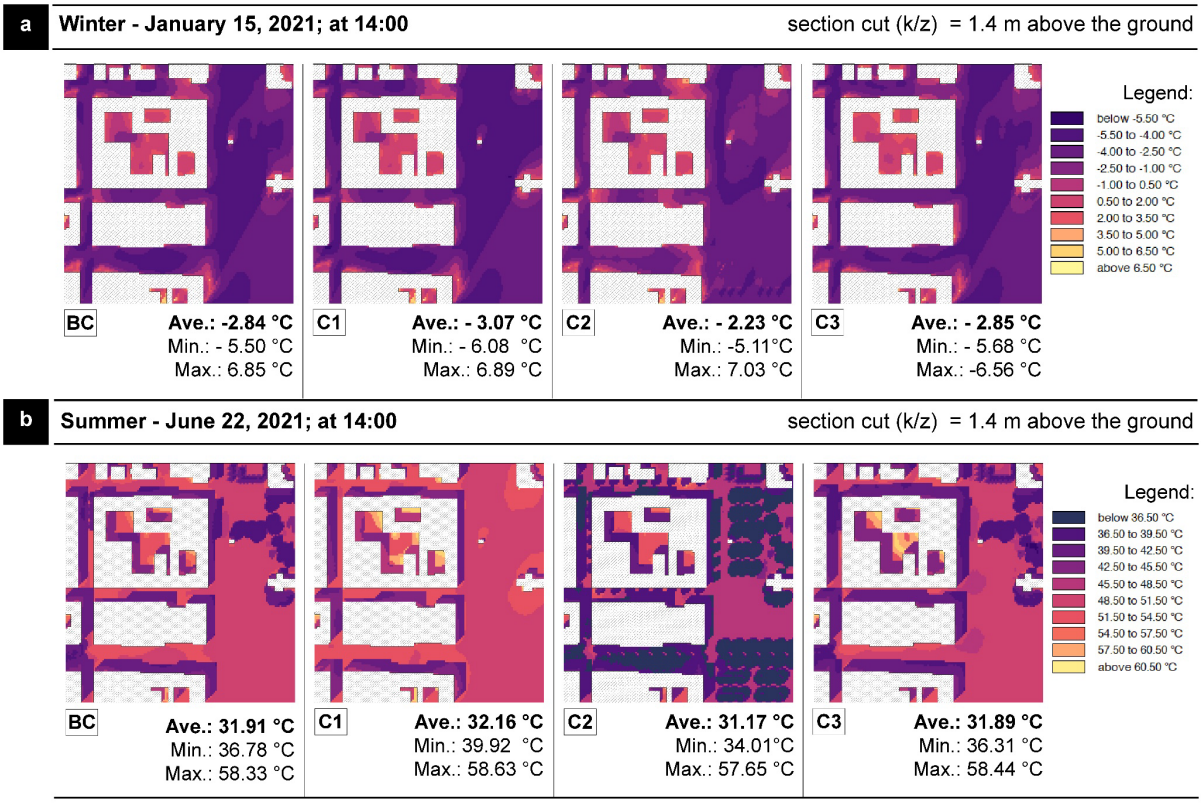

Figure 4.16 PET simulation result on a (a) critical cold winter day, and (b) critical hot summer day

CHAPTER 5: DISCUSSION

Structured into three sections, this chapter discusses the key findings of the research in relation to previous studies. The first section focuses on the existing UHI study of the city centre developed by Sitowise for the City of Tampere, followed by the city scale level analysis of LST, NDVI and LCZ, achieved through remote sensing and statistical methods. Lastly, the third section focuses on the microclimate analysis of outdoor thermal comfort using the ENVI-met software.

5.1 Tampere's UHI Study as a Baseline

The study is based on the inner-city centre's UHI report (2022), which provides a preliminary assessment of the city's current risks and vulnerabilities concerning UHI. In the study, the LST composite map (Fig 5.1) was obtained through using the Remote Sensing Lab's service which automatically calculates LST, to analyse the summer surface temperatures.

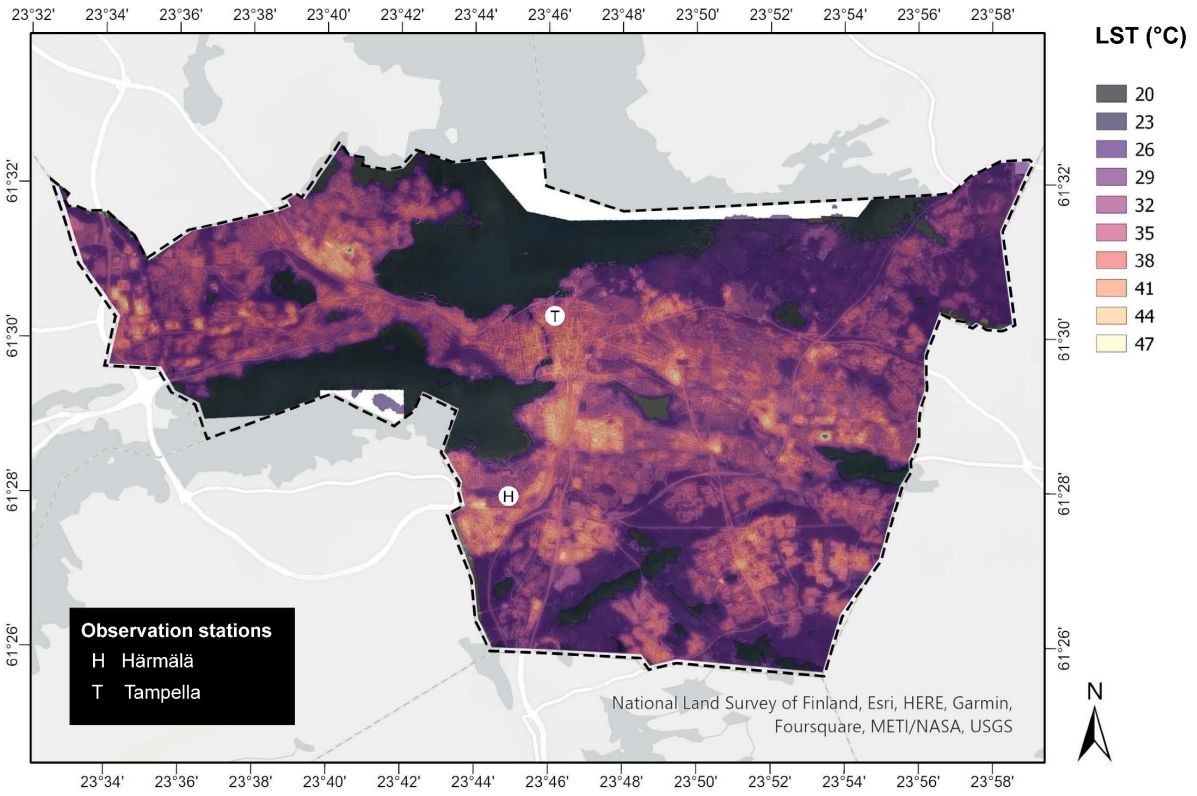

Figure 5.1 Tampere City Centre LST composite map from 2015-2018 (adapted from Sitowise, 2022b)

The study concluded that the coolest areas are the found in the forested areas near the banks of water bodies, while the hottest areas are within the industrial zones which are characterised by large surfaces, built up areas, and wide streets. In terms of factors affecting LST, the study uses the city's land cover material (trees, vegetation, roads and impervious surfaces and buildings) and found out that impervious surface has a high explanatory power on summer LST variation.

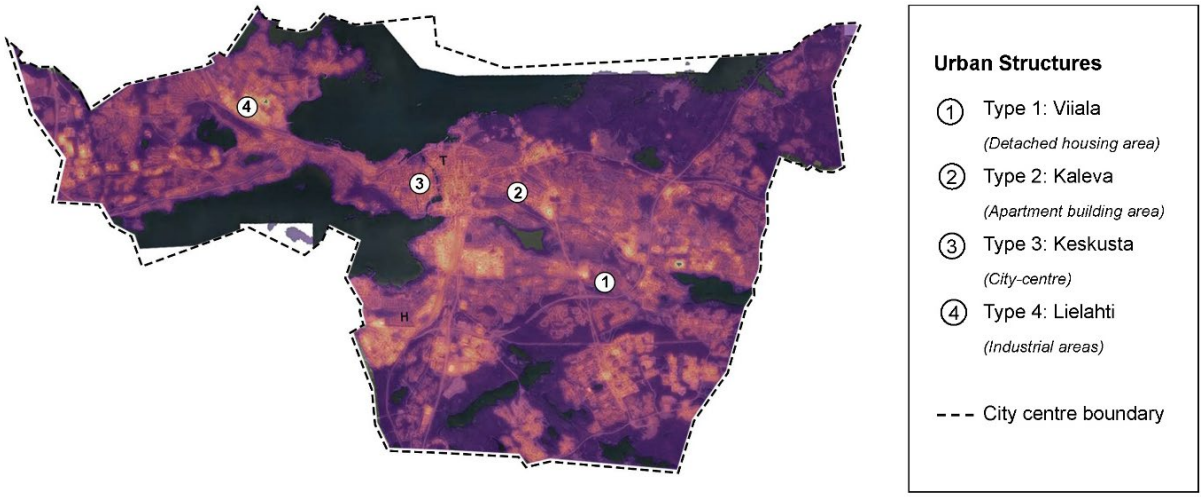

Figure 5.2 LST composite map showing the four urban structures used for microclimate modelling (adapted from Sitowise, 2022b)

In the second phase of the city's UHI study, microclimate modelling was done in four different urban structures (Fig 5.2): (1) Viiala (single-family house areas), (2) Kaleva (apartment blocks), (3) Keskusta (city centre), and (4) Lielahti (industrial area). The simulation was done with the Rhino-Grasshopper program with Ladybug plug-in, using the Universal Thermal Comfort Index (UTCI) as a thermal comfort indicator together with wind and MRT as additional parameters. Appendix H presents the detailed summary of the microclimate modelling of the four urban areas. Focusing on the simulation in Keskusta (city centre) (Fig 5.3), the report displays that in summer, the hottest parts are situated in the plaza, while the cooler parts are within the courtyards as well as in buildings and tree shadows. Green infrastructure was primarily recommended by the study, together with surface material consideration as ways to curb heatwave phenomena (Sitowise, 2022b).

a **Land Cover**

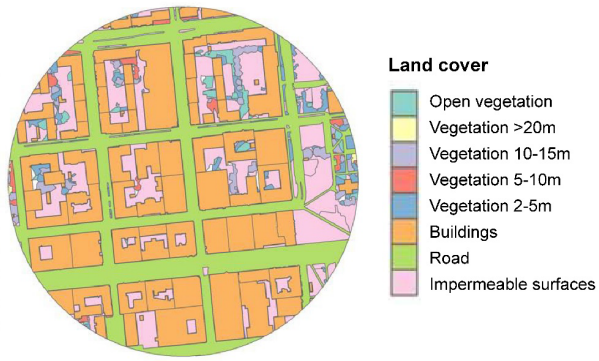

b **Windiness**

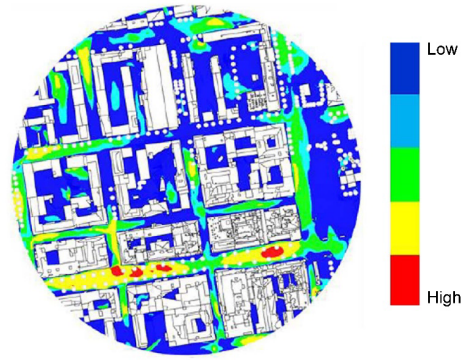

c **MRT**

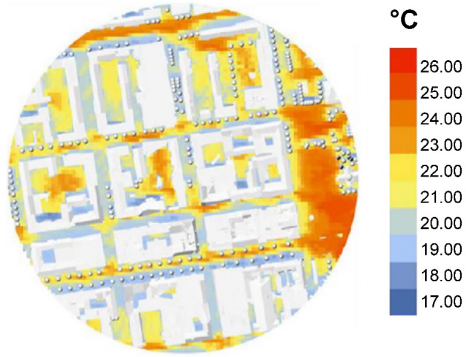

d **UTCI**

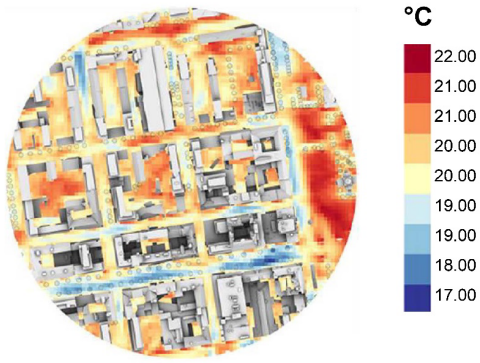

Type 3: Keskusta Area

Simulation Result

"The block structure in the city center was modeled between the central square and Hämeenpuisto.

The vegetation cover accounts for 5% of the ground, while buildings and impermeable surfaces make up 90%.

The land surface temperature combination map (lowest quartile - highest quartile) ranges from +37.4 to 38.8 °C.

The temperatures are evenly distributed across the area, with open spaces being warmer and shaded areas of tall buildings being cooler.

In the thermal comfort modeling of the city center, ***the streets stand out as relatively cooler areas compared to squares and inner courtyards****. This is due to the shading effect of buildings and trees, as well as the cooling effect of winds passing through the area.*

This is particularly evident on Hämeenkatu, which is quite windy, especially on its southern edge, where it is also shaded. However, the inner courtyards of closed blocks can be quite hot at times.

This is partly because the buildings do not offer significant protection from the summer sun, and partly because they are very sheltered from the wind. ***The central square is the hottest area, as it has the least amount of shade and is not significantly affected by wind."***

(Sitowise, 2022b)

Figure 5.3 Keskusta area description and simulation results by Sitowise, 2022b

5.2 City Scale Level: LST, NDVI, and LCZ Analysis

According to Oke *et al.* (2017), scale plays a crucial role in the climate impact assessment and policy intervention measures. In this study, the city scale analysis, including seasonal LST-NDVI correlation and LST-LCZ distribution, provides a broader understanding of thermal patterns and urban characteristics across the entire city, identifying hotspots, cool areas, variations in vegetation cover, and providing as a reference data for microclimate modelling.

5.2.1 Seasonal Correlation of LST and NDVI

The LST- NDVI analysis results revealed key insights on the temporal patterns between LST and vegetation dynamic, which supplements the existing UHI study considering that the report proposed the use of vegetation to mitigate UHI effects. In this study, the findings show that there is a clear variation on the LST and NDVI values across seasons. It also displays that there is stronger correlation in summer than in winter, suggesting that surface covers have greater influences in LST during this season which agrees to the previous studies (Sun and Kafatos, 2007; Yuan and Bauer, 2007; Naserikia *et al.*, 2022; Ullah *et al.*, 2023).

During winters, LST has a weak yet direct correlation with NDVI, which could be attributed to Tampere's climate as it gains lesser solar radiation due to decreased sunlight duration and is mostly covered by snow during this season. Another factor is the vegetation distribution, especially the presence of the season-dependent deciduous trees (Naserikia *et al.*, 2022). In the tree register of Tampere (Fig. 5.4), deciduous trees make up about 80% of the urban trees in the city centre (City of Tampere, 2022b). The leaf-shedding characteristics of these trees during winter leads to a decreased evapotranspiration rate, thus resulting to lesser effect on LST (Naserikia *et al.*, 2022). In cold climate cities, some studies revealed that NDVI, together with Normalised Difference Built-up Index (NDBI) has lesser influence in LST variation, which supports the weak correlation between LST and NDVI found in this study. Meanwhile previous studies mentioned that other indices such as albedo, elevation, coast distance (Naserikia *et al.*, 2022), and percent impervious surface area

(ISA) (Yuan and Bauer, 2007; Zhang, Odeh and Han, 2009; Naserikia *et al.*, 2022; Sitowise, 2022b) has more significance during this period.

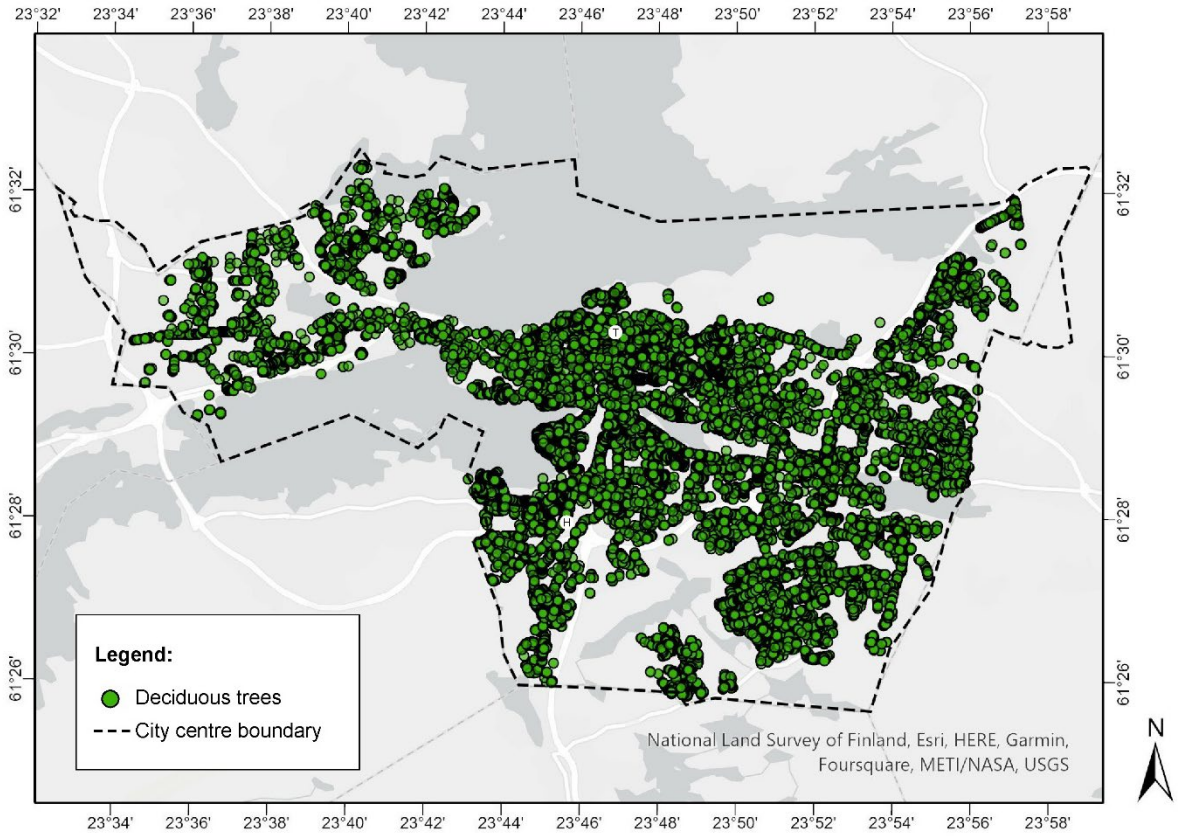

Figure 5.4 Tree register of Tampere showing deciduous trees (adapted from City of Tampere, 2022b)

During the summer season, the inverse relationship with moderate correlation between LST and NDVI implies the cooling effect of vegetation during summer months. Similar to the previous studies, the results show that high LSTs are concentrated on built up areas (Brozovsky, Gaitani and Gustavsen, 2021; Welegedara, Agrawal and Lotfi, 2023), while cooler areas are observed in the densely vegetated areas. The moderate correlation between LST and NDVI during this season implies that other factors, such as NDBI, and ISA mentioned in previous studies (Yuan and Bauer, 2007; Zhang, Odeh and Han, 2009; Naserikia *et al.*, 2022; Sitowise, 2022b), are to be accounted for the variation of LST. While adopting a different method from the existing UHI study by Sitowise in terms of LST retrieval, this research yielded consistent results during the summer season. The identified hot and cool areas agree to previous UHI findings (Sitowise, 2022b), while results gathered in the winter analysis provides valuable additional insights. However, due to limitations in accessing

Landsat 8 images with less than 10% cloud cover, the assessment was limited to the years 2018 and 2022.

5.2.2 LCZ Classification and LST Distribution

Classifying the city into LCZ provides a more comprehensive and uniformed approach on addressing urban climate challenges through climate-sensitive planning. As LCZ is categorised into different urban types, analysing how LST is distributed among different urban densities provides additional understanding especially in the preparation and execution of urban interventions (Stewart and Oke, 2012; Das and Das, 2020; Choudhury, Das and Das, 2021) . In built types, the LST distribution exhibits similar results to the previous studies (Bechtel *et al.*, 2019; Del Pozo *et al.*, 2021; Wang *et al.*, 2021; Zhou *et al.*, 2022), as compact types like LCZ 2 consistently exhibits the highest LST among all classes in both seasons, followed by large low-rise buildings with less vegetation (LCZ 8), while open types such as LCZ 9 generally have the lowest.

In land cover types, several studies (Bechtel *et al.*, 2019; Del Pozo *et al.*, 2021; Wang *et al.*, 2021; Zhou *et al.*, 2022) proved that extensive impervious surface in LCZ E generates higher LST and the abundance of pervious cover seen in LCZ A and LCZ G generally exhibits the lowest LST, which has both been consistent in this study especially during the summer (Choudhury, Das and Das, 2021; Del Pozo *et al.*, 2021; Aslam and Rana, 2022). The LST-LCZ distribution trend in summer proves to be more stable than in winter. Similar to a previous study (Del Pozo *et al.*, 2021), this variation could be due to the change in surface cover in cold climate cities like Finland, where snow covers the city during winters. According to Stewart and Oke (2012), including variable land cover properties such as *'bare trees'* (b) and *'snow cover'* (s) are important in short term seasonal analysis. However, due to data limitations (e.g., actual extent and placement of bare trees and depth of snow cover), this is not executed in the study. Stewart and Oke (2012) also claimed that as subclasses may add flexibility in the system, however there wouldn't be a significant change on the thermal climate as there is only a minimal difference on the maximum thermal contrasts between zones (1-2 K) (Appendix A2).

Nevertheless, the analysis in winter could still be proven useful, especially on built types as the result show that LCZs 2, 5, and 8, all have relatively high LSTs for both seasons. The inverse relationship of pervious surface cover and LST agrees with previous studies done that have recognised the significance of surface cover in UHI distribution, and that higher LSTs are generally found in built land types compared to the land cover types with extensive pervious land cover (Das and Das, 2020; Choudhury, Das and Das, 2021; Aslam and Rana, 2022; Sitowise, 2022b; Welegedara, Agrawal and Lotfi, 2023). Remarkably, this result also supports the findings in LST-NDVI maps as the result shows that the hottest areas are in LCZ 2 and LCZ 8, where vegetation is scarce.

However, there are some inconsistencies with the city LCZ map obtained from the WUDAPT database. In Nekala area, the LCZ map shows that it is within LCZ 5 (open midrise) whereas the actual site could be categorised in LCZ 6 (open low-rise). This is not surprising as the original European LCZ map from which the Tampere city LCZ map was extracted, covers a wider range and it showed minor inaccuracies in some areas as there is a confusion between mid-rise and low-rise classes (Demuzere *et al.*, 2019). In this regard, a city-specific calibration could be explored for the city using methods other than WUDAPT for a more precise analysis. In this study, using the extracted city LCZ map was more practical than generating it in the WUDAPT database due to the limitation of knowledge about the city. Nonetheless, this study still suggests that LCZ classification could be proven useful especially in urban climate analysis and in targeted greening interventions across the city. The initial LCZ map provides valuable information about the urban fabric and the local environmental characteristics of different areas within the city map and helps identify different types of urban areas with varying characteristics (building density, pervious cover, etc.) which is crucial for understanding UHI.

5.3 Block Scale Level: OTC analysis in the Inner-City Centre

In an urban planning perspective, the high LST in the inner city-centre which is comprised of several commercial and cultural sites could have potential risks and vulnerabilities not only in the environment but also in cultural, economic, and social aspects (Sitowise, 2022b). Higher LSTs contribute to UHI effect, which could have several implications including heat-related health issues, reduced outdoor activity due to discomfort, and increased energy consumption (Battista, De Lieto Vollaro and Zinzi, 2019; Acosta *et al.*, 2021). This could also have implications for local business, tourism, and the vitality of the urban centre. One of the main purposes of this research is to analyse the role of the presence of vegetation in OTC in cold climate cities like Tampere especially in the city centre where achieving pedestrian comfort is crucial.

5.3.1 Influence of the City's Plan in Site Selection and Scenario Development

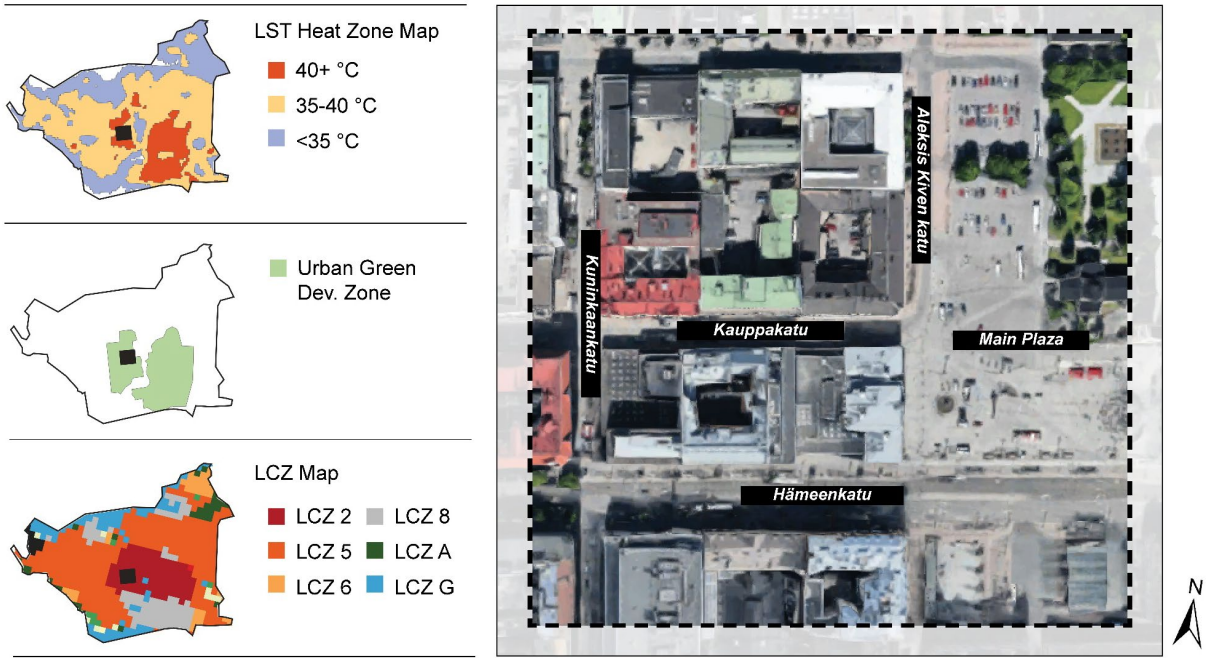

Figure 5.5 Focus area in relation to LST Heat Zones (adapted from Sitowise, 2022b) and Urban Green Development Zones (adapted from City of Tampere, 2023), and from this study's LCZ map

To further align with the city's urban development, the scenarios and site selection of this study relies on the Inner City's Phase Master (2021-2025). As seen in (Fig. 5.5) the selected site which is in Keskusta area is within the urban green development zone (City of Tampere, 2023), 40+ °C heat zone (Sitowise, 2022b), as well as in the LCZ 2 as identified in city-scale analysis. This exhibits the rationale of the site selection which relates to the aim of analysing the role of vegetation's presence in warmer areas. Moreover, the area includes outdoor spaces where users are mostly frequent including the culturally significant main plaza (Keskustori) and the Hämeenkatu street. In the future master plan, (Fig. 5.6a), the site is in the centre functions area reserved for future commercial spaces and activities. Additionally, a market area is also to be developed in the main plaza, thus adding more value to this site. In terms of mobility, (Fig. 5.6b) the whole area is to be developed as a pedestrian centre which indicates that conditions for pedestrians in the area must be improved, and urban greenery to be added. Based on the transport plan, certain streets are to be developed as pedestrian axes and main cycling routes. Moreover, spaces are to be designed for the underground parking provision (City of Tampere, 2023).

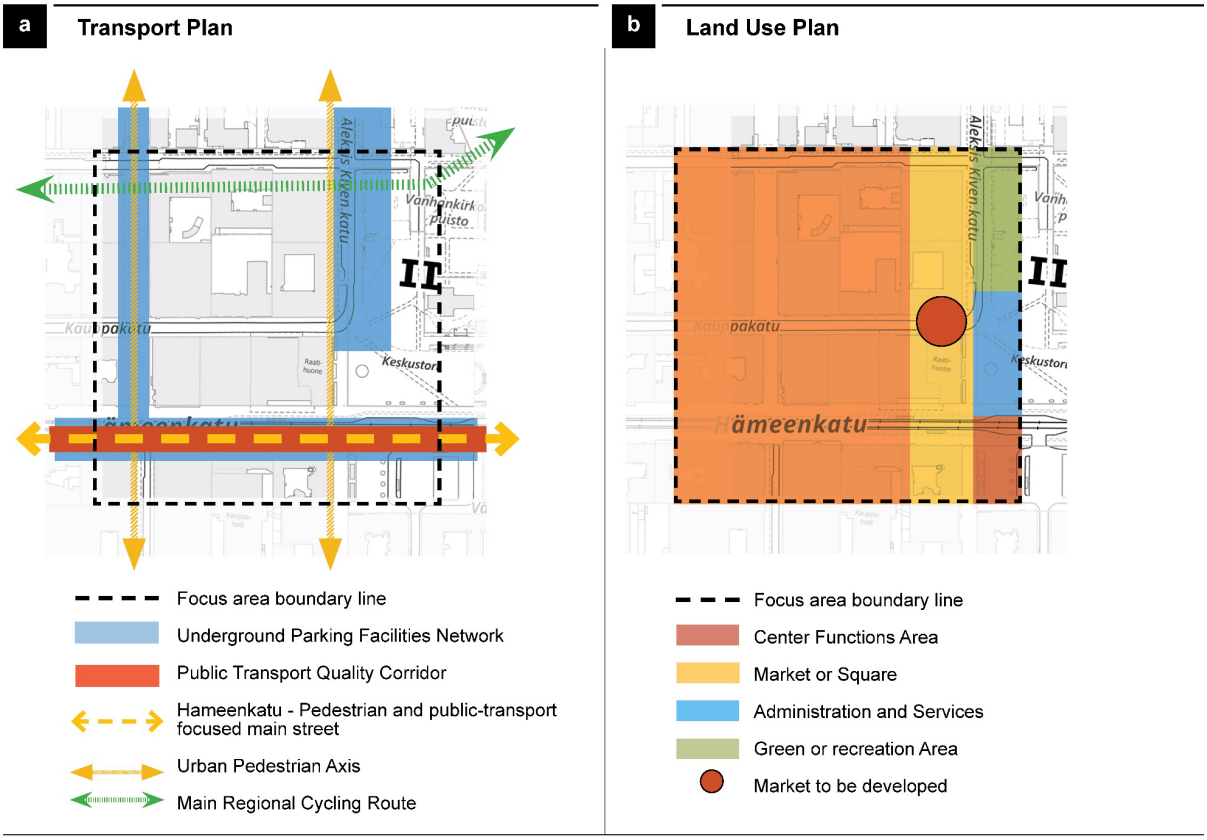

Figure 5.6 (a)Transport and (b) Land Use strategic master plan of the inner-city centre (adapted from City of Tampere, 2023)

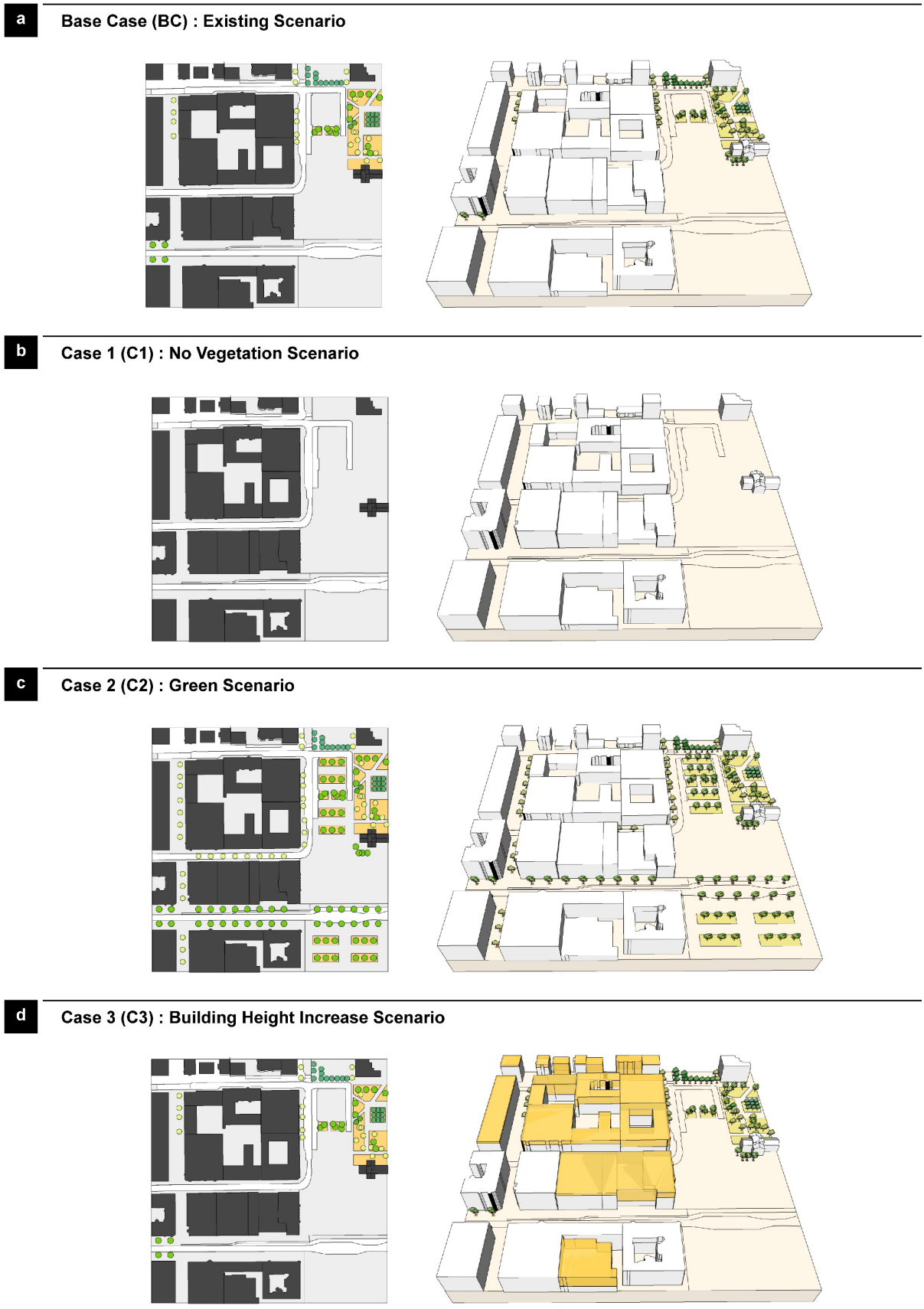

Figure 5.7 Conceptual 3D Models of the four (4) scenarios

Figure 5.7 shows the scenarios used in the study. In C2, greening scenario, deciduous trees are used in streets to support the master plan's vision in making comfortable pedestrian-focused streets. Additional trees and green cover were placed in open spaces, excluding the main plaza, to analyse the change in microclimate with the replacement of pervious cover. Aside from the master plan, this greening scenario (C2) was then utilised to align with several programs and reports as mentioned in the previous chapters. Several studies have indicated the benefit of combining different kinds of vegetation in microclimate regulation (Balany *et al.*, 2020; Sitowise, 2022b), while in this study, urban trees, specifically deciduous trees were given more focus in alignment with the city's Urban Tree Policy, as well as the available tree datasets. While C1 or the no vegetation scenario was included to give insight on the impacts of the absence of vegetation in the area, it also gives a glimpse of the extreme future scenario that could happen should pervious cover are diminished or completely replaced by impervious surfaces. Finally, the C3 or building height scenario was implemented to analyse whether the greening scenario would still be the best option for OTC in both seasons.

5.3.2 The Role of Urban Trees in the Inner-City Centre's OTC

Similar to previous studies, T_{air}, MRT, and PET index were used to analyse the effect of trees in microclimate and thermal comfort. It is also worth noting that while difference T_{air} is minimal, there has a there is a huge variation seen in MRT and PET, both of which are more appropriate in the thermal comfort assessment. Several studies claimed that in cold climate cities, lower temperatures in summer and increased temperatures in winter generally leads to OTC improvement (Afshar *et al.*, 2018; Potchter *et al.*, 2018; Gatto *et al.*, 2020; Yilmaz *et al.*, 2021).

In this regard, the simulated scenarios brought various impacts on the microclimate and OTC. Specifically:

- ***Case 1 (C1): No Vegetation Scenario***

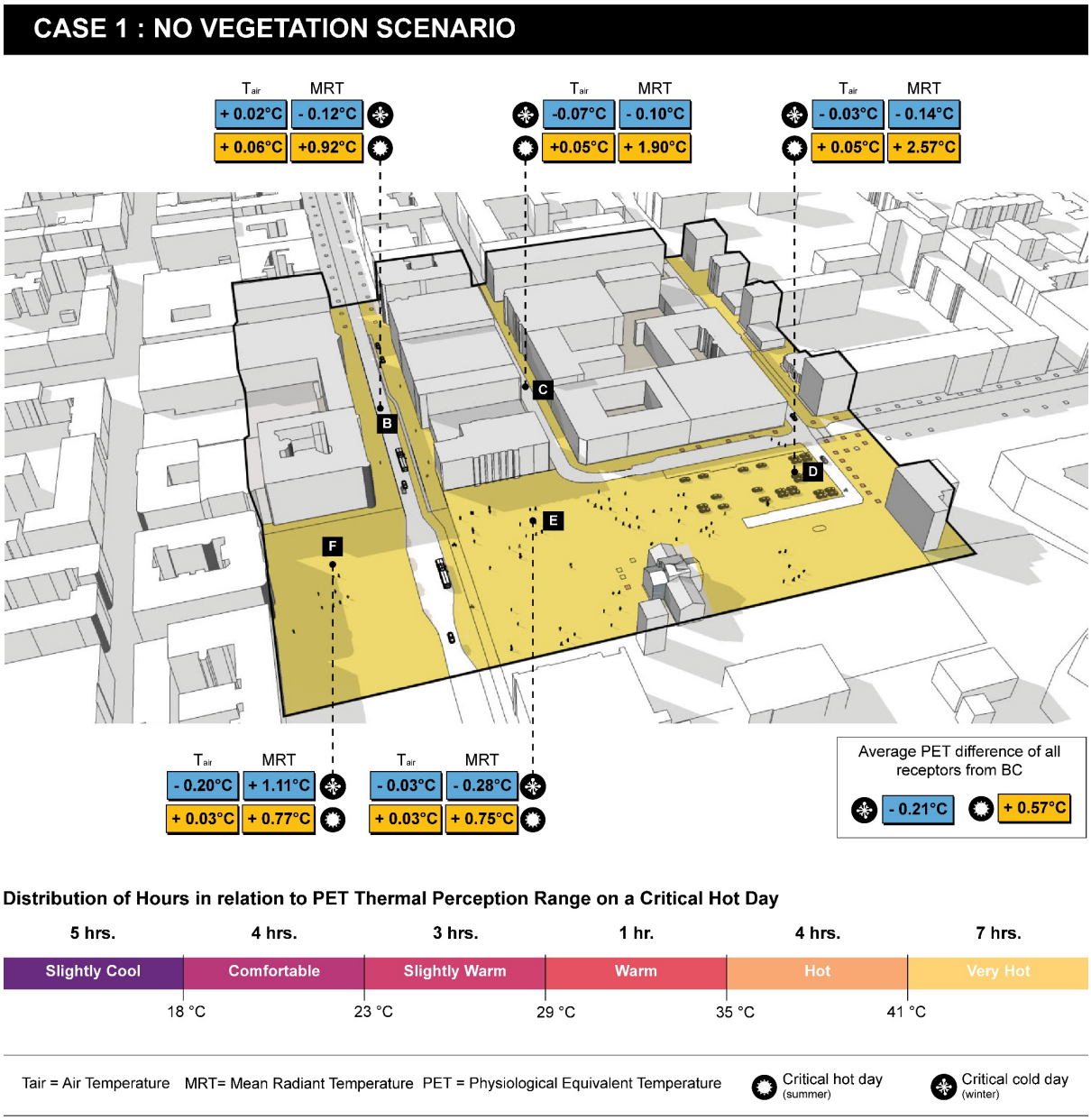

Figure 5.8 Conceptual 3D model of C1 with the summary of results

Case 1 (C1) or the no vegetation scenario (Fig. 5.8) consistently brings discomfort as T_{air}, MRT, and PET are consistently the lowest during winters and highest during summers. This result agrees to the previous study (Gatto *et al.*, 2020), where lessened or removal of vegetation in the area resulted to colder and warmer temperatures in winter and summers respectively. Moreover, the PET results show that in this scenario users may experience heightened and extended periods of discomfort. The small disparity between C1 and BC (existing scenario) indicates that the present situation might need to implement strategies to improve thermal comfort

within the area. In the city's urban planning, this change in C1 bears same result with the previous studies where it was found that extensive impervious streets and parking areas led to higher temperatures (Gatto *et al.*, 2020; Sitowise, 2022b). This is also relevant with the underground parking network provision (Fig. 5.6a) which could affect this area, as in extreme cases, trees and vegetation cover could be removed to give way to the construction. This scenario could also negate the city's vision to improve pedestrian comfort as the analysis show that shadows from the buildings will not be enough to compensate the loss of vegetation cover. It indicates that the absence of vegetation comes with possible risks and user thermal comfort especially in an area where social, cultural, and commercial activities are present.

- ***Case 2 (C2): Greening Scenario***

In this study, Case 2 (C2) or the greening scenario (Fig. 5.9) proves to be the best scenario overall in terms of OTC improvement as the addition of deciduous trees on streets and open spaces brings higher T_{air}, MRT, and PET on winter days and lower during summer days across all receptors. The use of deciduous trees brought improvement for both seasons which agrees to the previous studies stating that deciduous trees are more favourable in cold climate cities because of their seasonal characteristics (Potchter *et al.*, 2018; Balany *et al.*, 2020; Wang *et al.*, 2021; Li, Sun and Chen, 2023). While this scenario brings overall improvement across all the receptors during winter, it could bring a further decrease in temperature during specific hours. This result agrees with the previous study (Lindberg *et al.*, 2014), where it was recommended to create a more diverse outdoor space. This also indicates that proper distribution of trees should be taken into consideration in urban greening interventions. During the summer, MRT results emphasize the benefits of flexible tree placement in comparison to relying solely on fixed sources of shade, such as increasing building height, to enhance OTC. This scenario demonstrates that the strategic placement of trees offers more advantageous outcomes for mitigating heat and improving overall comfort levels. Moreover, this scenario provides longer hours that the PET values are in the *'comfortable'* range. It also resulted to a lower range during the peak hot hours among all the scenarios. This indicates that in the urban centre, users could experience extended comfort outdoors thus providing more vitality in the urban centre's public spaces. C2 supports the city's objective in increasing the vegetation in

the area, protecting, and enhancing urban trees, as well as providing comfortable conditions to pedestrians.

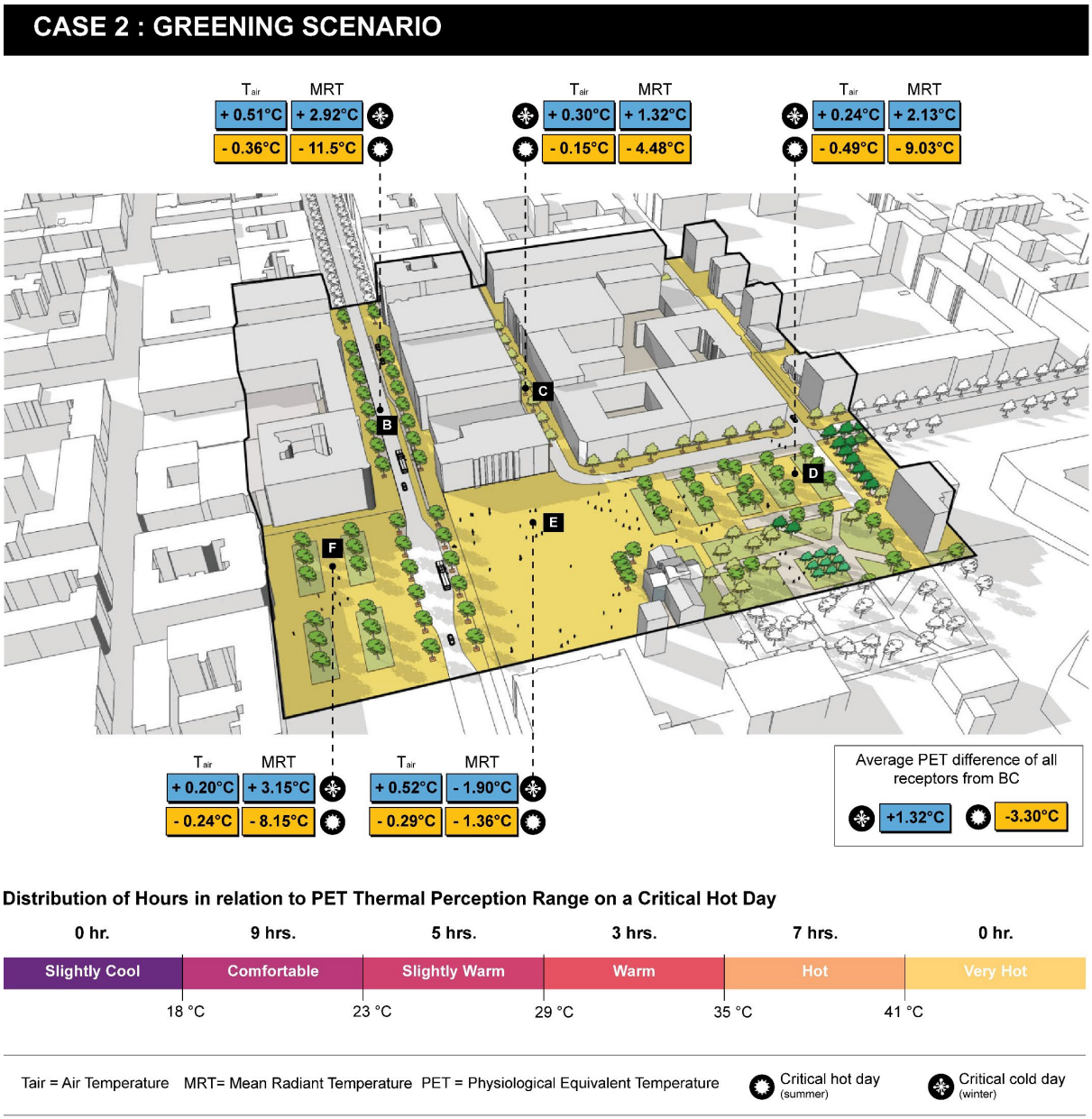

Figure 5.9 Conceptual 3D model of C2 with the summary of results

- ***Case 3 (C3): Building Height Increase Scenario***

Lastly, Case 3 (C3), or the building height increase scenario (Fig 5.10) resulted to similar trend in results as C2, however only to a minimum. This finding implies that the combination of increasing building height and tree cover could provide better

solutions for thermal comfort improvement, however, additional investigation should be considered as extensive shadows could bring more discomfort during winters.

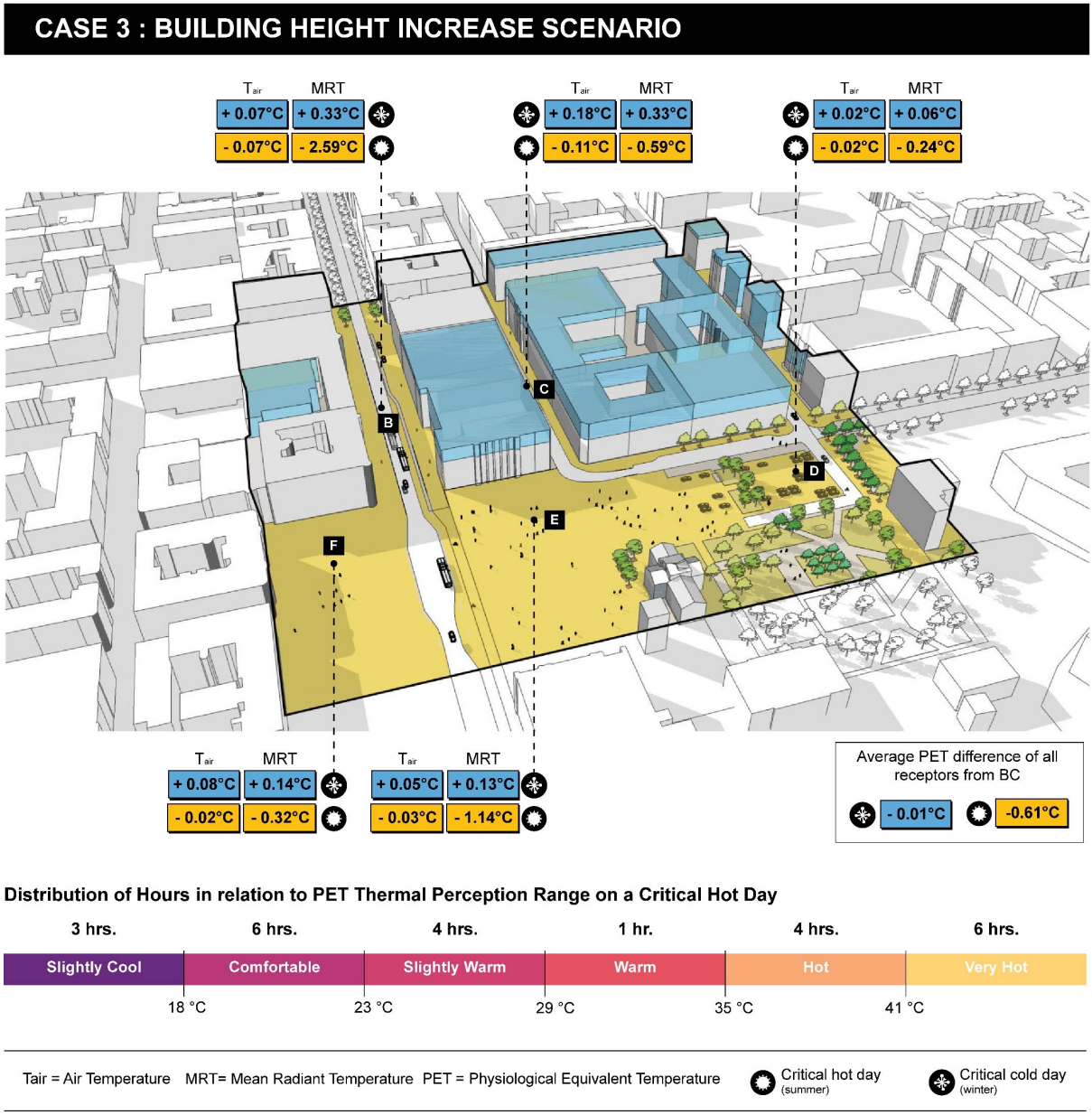

Figure 5.10 Conceptual 3D model of C3 with the summary of results

5.3.3 Implications of Block Scale Greening to the City's Adaptation Plan

In urban planning, the results of the block scale greening interventions strongly align with the city's key adaptation themes. The city's Climate Change Adaptation and Preparation Plan (2022), emphasizes the importance of green infrastructure as an

adaptation measure, and the addition of trees as highlighted in this study, directly supports this objective.

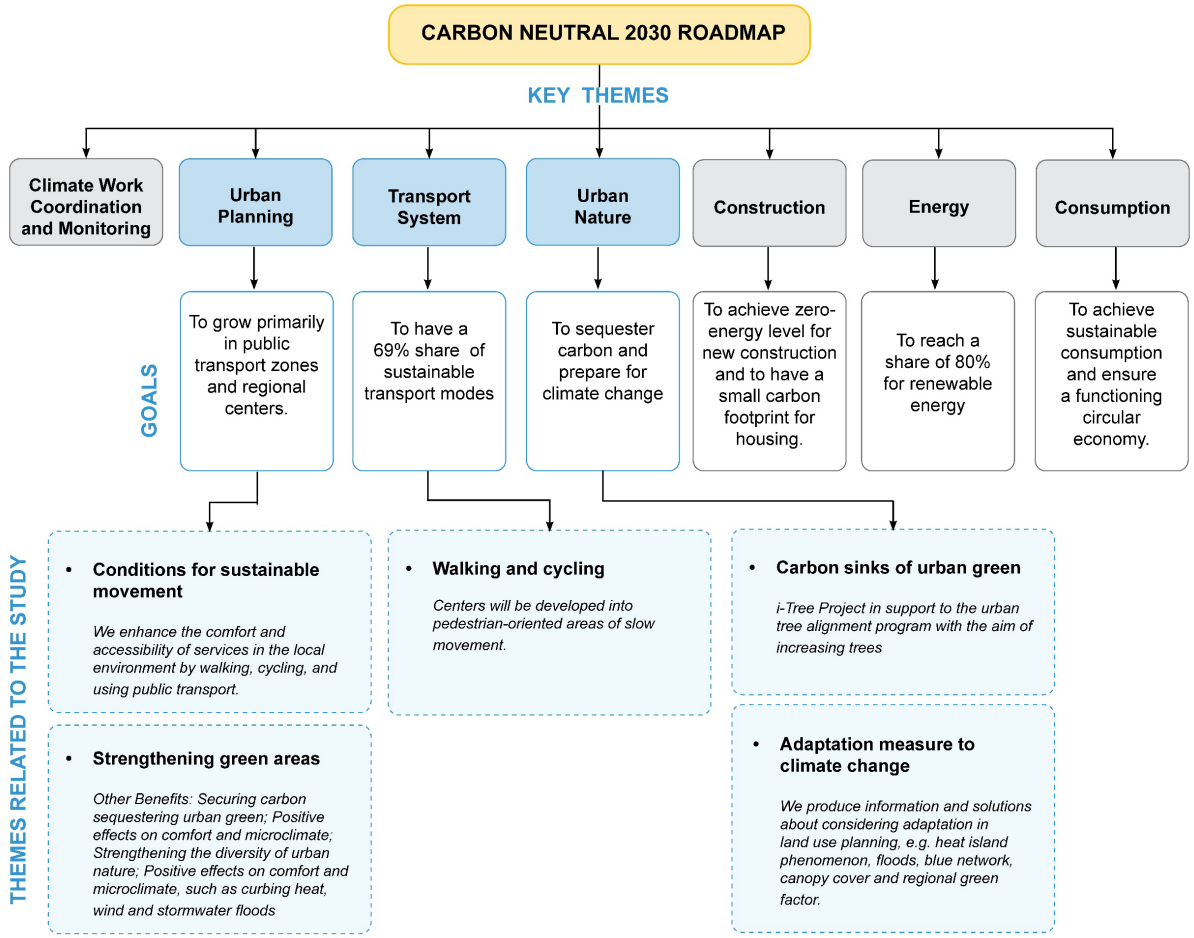

Figure 5.11 Carbon Neutral 2030 Roadmap with goals and themes related to the results of the block-scale intervention (adapted from the City of Tampere, 2021)

Moreover, the results compliment multiple themes outlined in the Carbon Neutral 2030 Roadmap (Fig. 5.11), which is directly related to the adaptation plan. The intervention aligns with the *'urban nature'* theme, where the city aims to increase the number and value of urban trees. The findings of the block-scale intervention also support the *'urban planning'* and '*transport system'* sections, where the city aims to provide comfortable conditions for sustainable movement (walking, biking, public transport), and to strengthen green areas to improve comfort and regulate the microclimate (City of Tampere, 2021). In this study, the extended comfortable outdoor conditions for pedestrians brought by additional greening proves to be a key factor in the enhancement of the city's resilience to the impacts of climate change and improvement of the well-being of its residents.

CHAPTER 6: CONCLUSION AND RECOMMENDATIONS

The chapter presents the conclusions drawn from the research. It encompasses the answers to the main research problem, considering the limitations encountered during the study, and provides recommendations for future studies to further enhance the understanding of the topic.

6.1 Summary of Findings

With the increasing occurrence of urban overheating, even in cold climate cities, it has become imperative to implement measures that address and adapt to this phenomenon. Tampere, guided by plans, policies and climate reports, recognizes the significance of vegetation as a priority measure for mitigating the adverse effects of UHI brought by climate change.

Through the city scale and block scale analysis, this study supplements the city's vision and further supports its urban planning decisions by (a) analysing the seasonal relationship of LST and NDVI, (b) assessing the spatial distribution of LSTs across different urban densities guided by LCZ classes, and (c) assessing the role of urban deciduous trees in UHI mitigation and outdoor thermal comfort (OTC) improvement. This study draws the following conclusions:

1. The analysis of LST and NDVI reveals a significant variation in their relationship within cold climate cities. The correlation is observed to be stronger during summer compared to winter, as NDVI is influenced by seasonal changes. However, the correlation during winter (Feb 2018: r = 0.18; Feb 2022: r = 0.25) and summer (July 2018: r = -0.55; July 2022: r = -0.59) is weak and moderate respectively, suggesting that other factors exert a more pronounced influence on LST variation. The weak positive correlation observed during winter indicates the need to consider vegetation density to maximize heat retention and facilitate OTC improvement during the colder months. On the other hand, the inverse relationship between LST and NDVI during summer highlights the cooling potential and heat stress reduction benefits offered by urban vegetation

in hot summer months. These findings underscore the importance of recognizing and leveraging the seasonal dynamics of LST and NDVI in urban environments, as it can guide decisions related to climate adaptation and mitigation strategies. By optimizing vegetation density and distribution, cities can enhance heat retention during winter and capitalize on the cooling effects of urban vegetation during the summer, contributing to overall thermal comfort and urban liveability.

2. The LST-LCZ distribution the significance of surface cover in UHI_{surf} distribution. Built type LCZs characterised by lesser pervious surface generates higher LSTs than land-cover types LCZs. This inverse relationship between LST and pervious surface cover ratio suggests that addition of more pervious surface such as vegetation, can help in LST reduction and generate a more comfortable urban environment. In this study, LCZs belonging to built types specifically LCZ 2 and 8 consistently has the highest LST values, while LCZs in the land cover types (LCZ A and G) generally has the lowest value in both winter and summer months. This distribution is more consistent in summers than in winters. Moreover, this concluded the advantages of mapping the city into LCZs especially in urban climate analysis as it provides a spatial framework for urban planners, policymakers, and researchers to understand the urban structure and identify areas that are more vulnerable to heat stress. These insights contribute to a more informed decision-making process for urban planners and policymakers, allowing them to prioritize and implement appropriate greening interventions in areas where they will have the greatest impact in mitigating the adverse effects of UHI.

3. The results of the microclimate simulation and OTC analysis revealed that in the inner-city centre, the presence and addition of vegetation, specifically urban deciduous trees (C2), brings significant OTC improvement in both summer and winter season, in comparison with increasing the building height (C3) in the area. Meanwhile the absence of vegetation which leads to the increase in impervious surface cover resulted an inverse effect, bringing more discomfort to users. The microclimate simulations and scenarios based on the inner-city master plan provides crucial information for designing urban environments that

promote public health, well-being, and social interaction, as it provides information on the placement and benefits of certain types of vegetation, such as trees, to enhance outdoor thermal comfort for pedestrians and residents.

4. Additionally, the city level and block level analysis highlight the importance of tree species, specifically the deciduous trees and their role in UHI mitigation in cold climate cities.

Overall, the city can leverage these findings to inform its urban planning decisions, prioritize greening interventions, and create urban environments that enhance the well-being and comfort of its residents while mitigating the effects of UHI brought about by climate change.

6.2 Limitations of the Study

Although this research has provided key insights for the city, there are certain limitations that needs further improvement or investigation. The following points highlight the specific limitations of the study:

1. The availability of Landsat 8 images with minimal cloud cover, particularly during winters in Finland, restricted the study's LST (Land Surface Temperature) and NDVI (Normalized Difference Vegetation Index) mapping to the years 2018 and 2022.

2. Due to limited expertise in the area, the study relied on a readily available LCZ (Local Climate Zone) map, which contains inaccuracies in certain areas, particularly in distinguishing between mid-rise and low-rise classes. The LCZ-LST analysis in winter did not consider the land cover subclasses *'bare trees'* and *'snow cover'* due to lack of data.

3. In the ENVI-met microclimate modelling, the calibration of air temperature was not conducted using field measurements, which could have improved the accuracy of the data. Additionally, the model for the study did not consider

surface elevation and in terms of trees, had to rely on default settings for certain species due to limited information in the tree dataset. Moreover, in the simulation process, the study utilized a simple forcing simulation method to account for limited input parameters (wind speed, direction), lengthy simulation duration, and limited computational power.

4. As this study only focuses on the role of the presence of vegetation in land surface temperature and outdoor thermal comfort improvement, it did not exactly quantify the cooling benefit of each tree, as well as its other benefits like the economic, cultural, and social impact to the city.

6.3 Recommendations for Future Works

The following recommendations are proposed for future studies and investigations:

1. Follow up studies are recommended to perform an LST-NDVI analysis across all seasons and it would be best to consider utilizing additional indices to gain a more comprehensive understanding of LST variations across different seasons.

2. For the LCZ mapping, it is recommended to enhance the precision of the analysis by utilizing alternative methods, such as GIS-based approaches.

3. In thermal comfort analysis, it is best to consider calibrating the PET range through field methods and surveys to account for behavioural and psychological adaptation and the influence of subjective parameters like thermal adaptation.

4. For microclimate simulations, it is recommended to conduct in-depth site investigations to gather site-specific data and actual air temperature measurements to enhance the accuracy of the results.

5. Conducting in-depth analyses on the benefits of trees in other areas (social, economic, cultural, etc), and exploring tree species and leaf-area density (LAD) is recommended to gain a broader perspective on their contributions beyond temperature regulation.

6. For the city planners, it is recommended to incorporate microclimate analysis into future urban planning projects to gain insights into the benefits, risks, and potential vulnerabilities associated with the proposed developments. This will enable informed decision-making and the integration of climate considerations into the planning process.

REFERENCES

Abdulateef, M.F. and A. S. Al-Alwan, H. (2022) 'The effectiveness of urban green infrastructure in reducing surface urban heat island', *Ain Shams Engineering Journal*, 13(1), p. 101526. Available at: https://doi.org/10.1016/j.asej.2021.06.012.

Acosta, M.P. *et al.* (2021) 'How to bring UHI to the urban planning table? A data-driven modeling approach', *Sustainable Cities and Society*, 71, p. 102948. Available at: https://doi.org/10.1016/j.scs.2021.102948.

Afshar, N.K. *et al.* (2018) 'Influence of planting designs on winter thermal comfort in an urban park', *Journal of Environmental Engineering and Landscape Management*, 26(3), pp. 232–240. Available at: https://doi.org/10.3846/jeelm.2018.5374.

Ahmadpour, N. *et al.* (2021) 'Analysing the impact of urban morphology on the thermal comfort of the street canyon in a hot and dry climate (Case Study of Kashan, Iran)', *Italian Journal of Planning Practice*, 12(1), pp. 1–19.

Al-Saadi, L.M., Jaber, S.H. and Al-Jiboori, M.H. (2020) 'Variation of urban vegetation cover and its impact on minimum and maximum heat islands', *Urban Climate*, 34, p. 100707. Available at: https://doi.org/10.1016/j.uclim.2020.100707.

Aslam, A. and Rana, I.A. (2022) 'The use of local climate zones in the urban environment: A systematic review of data sources, methods, and themes', *Urban Climate*, 42, p. 101120. Available at: https://doi.org/10.1016/j.uclim.2022.101120.

Avdan, U. and Jovanovska, G. (2016) 'Algorithm for automated mapping of land surface temperature using LANDSAT 8 satellite data', *Journal of Sensors*, 2016, pp. 1–8. Available at: https://doi.org/10.1155/2016/1480307.

Balany, F. *et al.* (2020) 'Green infrastructure as an urban heat island mitigation strategy—a review', *Water*, 12(12), p. 3577. Available at: https://doi.org/10.3390/w12123577.

Battista, G., De Lieto Vollaro, R. and Zinzi, M. (2019) 'Assessment of urban overheating mitigation strategies in a square in Rome, Italy', *Solar Energy*, 180, pp. 608–621. Available at: https://doi.org/10.1016/j.solener.2019.01.074.

Bechtel, B. *et al.* (2019) 'SUHI analysis using local climate zones—A comparison of 50 cities', *Urban Climate*, 28, p. 100451. Available at: https://doi.org/10.1016/j.uclim.2019.01.005.

Brozovsky, J., Gaitani, N. and Gustavsen, A. (2021) 'A systematic review of urban climate research in cold and polar climate regions', *Renewable and Sustainable Energy Reviews*, 138, p. 110551. Available at: https://doi.org/10.1016/j.rser.2020.110551.

Choudhury, D., Das, A. and Das, M. (2021) 'Investigating thermal behavior pattern (TBP) of local climatic zones (LCZs): A study on industrial cities of Asansol-Durgapur

development area (ADDA), eastern India', *Urban Climate*, 35, p. 100727. Available at: https://doi.org/10.1016/j.uclim.2020.100727.

City of Tampere (2019) *I-Tree Ecosystem Analysis: Tampere 2019*. Available at: https://www.tampere.fi/luonto-ja-ymparisto/puistot/kaupunkipuut (Accessed: 20 March 2023).

City of Tampere (2020a) *Hiilineutraali Tampere 2030 tiekartta*. Available at: https://www.tampere.fi/en/nature-and-environment/climate-action-tampere (Accessed: 25 May 2023).

City of Tampere (2020b) 'Tampereen kaupunkipuulinjaus 2020'. Available at: https://www.tampere.fi/luonto-ja-ymparisto/puistot/kaupunkipuut#kaupunkipuulinjaus (Accessed: 20 April 2023).

City of Tampere (2021) *Tampereen ilmastovahti*. Available at: https://ilmastovahti.tampere.fi/.

City of Tampere (2022a) *City of sustainable action – The voluntary local review of the UN sustainable development goals in Tampere 2022*. Available at: https://www.tampere.fi/en/tampere-city-strategy/sustainable-development (Accessed: 20 March 2023).

City of Tampere (2022b) 'Street and Park Trees of the City of Tampere'. Available at: https://kartat.tampere.fi/oskari/ (Accessed: 10 May 2023).

City of Tampere (2023) *Kantakaupungin vaiheyleiskaava - valtuustokausi 2021 - 2025*. Available at: https://www.tampere.fi/kaupunkisuunnittelu/kaupunkiymparisto-uudistuu/kantakaupungin-vaiheyleiskaava-valtuustokausi-2021-2025/kaava-aineistot (Accessed: 22 March 2023).

Das, M. and Das, A. (2020) 'Assessing the relationship between local climatic zones (LCZs) and land surface temperature (LST) – A case study of Sriniketan-Santiniketan Planning Area (SSPA), West Bengal, India', *Urban Climate*, 32, p. 100591. Available at: https://doi.org/10.1016/j.uclim.2020.100591.

Del Pozo, S. *et al.* (2021) 'Evaluation of the seasonal nightime LST-air temperature discrepancies and their relation to local climate zones (LCZ) in Strasbourg', *The International Archives of the Photogrammetry, Remote Sensing and Spatial Information Sciences*, XLIII-B3-2021, pp. 391–398. Available at: https://doi.org/10.5194/isprs-archives-XLIII-B3-2021-391-2021.

Demuzere, M. *et al.* (2019) 'Mapping Europe into local climate zones', *PLOS ONE*. Edited by M. Mourshed, 14(4), p. e0214474. Available at: https://doi.org/10.1371/journal.pone.0214474.

Drebs, A., Suomi, J. and Mäkelä, A. (2023) 'Urban heat island research at high latitudes — utilising Finland as an example', *Boreal Environmental Research*, 28, pp. 81–96.

Duarte, D.H.S. *et al.* (2015) 'The impact of vegetation on urban microclimate to counterbalance built density in a subtropical changing climate', *Urban Climate*, 14, pp. 224–239. Available at: https://doi.org/10.1016/j.uclim.2015.09.006.

Emmanuel, R. *et al.* (2023) 'Urban Heat Risk: Protocols for Mapping and Implications for Colombo, Sri Lanka', *Atmosphere*, 14(2), p. 343. Available at: https://doi.org/10.3390/atmos14020343.

Feng, W. and Liu, J. (2022) 'A Literature Survey of Local Climate Zone Classification: Status, Application, and Prospect', *Buildings*, 12(10), p. 1693. Available at: https://doi.org/10.3390/buildings12101693.

Finnish Meteorological Institute (2021) *June this year was Finland's warmest in recorded history*, *Finnish Meteorological Institute*. Available at: https://en.ilmatieteenlaitos.fi/press-release/5vByjewgsYT1lbvgSv2FQ6 (Accessed: 27 March 2023).

Gago, E.J. *et al.* (2013) 'The city and urban heat islands: A review of strategies to mitigate adverse effects', *Renewable and Sustainable Energy Reviews*, 25, pp. 749–758. Available at: https://doi.org/10.1016/j.rser.2013.05.057.

Gatto, E. *et al.* (2020) 'Impact of Urban Vegetation on Outdoor Thermal Comfort: Comparison between a Mediterranean City (Lecce, Italy) and a Northern European City (Lahti, Finland)', *Forests*, 11(2), p. 228. Available at: https://doi.org/10.3390/f11020228.

Google Maps (2023) *Identified Focus Area*. Available at: https://www.google.com/maps/place/Tampere,+Finland/ (Accessed: 20 February 2023).

Grimmond, C.S.B., Ward, H.C. and Kotthaus, S. (eds) (2015) *How is urbanization altering local and regional climate? In: Seto, K. C., Solecki, W. D. and Griffith, C. A. (eds.) The Routledge Handbook of Urbanization and Global Environmental Change. Routledge*. 1 Edition. London ; New York: Routledge, Taylor & Francis Group.

Hashim, H., Abd Latif, Z. and Adnan, N.A. (2019) 'Urban vegetation classification with NDVI threshold value methods with very high resolution (VHR) pleiades imagery', *The International Archives of the Photogrammetry, Remote Sensing and Spatial Information Sciences*, XLII-4/W16, pp. 237–240. Available at: https://doi.org/10.5194/isprs-archives-XLII-4-W16-237-2019.

Höppe, P. (1999) 'The physiological equivalent temperature - a universal index for the biometeorological assessment of the thermal environment', *International Journal of Biometeorology*, 43(2), pp. 71–75. Available at: https://doi.org/10.1007/s004840050118.

IPCC (2023) *Summary for Policymakers. In: Climate Change 2023: Synthesis Report. A Report of the Intergovernmental Panel on Climate Change. Contribution of Working Groups I, II and III to the Sixth Assessment Report of the Intergovernmental Panel on Climate Change [Core Writing Team, H. Lee and J. Romero (eds.)].* Geneva, Switzerland, p. 36. Available at: https://www.ipcc.ch/report/ar6/syr/ (Accessed: 20 July 2023).

Jansson, C., Jansson, P.-E. and Gustafsson, D. (2007) 'Near surface climate in an urban vegetated park and its surroundings', *Theoretical and Applied Climatology*, 89(3–4), pp. 185–193. Available at: https://doi.org/10.1007/s00704-006-0259-z.

Jokinen, P. *et al.* (2021) *Climatological and oceanographic statistics of Finland 1991–2020*. Finnish Meteorological Institute. Available at: https://doi.org/10.35614/isbn.9789523361485.

Kaplan, G., Avdan, U. and Avdan, Z.Y. (2018) 'Urban Heat Island Analysis Using the Landsat 8 Satellite Data: A Case Study in Skopje, Macedonia', in *The 2nd International Electronic Conference on Remote Sensing*. *International Electronic Conference on Remote Sensing*, MDPI, p. 358. Available at: https://doi.org/10.3390/ecrs-2-05171.

Kollanus, V., Tiittanen, P. and Lanki, T. (2021) 'Mortality risk related to heatwaves in Finland – Factors affecting vulnerability', *Environmental Research*, 201, p. 111503. Available at: https://doi.org/10.1016/j.envres.2021.111503.

Li, H. (2016) 'Impacts of Pavement Strategies on Human Thermal Comfort', in *Pavement Materials for Heat Island Mitigation*. Elsevier, pp. 281–306. Available at: https://doi.org/10.1016/B978-0-12-803476-7.00013-1.

Li, J., Sun, R. and Chen, L. (2023) 'A review of thermal perception and adaptation strategies across global climate zones', *Urban Climate*, 49, p. 101559. Available at: https://doi.org/10.1016/j.uclim.2023.101559.

Lindberg, F. *et al.* (2014) 'Characteristics of the mean radiant temperature in high latitude cities—implications for sensitive climate planning applications', *International Journal of Biometeorology*, 58(5), pp. 613–627. Available at: https://doi.org/10.1007/s00484-013-0638-y.

Marando, F. *et al.* (2022) 'Urban heat island mitigation by green infrastructure in European Functional Urban Areas', *Sustainable Cities and Society*, 77, p. 103564. Available at: https://doi.org/10.1016/j.scs.2021.103564.

Matzarakis, A., Mayer, H. and Iziomon, M.G. (1999) 'Applications of a universal thermal index: physiological equivalent temperature', *International Journal of Biometeorology*, 43(2), pp. 76–84. Available at: https://doi.org/10.1007/s004840050119.

Morakinyo, T.E. *et al.* (2017) 'A study on the impact of shadow-cast and tree species on in-canyon and neighborhood's thermal comfort', *Building and Environment*, 115, pp. 1–17. Available at: https://doi.org/10.1016/j.buildenv.2017.01.005.

Naserikia, M. *et al.* (2022) 'Background climate modulates the impact of land cover on urban surface temperature', *Scientific Reports*, 12(1), p. 15433. Available at: https://doi.org/10.1038/s41598-022-19431-x.

Nie, T. *et al.* (2022) 'Discussion on inapplicability of Universal Thermal Climate Index (UTCI) for outdoor thermal comfort in cold region', *Urban Climate*, 46, p. 101304. Available at: https://doi.org/10.1016/j.uclim.2022.101304.

Oke, T.R. *et al.* (2017) *Urban Climates*. 1st edn. Cambridge University Press. Available at: https://doi.org/10.1017/9781139016476.

Perini, K., Chokhachian, A. and Auer, T. (2018) 'Green streets to enhance outdoor comfort', in *Nature Based Strategies for Urban and Building Sustainability*. Elsevier, pp. 119–129. Available at: https://doi.org/10.1016/B978-0-12-812150-4.00011-2.

Potchter, O. *et al.* (2018) 'Outdoor human thermal perception in various climates: A comprehensive review of approaches, methods and quantification', *Science of The Total Environment*, 631–632, pp. 390–406. Available at: https://doi.org/10.1016/j.scitotenv.2018.02.276.

Remote Sensing Phenology (2018) *NDVI, the foundation for remote sensing phenology*, *USGS*. Available at: https://www.usgs.gov/special-topics/remote-sensing-phenology/science/ndvi-foundation-remote-sensing-phenology#science (Accessed: 10 July 2023).

Ruuhela, R. *et al.* (2017) 'Biometeorological Assessment of Mortality Related to Extreme Temperatures in Helsinki Region, Finland, 1972–2014', *International Journal of Environmental Research and Public Health*, 14(8), p. 944. Available at: https://doi.org/10.3390/ijerph14080944.

Saaroni, H. *et al.* (2018) 'Urban Green Infrastructure as a tool for urban heat mitigation: Survey of research methodologies and findings across different climatic regions', *Urban Climate*, 24, pp. 94–110. Available at: https://doi.org/10.1016/j.uclim.2018.02.001.

Sitowise (2022a) *Ilmastonmuutokseen sopeutuminen ja varautuminen, Tampereen kaupunki*. Available at: https://www.tampere.fi/luonto-ja-ymparisto/ilmastotyo-tampereella/ilmastonmuutokseen-sopeutuminen-ja-varautuminen (Accessed: 20 June 2023).

Sitowise (2022b) *Tampereen kantakaupungin lämpösaarekeilmiö*. Available at: https://www.tampere.fi/kaupunkisuunnittelu/kaupunkiymparisto-uudistuu/kantakaupungin-vaiheyleiskaava-valtuustokausi-2021-2025/kaava-aineistot (Accessed: 20 March 2023).

Solecki, W.D. *et al.* (2005) 'Mitigation of the heat island effect in urban New Jersey', *Environmental Hazards*, 6(1), pp. 39–49. Available at: https://doi.org/10.1016/j.hazards.2004.12.002.

Sresto, M.A. *et al.* (2022) 'A GIS and remote sensing approach for measuring summer-winter variation of land use and land cover indices and surface temperature in Dhaka district, Bangladesh', *Heliyon*, 8(8), p. e10309. Available at: https://doi.org/10.1016/j.heliyon.2022.e10309.

Stewart, I.D. and Oke, T.R. (2012) 'Local climate zones for urban temperature studies', *Bulletin of the American Meteorological Society*, 93(12), pp. 1879–1900. Available at: https://doi.org/10.1175/BAMS-D-11-00019.1.

Sun, D. and Kafatos, M. (2007) 'Note on the NDVI-LST relationship and the use of temperature-related drought indices over North America', *Geophysical Research Letters*, 34(24), p. L24406. Available at: https://doi.org/10.1029/2007GL031485.

Suomi, J. (2018) 'Extreme temperature differences in the city of Lahti, southern Finland: Intensity, seasonality and environmental drivers', *Weather and Climate Extremes*, 19, pp. 20–28. Available at: https://doi.org/10.1016/j.wace.2017.12.001.

Tesfamariam, S., Govindu, V. and Uncha, A. (2023) 'Spatio-temporal analysis of urban heat island (UHI) and its effect on urban ecology: The case of Mekelle city, Northern Ethiopia', *Heliyon*, 9(2), p. e13098. Available at: https://doi.org/10.1016/j.heliyon.2023.e13098.

Ullah, W. *et al.* (2023) 'Analysis of the relationship among land surface temperature (LST), land use land cover (LULC), and normalized difference vegetation index (NDVI) with topographic elements in the lower Himalayan region', *Heliyon*, 9(2), p. e13322. Available at: https://doi.org/10.1016/j.heliyon.2023.e13322.

United Nations Human Settlements Programme (2022) *World cities report 2022: Envisaging the future of cities*. Nairobi, Kenya. Available at: https://unhabitat.org/wcr/ (Accessed: 15 July 2023).

Venter, Z.S., Krog, N.H. and Barton, D.N. (2020) 'Linking green infrastructure to urban heat and human health risk mitigation in Oslo, Norway', *Science of The Total Environment*, 709, p. 136193. Available at: https://doi.org/10.1016/j.scitotenv.2019.136193.

Wang, Y. *et al.* (2019) 'Microclimate regulation and energy saving potential from different urban green infrastructures in a subtropical city', *Journal of Cleaner Production*, 226, pp. 913–927. Available at: https://doi.org/10.1016/j.jclepro.2019.04.114.

Wang, Y. *et al.* (2021) 'A practical approach of urban green infrastructure planning to mitigate urban overheating: A case study of Guangzhou', *Journal of Cleaner Production*, 287, p. 124995. Available at: https://doi.org/10.1016/j.jclepro.2020.124995.

Ward, K. *et al.* (2016) 'Heat waves and urban heat islands in Europe: A review of relevant drivers', *Science of The Total Environment*, 569–570, pp. 527–539. Available at: https://doi.org/10.1016/j.scitotenv.2016.06.119.

Welegedara, N.P.Y., Agrawal, S.K. and Lotfi, G. (2023) 'Exploring spatiotemporal changes of the urban heat Island effect in high-latitude cities at a neighbourhood level: A case of Edmonton, Canada', *Sustainable Cities and Society*, 90, p. 104403. Available at: https://doi.org/10.1016/j.scs.2023.104403.

World Meteorological Organization (2023) *Guidance on measuring, modelling and monitoring the canopy layer urban heat island (CL-UHI)*. Available at: chrome-extension://efaidnbmnnnibpcajpcglclefindmkaj/https://library.wmo.int/doc_num.php?explnum_id=11537 (Accessed: 20 June 2023).

Yang, Y. *et al.* (2018) ‘Simulation on the impacts of the street tree pattern on built summer thermal comfort in cold region of China’, *Sustainable Cities and Society*, 37, pp. 563–580. Available at: https://doi.org/10.1016/j.scs.2017.09.033.

Yilmaz, S. *et al.* (2021) ‘Analysis of winter thermal comfort conditions: street scenarios using ENVI-met model’, *Environmental Science and Pollution Research*, 28(45), pp. 63837–63859. Available at: https://doi.org/10.1007/s11356-020-12009-y.

Yuan, F. and Bauer, M.E. (2007) ‘Comparison of impervious surface area and normalized difference vegetation index as indicators of surface urban heat island effects in landsat imagery’, *Remote Sensing of Environment*, 106(3), pp. 375–386. Available at: https://doi.org/10.1016/j.rse.2006.09.003.

Zhang, Y., Odeh, I.O.A. and Han, C. (2009) ‘Bi-temporal characterization of land surface temperature in relation to impervious surface area, NDVI and NDBI, using a sub-pixel image analysis’, *International Journal of Applied Earth Observation and Geoinformation*, 11(4), pp. 256–264. Available at: https://doi.org/10.1016/j.jag.2009.03.001.

Zhou, L. *et al.* (2022) ‘Understanding the effects of 2D/3D urban morphology on land surface temperature based on local climate zones’, *Building and Environment*, 208, p. 108578. Available at: https://doi.org/10.1016/j.buildenv.2021.108578.

APPENDICES

Appendix A. Local Climate Zone Classes Properties

A.1. Values of geometric and surface cover properties for local climate zones. (Stewart and Oke, 2012)

Local Climate Zone (LCZ)		Sky View Factor (a)	Aspect Ratio (b)	Building Surface Fraction (c)	Impervious Surface Fraction (d)	Pervious Surface Fraction (e)	Height of Roughness Elements (f)	Terrain Roughness Class (g)
1	Compact high-rise	0.2–0.4	>2	40–60	40–60	<10	>25	8
2	Compact midrise	0.3–0.6	0.75–2	40–70	30–50	<20	10–25	6–7
3	Compact low-rise	0.2–0.6	0.75–1.5	40–70	20–50	<30	3–10	6
4	Open high-rise	0.5–0.7	0.75–1.25	20–40	30–40	30–40	>25	7–8
5	Open midrise	0.5–0.8	0.3–0.75	20–40	30–50	20–40	10–25	5–6
6	Open low-rise	0.6–0.9	0.3–0.75	20–40	20–50	30–60	3–10	5–6
7	Lightweight low-rise	0.2–0.5	1–2	60–90	<20	<30	2–4	4–5
8	Large low-rise	>0.7	0.1–0.3	30–50	40–50	<20	3–10	5
9	Sparsely built	>0.8	0.1–0.25	10–20	<20	60–80	3–10	5–6
10	Heavy industry	0.6–0.9	0.2–0.5	20–30	20–40	40–50	5–15	5–6
A	Dense trees	<0.4	>1	<10	<10	>90	3–30	8
B	Scattered trees	0.5–0.8	0.25–0.75	<10	<10	>90	3–15	5–6
C	Bush, scrub	0.7–0.9	0.25–1.0	<10	<10	>90	<2	4–5
D	Low plants	>0.9	<0.1	<10	<10	>90	<1	3–4
E	Bare rock or paved	>0.9	<0.1	<10	>90	<10	<0.25	1–2
F	Bare soil or sand	>0.9	<0.1	<10	<10	>90	<0.25	1–2
G	Water	>0.9	<0.1	<10	<10	>90	–	1

a. Ratio of the amount of sky hemisphere visible from ground level to that of an unobstructed hemisphere
b. Mean height-to-width ratio of street canyons (LCZs 1–7), building spacing (LCZs 8–10), and tree spacing (LCZs A–G)
c. Ratio of building plan area to total plan area (%)
d. Ratio of impervious plan area (paved, rock) to total plan area (%)
e. Ratio of pervious plan area (bare soil, vegetation, water) to total plan area (%)
f. Geometric average of building heights (LCZs 1–10) and tree/plant heights (LCZs A–F) (m)
g. Davenport et al.'s (2000) classification of effective terrain roughness ($z0$) for city and country landscapes. See Table 5 for class descriptions

A.2. Values of thermal, radiative, and metabolic properties for local climate zones (Stewart and Oke, 2012)

Local Climate Zone (LCZ)		Surface Admittance (a)	Surface Albedo (b)	Anthropogenic Heat Output (c)
1	Compact high-rise	1,500–1,800	0.10–0.20	50–300
2	Compact midrise	1,500–2,200	0.10–0.20	<75
3	Compact low-rise	1,200–1,800	0.10–0.20	<75
4	Open high-rise	1,400–1,800	0.12–0.25	<50
5	Open midrise	1,400–2,000	0.12–0.25	<25
6	Open low-rise	1,200–1,800	0.12–0.25	<25
7	Lightweight low-rise	800–1,500	0.15–0.35	<35
8	Large low-rise	1,200–1,800	0.15–0.25	<50
9	Sparsely built	1,000–1,800	0.12–0.25	<10
10	Heavy industry	1,000–2,500	0.12–0.20	>300
A	Dense trees	unknown	0.10–0.20	0
B	Scattered trees	1,000–1,800	0.15–0.25	0
C	Bush, scrub	700–1,500	0.15–0.30	0
D	Low plants	1,200–1,600	0.15–0.25	0
E	Bare rock or paved	1,200–2,500	0.15–0.30	0
F	Bare soil or sand	600–1,400	0.20–0.35	0
G	Water	1500	0.02–0.10	0

a. Ability of surface to accept or release heat (J m–2 s–1/2 K–1). Varies with soil wetness and material density. Few estimates of local-scale admittance exist in the literature; values given here are therefore subjective and should be used cautiously. Note that the “surface” in LCZ A is undefined and its admittance unknown.

b. Ratio of the amount of solar radiation reflected by a surface to the amount received by it. Varies with surface colour, wetness, and roughness.

c. Mean annual heat flux density (W m−2) from fuel combustion and human activity (transportation, space cooling/heating, industrial processing, human metabolism). Varies significantly with latitude, season, and population density.

Appendix B. LST AND NDVI Calculation Process

In this study, TIR band 10 was used for brightness estimation and bands 4 and 5 for the NDVI calculation. The algorithm process was based on previous studies (Avdan and Jovanovska, 2016; Emmanuel *et al.,* 2023)

B.1. Top of Atmospheric Spectral Radiance

After the input of Band 10, the first step to LST calculation (A4) is the conversion of digital number to top of atmospheric (TOA) spectral radiance *(L λ)*:

$$L\lambda = M_L * Q_{cal} + A_L$$

Where: M_L represents the band-specific multiplicative rescaling factor; Q_{cal} represents the band 10 images, and A_L is the band-specific additive rescaling factor.

Table B.1 Constant for radiance calculation

Parameter	Landsat 8 Description	Average Values
A_L	Radiance add band 10	0.1000
M_L	Radiance multi-band 10	0.0003342

B.2. Radiance conversion to At-Sensor Temperature

Data should be converted to brightness temperature (BT) using thermal constants.

$$BT = \frac{K_2}{ln\left[\left(\frac{K_1}{L\lambda}\right) + 1\right]} - 273.15$$

Where: *K1 and* K_2 are the band-specific thermal conversion constants derived from the metadata (Table A.2).

Table B.2 Constants for brightness temperature (BT) calculation

Calibrated Constant for Landsat 8	Band	Constant
K1	Band 10	774.8853
K2	Band 10	1321.0789

B.3. NDVI methods for Emissivity Correction

B.3.1. Normalised Difference Vegetation Index (NDVI) Calculation

Landsat visible and near-infrared bands were used for the NDVI calculation. Affected by atmospheric conditions, the brightness temperature (BT) is further enhanced using NDVI to determine spectral emissivity of various land surface value (Table A.3).

$$\mathrm{NDVI} = \frac{NIR(band\ 5) - NIR(band\ 4)}{NIR + NIR(band\ 4)}$$

Table B.3 NDVI thresholds for spectral emissivity of land surfaces

NDVI Thresholds	Spectral Emissivity of Land Surface ()
NDVI < -0.185	0.995
-0.185 < NDVI < -0.157	0.970
-0.157 < NDVI < 0.727	1.0094 + Ln (NDVI)
NDVI > 0.727	0.990

B.3.2. Proportion of Vegetation (P_v) calculation

$$P_v = \left[\frac{NDVI - NDVI_{min}}{NDVI_{mzx} - NDVI_{min}}\right]^2$$

B.3.3. Land Surface Emissivity Calculation (ε)

$$\varepsilon = 0.004\ P_V + 0.986$$

B.4. LST Calculation

$$\mathrm{LST} = \frac{BT}{1 + \left(\lambda * \frac{BT}{\rho}\right) * ln\ (\varepsilon)}$$

$$\rho = h * c/\sigma$$

Where: BT is the brightness temperature; λ is the wavelength of emitted radiance (λ =10.9 μm for band 10, and 12 μm for band 11); *h* is the Planck's constant (6.626 x 10^{-34} m^2kg/s); *c* represents the velocity of light (2.998 * 108 m/s); σ is the Boltzmann constant (1.38 *10^{-23} J/K), and calculated ρ value is 1.438 * 10^{-2} mk.

Appendix C. Air temperature Time Behaviour at Receptors

Legend: BC C1 C2 C3

Winter - January 15, 2021 *at 1.4m above the ground*

Streets

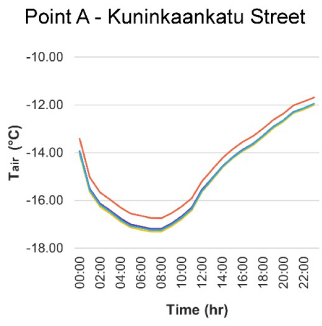

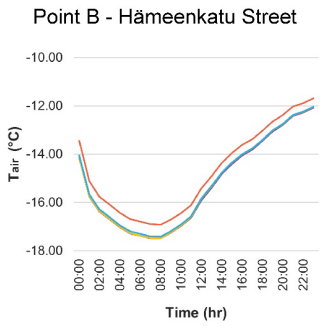

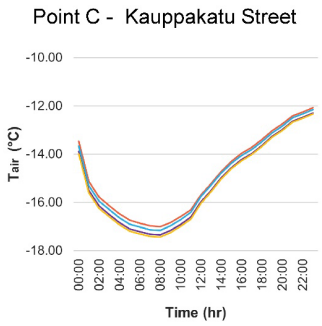

Open Spaces

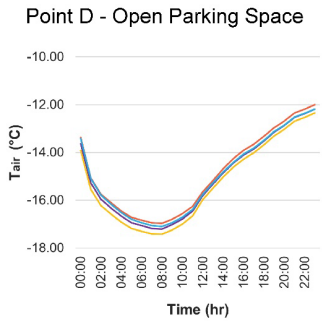

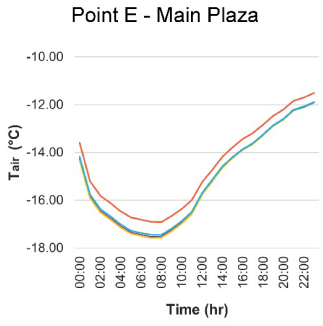

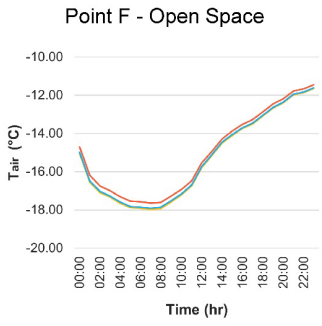

Legend: BC C1 C2 C3

Summer - June 22, 2021 *at 1.4m above the ground*

Streets

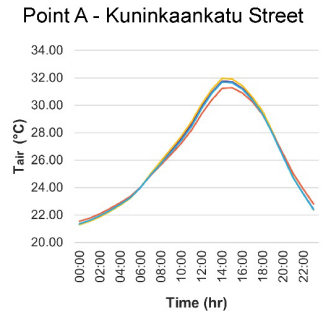

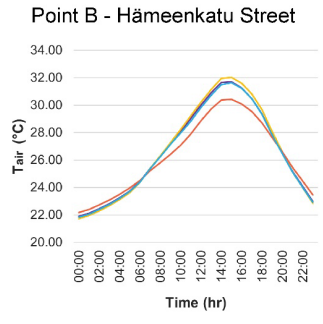

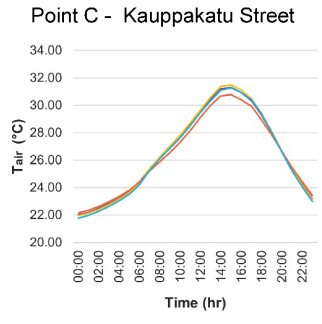

Open Spaces

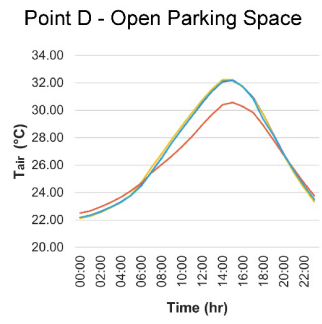

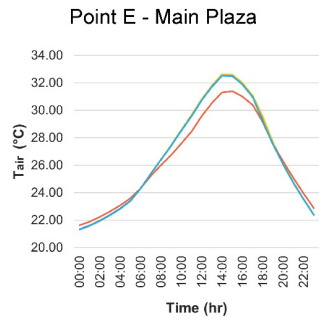

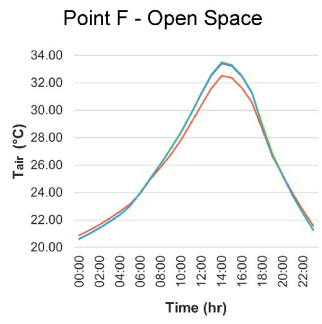

Appendix D. MRT Time Behaviour at Receptors

Legend: BC C1 C2 C3

Winter - January 15, 2021 *at 1.4m above the ground*

Streets

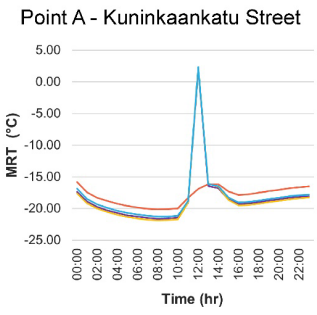

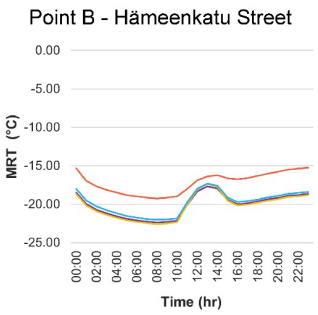

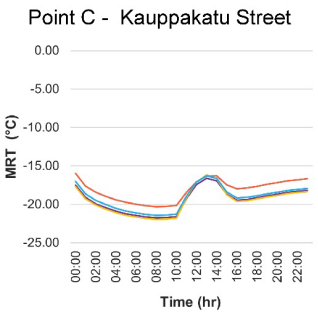

Open Spaces

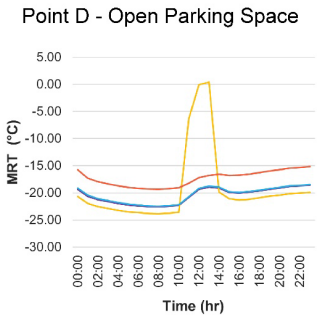

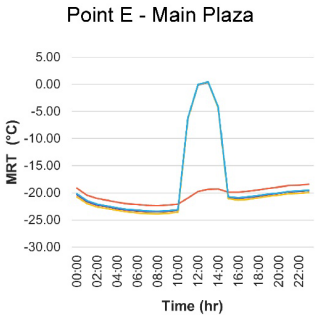

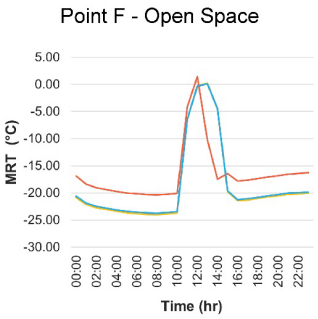

Legend: BC C1 C2 C3

Summer - June 22, 2021 *at 1.4m above the ground*

Streets

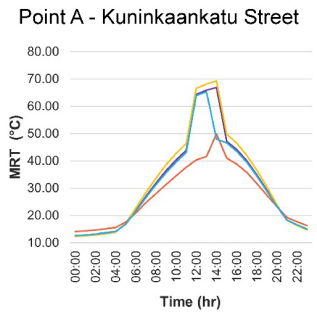

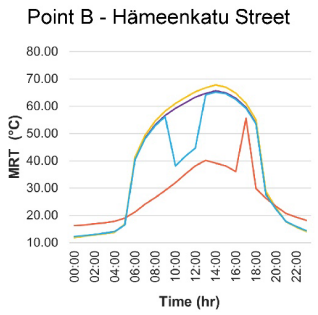

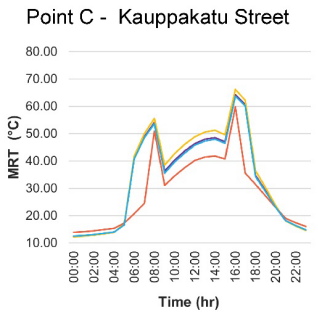

Open Spaces

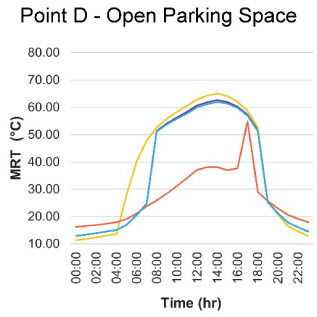

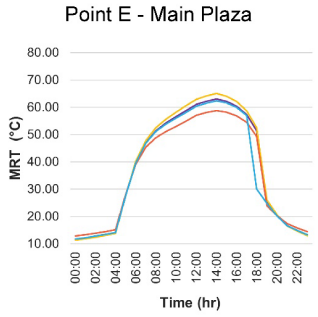

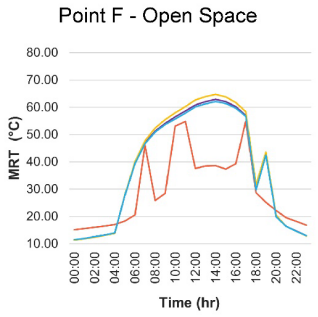

Appendix E. PET Time Behaviour at Receptors

Legend: BC C1 C2 C3

Winter - January 15, 2021 *at 1.4m above the ground*

Streets

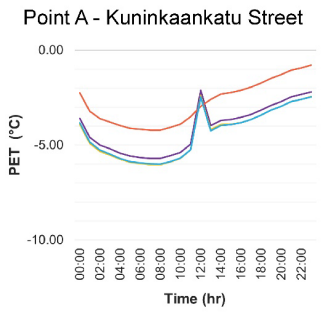

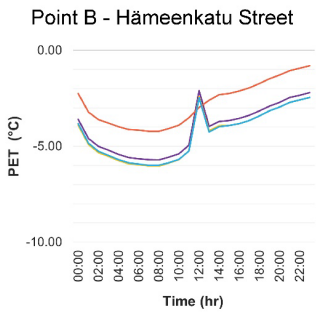

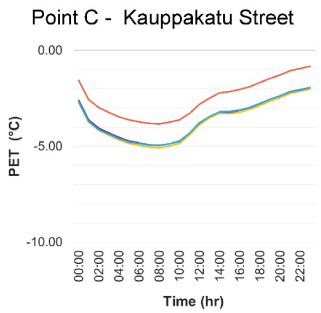

Open Spaces

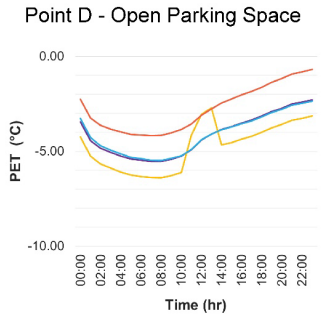

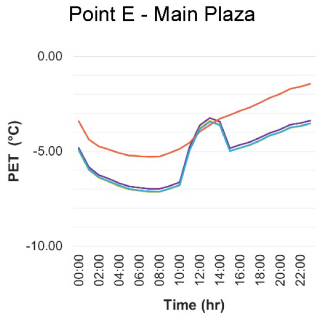

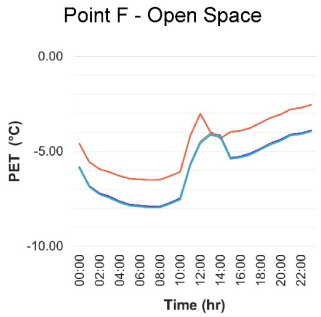

Legend: BC C1 C2 C3

Summer - June 22, 2021 *at 1.4m above the ground*

Streets

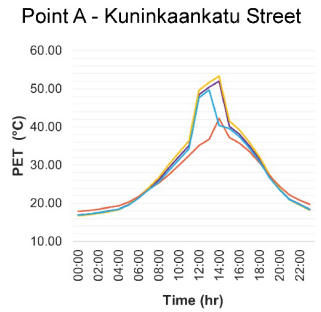

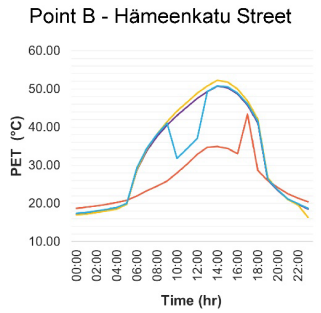

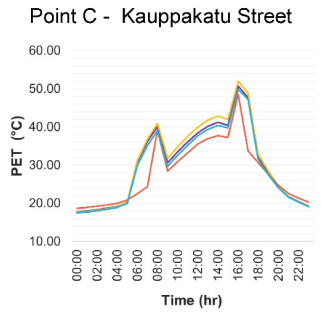

Open Spaces

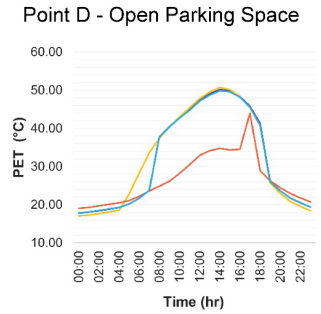

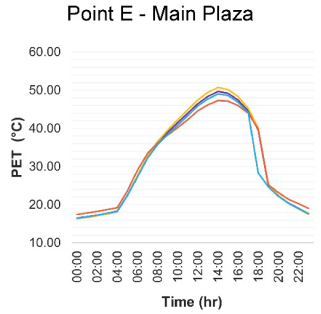

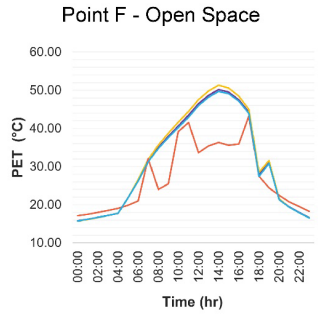

Appendix F. PET Range of Receptors on a Critical Cold Winter Day

AVERAGE				
Time	BC	C1	C2	C3
0:00	-4.05	-4.31	-2.79	-4.01
1:00	-5.06	-5.31	-3.78	-5.02
2:00	-5.47	-5.73	-4.17	-5.44
3:00	-5.68	-5.95	-4.36	-5.66
4:00	-5.91	-6.17	-4.55	-5.88
5:00	-6.07	-6.34	-4.70	-6.06
6:00	-6.15	-6.41	-4.74	-6.13
7:00	-6.21	-6.48	-4.79	-6.20
8:00	-6.22	-6.49	-4.79	-6.21
9:00	-6.08	-6.35	-4.64	-6.08
10:00	-5.91	-6.18	-4.46	-5.91
11:00	-5.04	-5.02	-3.87	-5.05
12:00	-3.92	-3.79	-3.25	-3.94
13:00	-3.92	-3.77	-3.12	-3.94
14:00	**-3.80**	**-4.02**	**-2.93**	**-3.81**
15:00	-4.18	-4.42	-2.75	-4.19
16:00	-4.05	-4.30	-2.60	-4.07
17:00	-3.90	-4.15	-2.43	-3.92
18:00	-3.67	-3.92	-2.20	-3.70
19:00	-3.42	-3.67	-1.95	-3.45
20:00	-3.24	-3.50	-1.76	-3.28
21:00	-3.00	-3.25	-1.52	-3.04
22:00	-2.91	-3.16	-1.41	-2.94
23:00	-2.77	-3.03	-1.27	-2.82

Physiological Equivalent Temperature (PET) Range

adapted from Matzarakis, Mayer and Iziomon, 1999

	°C	Thermal Perception	Physiological Stress Grade
Coolest	< 4	Very Cold	Extreme Cold Stress

Point A - Kuninkaankatu				
Time	BC	C1	C2	C3
0:00	-3.58	-3.90	-2.24	-3.82
1:00	-4.59	-4.91	-3.22	-4.84
2:00	-5.00	-5.32	-3.60	-5.26
3:00	-5.20	-5.52	-3.79	-5.48
4:00	-5.42	-5.74	-3.97	-5.70
5:00	-5.58	-5.90	-4.12	-5.87
6:00	-5.65	-5.96	-4.17	-5.93
7:00	-5.70	-6.03	-4.22	-5.99
8:00	-5.71	-6.03	-4.21	-5.99
9:00	-5.56	-5.89	-4.07	-5.86
10:00	-5.39	-5.70	-3.90	-5.68
11:00	-4.94	-5.23	-3.51	-5.25
12:00	-2.10	-2.40	-2.96	-2.46
13:00	-3.96	-4.19	-2.59	-4.25
14:00	**-3.70**	**-3.92**	**-2.31**	**-3.97**
15:00	-3.66	-3.91	-2.24	-3.92
16:00	-3.54	-3.81	-2.11	-3.81
17:00	-3.38	-3.65	-1.95	-3.65
18:00	-3.15	-3.42	-1.72	-3.42
19:00	-2.90	-3.15	-1.48	-3.15
20:00	-2.70	-2.96	-1.29	-2.96
21:00	-2.46	-2.71	-1.06	-2.71
22:00	-2.33	-2.59	-0.93	-2.59
23:00	-2.19	-2.45	-0.79	-2.45

Point B - Hämeenkatu Main Street				
Time	BC	C1	C2	C3
0:00	-4.05	-4.12	-2.69	-3.48
1:00	-5.05	-5.13	-3.71	-4.49
2:00	-5.47	-5.55	-4.11	-4.92
3:00	-5.69	-5.77	-4.31	-5.15
4:00	-5.91	-6.00	-4.50	-5.39
5:00	-6.09	-6.17	-4.65	-5.57
6:00	-6.16	-6.26	-4.71	-5.67
7:00	-6.24	-6.33	-4.76	-5.75
8:00	-6.26	-6.35	-4.76	-5.78
9:00	-6.13	-6.23	-4.63	-5.67
10:00	-5.97	-6.07	-4.46	-5.52
11:00	-5.59	-5.67	-4.16	-5.15
12:00	-5.04	-5.08	-3.66	-4.59
13:00	-4.68	-4.71	-3.32	-4.26
14:00	**-4.40**	**-4.45**	**-2.99**	**-3.99**
15:00	-4.32	-4.39	-2.82	-3.93
16:00	-4.18	-4.28	-2.64	-3.83
17:00	-4.05	-4.14	-2.47	-3.69
18:00	-3.83	-3.92	-2.25	-3.49
19:00	-3.58	-3.69	-2.00	-3.27
20:00	-3.42	-3.52	-1.82	-3.10
21:00	-3.19	-3.29	-1.58	-2.89
22:00	-3.10	-3.21	-1.47	-2.80
23:00	-2.98	-3.09	-1.34	-2.69

Point C - Kauppakatu				
Time	BC	C1	C2	C3
0:00	-2.60	-2.73	-1.55	-2.68
1:00	-3.62	-3.73	-2.56	-3.70
2:00	-4.06	-4.17	-2.98	-4.13
3:00	-4.30	-4.43	-3.23	-4.36
4:00	-4.53	-4.66	-3.45	-4.59
5:00	-4.72	-4.85	-3.62	-4.76
6:00	-4.83	-4.94	-3.71	-4.86
7:00	-4.91	-5.03	-3.79	-4.93
8:00	-4.95	-5.07	-3.83	-4.96
9:00	-4.87	-4.98	-3.74	-4.87
10:00	-4.73	-4.85	-3.62	-4.72
11:00	-4.33	-4.42	-3.28	-4.31
12:00	-3.82	-3.87	-2.81	-3.77
13:00	-3.48	-3.50	-2.48	-3.43
14:00	**-3.24**	**-3.28**	**-2.21**	**-3.19**
15:00	-3.22	-3.29	-2.14	-3.18
16:00	-3.12	-3.22	-2.03	-3.10
17:00	-2.98	-3.07	-1.88	-2.96
18:00	-2.77	-2.87	-1.68	-2.76
19:00	-2.54	-2.64	-1.45	-2.54
20:00	-2.37	-2.46	-1.27	-2.37
21:00	-2.15	-2.24	-1.05	-2.16
22:00	-2.05	-2.13	-0.94	-2.06
23:00	-1.92	-2.01	-0.82	-1.94

Point D - Open Parking Space				
Time	BC	C1	C2	C3
0:00	-3.44	-4.25	-2.26	-3.27
1:00	-4.44	-5.26	-3.26	-4.28
2:00	-4.85	-5.67	-3.64	-4.71
3:00	-5.06	-5.89	-3.82	-4.94
4:00	-5.26	-6.09	-3.98	-5.15
5:00	-5.40	-6.25	-4.11	-5.31
6:00	-5.48	-6.32	-4.15	-5.39
7:00	-5.53	-6.38	-4.17	-5.47
8:00	-5.54	-6.39	-4.16	-5.49
9:00	-5.42	-6.28	-4.02	-5.37
10:00	-5.26	-6.12	-3.84	-5.23
11:00	-4.93	-4.16	-3.56	-4.91
12:00	-4.41	-3.05	-3.10	-4.40
13:00	-4.09	-2.71	-2.77	-4.09
14:00	**-3.85**	**-4.65**	**-2.46**	**-3.86**
15:00	-3.70	-4.53	-2.24	-3.72
16:00	-3.52	-4.36	-2.03	-3.55
17:00	-3.36	-4.22	-1.85	-3.39
18:00	-3.14	-3.99	-1.62	-3.19
19:00	-2.91	-3.76	-1.37	-2.96
20:00	-2.73	-3.58	-1.17	-2.79
21:00	-2.51	-3.36	-0.94	-2.57
22:00	-2.41	-3.26	-0.82	-2.48
23:00	-2.29	-3.14	-0.68	-2.36

Point E - Keskustori Main Plaza				
Time	BC	C1	C2	C3
0:00	-4.83	-4.98	-3.42	-4.93
1:00	-5.83	-5.98	-4.37	-5.94
2:00	-6.24	-6.40	-4.74	-6.36
3:00	-6.45	-6.61	-4.91	-6.57
4:00	-6.67	-6.84	-5.10	-6.80
5:00	-6.85	-7.01	-5.23	-6.98
6:00	-6.91	-7.08	-5.25	-7.05
7:00	-6.97	-7.14	-5.29	-7.12
8:00	-6.97	-7.14	-5.27	-7.12
9:00	-6.82	-6.98	-5.09	-6.96
10:00	-6.63	-6.79	-4.88	-6.77
11:00	-4.76	-4.93	-4.53	-4.94
12:00	-3.63	-3.78	-3.97	-3.82
13:00	-3.25	-3.39	-3.62	-3.44
14:00	**-3.43**	**-3.58**	**-3.28**	**-3.62**
15:00	-4.84	-4.99	-3.09	-4.99
16:00	-4.66	-4.82	-2.87	-4.82
17:00	-4.51	-4.67	-2.69	-4.66
18:00	-4.27	-4.44	-2.44	-4.43
19:00	-4.02	-4.18	-2.17	-4.17
20:00	-3.85	-4.01	-1.97	-3.99
21:00	-3.59	-3.76	-1.71	-3.75
22:00	-3.51	-3.68	-1.59	-3.66
23:00	-3.38	-3.55	-1.44	-3.53

Point F - Open Space				
Time	BC	C1	C2	C3
0:00	-5.83	-5.88	-4.59	-5.86
1:00	-6.82	-6.88	-5.56	-6.86
2:00	-7.21	-7.27	-5.93	-7.26
3:00	-7.39	-7.46	-6.09	-7.45
4:00	-7.64	-7.69	-6.30	-7.68
5:00	-7.80	-7.86	-6.44	-7.86
6:00	-7.85	-7.91	-6.47	-7.90
7:00	-7.90	-7.96	-6.51	-7.96
8:00	-7.89	-7.95	-6.49	-7.95
9:00	-7.70	-7.75	-6.29	-7.75
10:00	-7.47	-7.53	-6.07	-7.53
11:00	-5.68	-5.73	-4.19	-5.75
12:00	-4.49	-4.53	-3.02	-4.56
13:00	-4.07	-4.10	-3.96	-4.14
14:00	**-4.16**	**-4.21**	**-4.33**	**-4.24**
15:00	-5.33	-5.38	-3.98	-5.38
16:00	-5.26	-5.31	-3.91	-5.32
17:00	-5.10	-5.16	-3.75	-5.16
18:00	-4.84	-4.90	-3.50	-4.90
19:00	-4.56	-4.63	-3.23	-4.63
20:00	-4.38	-4.44	-3.05	-4.44
21:00	-4.11	-4.16	-2.78	-4.16
22:00	-4.03	-4.09	-2.70	-4.09
23:00	-3.89	-3.94	-2.55	-3.94

Appendix G. PET Range of Receptors on a Critical Hot Summer Day

Average PET Values				
Time	BC	C1	C2	C3
0:00	17.02	16.76	18.16	16.99
1:00	17.31	17.05	18.45	17.29
2:00	17.70	17.44	18.83	17.67
3:00	18.14	17.89	19.26	18.11
4:00	18.64	18.39	19.73	18.60
5:00	20.73	21.13	21.10	20.66
6:00	26.13	27.36	23.06	25.96
7:00	30.29	32.23	26.77	30.09
8:00	35.46	35.92	29.02	35.18
9:00	36.33	37.02	28.63	35.95
10:00	38.98	39.87	32.74	36.60
11:00	41.53	42.56	35.06	39.18
12:00	45.83	46.89	35.78	43.59
13:00	47.69	48.85	37.37	47.19
14:00	**48.99**	**50.21**	**38.88**	**46.70**
15:00	46.57	47.71	37.67	46.21
16:00	46.81	47.76	38.97	46.41
17:00	43.89	44.59	40.34	43.61
18:00	35.55	36.07	31.05	33.44
19:00	27.26	27.56	26.15	27.02
20:00	23.19	23.17	23.95	23.09
21:00	20.92	20.71	22.08	20.86
22:00	19.60	19.35	20.87	19.55
23:00	18.31	17.71	19.76	18.27

Physiological Equivalent Temperature (PET) Range

adapted from Matzarakis, Mayer and Iziomon, 1999

°C	Thermal Perception	Physiological Stress Grade
13 to 18	Slightly Cool	Slight Cold Stress
18 to 23	Comfortable	No Thermal Stress
23 to 29	Slightly Warm	Slight Heat Stress
29 to 35	Warm	Moderate Heat Stress
35 to 41	Hot	Strong Heat Stress
>41	Very Hot	Extreme Heat Stress

Point A - Kuninkaankatu				
Time	BC	C1	C2	C3
0:00	16.95	16.73	17.86	16.93
1:00	17.21	16.99	18.11	17.19
2:00	17.57	17.35	18.46	17.54
3:00	17.99	17.78	18.88	17.95
4:00	18.46	18.25	19.33	18.42
5:00	19.62	19.54	20.30	19.52
6:00	21.56	21.68	21.77	21.34
7:00	23.88	24.13	23.64	23.53
8:00	26.15	26.76	25.32	25.63
9:00	29.28	30.13	27.46	28.49
10:00	32.28	33.33	29.97	31.45
11:00	35.16	36.34	32.52	34.30
12:00	48.49	49.58	35.13	47.67
13:00	50.46	51.69	36.75	49.70
14:00	**51.96**	**53.28**	**42.23**	**40.39**
15:00	40.18	41.55	37.24	39.57
16:00	38.12	39.29	35.77	37.44
17:00	35.11	36.01	33.64	34.54
18:00	31.51	32.17	30.68	30.97
19:00	27.21	27.56	27.34	26.72
20:00	23.76	23.77	24.48	23.55
21:00	21.05	20.89	22.14	20.93
22:00	19.71	19.50	20.82	19.62
23:00	18.41	18.17	19.75	18.33

Point B - Hämeenkatu Main Street				
Time	BC	C1	C2	C3
0:00	17.22	17.03	18.76	17.41
1:00	17.49	17.30	19.02	17.67
2:00	17.86	17.67	19.37	18.03
3:00	18.28	18.10	19.78	18.46
4:00	18.76	18.58	20.24	18.93
5:00	19.82	19.77	20.83	19.99
6:00	28.72	28.87	21.95	29.37
7:00	33.85	34.27	23.40	34.51
8:00	37.60	38.29	24.61	38.19
9:00	40.55	41.48	25.92	41.04
10:00	43.06	44.19	28.01	31.83
11:00	45.34	46.60	30.37	34.47
12:00	47.57	48.91	32.88	37.06
13:00	49.34	50.80	34.80	49.43
14:00	**50.71**	**52.25**	**34.89**	**50.79**
15:00	50.33	51.81	34.41	50.55
16:00	48.67	50.03	33.09	48.92
17:00	45.74	46.91	43.44	46.11
18:00	41.12	42.10	28.64	41.53
19:00	26.11	26.78	25.95	26.34
20:00	23.38	23.55	24.19	23.54
21:00	21.05	20.98	22.57	21.20
22:00	19.79	19.66	21.41	19.94
23:00	18.54	16.40	20.42	18.69

Point C - Kauppakatu				
Time	BC	C1	C2	C3
0:00	17.82	17.69	18.68	17.53
1:00	18.03	17.90	18.89	17.74
2:00	18.34	18.22	19.21	18.06
3:00	18.73	18.61	19.58	18.45
4:00	19.16	19.05	20.01	18.88
5:00	20.35	20.39	20.86	20.02
6:00	30.83	31.13	22.50	29.86
7:00	36.17	36.72	24.41	35.16
8:00	40.08	40.89	39.14	39.01
9:00	30.64	31.76	28.43	29.72
10:00	33.51	34.81	30.86	32.59
11:00	36.14	37.57	33.23	35.24
12:00	38.46	39.94	35.51	37.69
13:00	40.22	41.82	36.96	39.40
14:00	**41.20**	**42.87**	**37.71**	**40.42**
15:00	40.44	42.00	37.23	39.79
16:00	50.70	51.99	48.59	49.85
17:00	47.78	48.82	33.71	47.14
18:00	32.00	32.89	30.71	31.59
19:00	27.89	28.49	27.58	27.50
20:00	24.38	24.55	24.82	24.16
21:00	21.76	21.72	22.59	21.58
22:00	20.49	20.42	21.32	20.30
23:00	19.26	19.15	20.31	19.05

Point D - Open Parking Space				
Time	BC	C1	C2	C3
0:00	17.79	17.03	19.08	17.85
1:00	18.05	17.29	19.33	18.10
2:00	18.41	17.66	19.68	18.45
3:00	18.83	18.09	20.08	18.87
4:00	19.31	18.57	20.54	19.33
5:00	20.21	22.84	21.10	20.23
6:00	21.72	28.35	22.20	21.71
7:00	23.77	33.64	23.63	23.78
8:00	37.74	37.41	24.83	37.73
9:00	40.51	40.42	26.15	40.41
10:00	42.85	43.02	28.21	42.65
11:00	45.12	45.47	30.51	44.83
12:00	47.46	47.85	32.89	47.20
13:00	49.03	49.54	34.14	48.72
14:00	**50.19**	**50.74**	**34.79**	**49.87**
15:00	49.84	50.15	34.39	49.62
16:00	48.40	48.40	34.50	48.19
17:00	45.85	45.47	44.03	45.65
18:00	41.26	40.68	28.90	40.81
19:00	26.19	25.74	26.29	26.03
20:00	23.72	23.08	24.51	23.68
21:00	21.74	20.90	22.99	21.75
22:00	20.57	19.67	21.86	20.59
23:00	19.35	18.42	20.77	19.39

Point E - Keskustori Main Plaza				
Time	BC	C1	C2	C3
0:00	16.53	16.37	17.46	16.49
1:00	16.88	16.71	17.80	16.83
2:00	17.31	17.14	18.23	17.26
3:00	17.80	17.63	18.71	17.74
4:00	18.33	18.17	19.23	18.26
5:00	22.50	22.37	23.66	22.37
6:00	27.52	27.52	28.99	27.21
7:00	32.59	32.77	33.44	32.28
8:00	36.14	36.55	36.22	35.74
9:00	38.98	39.59	38.30	38.48
10:00	41.50	42.28	40.21	40.91
11:00	43.98	44.88	42.24	43.31
12:00	46.54	47.50	44.63	45.91
13:00	48.37	49.42	46.18	47.71
14:00	**49.69**	**50.80**	**47.31**	**49.05**
15:00	49.18	50.20	47.14	48.63
16:00	47.47	48.35	46.01	46.94
17:00	44.61	45.28	44.02	44.18
18:00	39.59	40.06	39.87	28.33
19:00	24.93	25.14	25.27	24.67
20:00	22.44	22.46	23.24	22.27
21:00	20.45	20.33	21.43	20.34
22:00	19.04	18.89	20.28	18.95
23:00	17.72	17.55	19.05	17.64

Point F - Open Space				
Time	BC	C1	C2	C3
0:00	15.79	15.72	17.15	15.76
1:00	16.21	16.13	17.55	16.18
2:00	16.69	16.62	18.01	16.67
3:00	17.23	17.15	18.51	17.20
4:00	17.79	17.72	19.05	17.76
5:00	21.86	21.86	19.84	21.81
6:00	26.42	26.64	20.98	26.26
7:00	31.47	31.87	32.11	31.30
8:00	35.04	35.64	24.02	34.78
9:00	37.98	38.75	25.51	37.60
10:00	40.68	41.59	39.18	40.20
11:00	43.47	44.49	41.52	42.93
12:00	46.49	47.55	33.61	46.01
13:00	48.70	49.84	35.40	48.21
14:00	**50.17**	**51.33**	**36.34**	**49.68**
15:00	49.48	50.57	35.61	49.09
16:00	47.51	48.48	35.88	47.14
17:00	44.27	45.08	43.20	44.01
18:00	27.85	28.53	27.48	27.41
19:00	31.23	31.64	24.44	30.88
20:00	21.50	21.60	22.49	21.35
21:00	19.45	19.43	20.74	19.37
22:00	17.99	17.95	19.54	17.92
23:00	16.61	16.54	18.27	16.54

Appendix H. Summary of Tampere's UHI Study Microclimate Simulations (Sitowise, 2022b)

Urban Structure	**Windiness** (Based on simulation)	**MRT** (Based on simulation)	**LST** (Based on composite map)	**Land Cover** (From City of Tampere geospatial data)
Type 1: Viiala	Low windiness	22 - 26 °C	31.7 - 32.5 °C	Vegetation 47% Buildings 10% Impermeable surface 26%
Type 2: Kaleva	Quite windy. However, some of the yards are sheltered.	Streets and parking = 24-26 °C Courtyards = 22-23 °C	34.5 - 36.5 °C	Vegetation 16% Buildings 17% Impermeable surface 43%
Type 3: Keskusta	Streets quite windy, courtyards mainly very calm	Street in the shade = 19-20°C; Street in the sun = 22-25 °C; Market square = 24-26 °C; Differs based on shading	37.4 - 38.8 °C	Vegetation 5 % Buildings 44% Impermeable surface 46%
Type 4: Lielahti	The windiest of the areas examined	24-26 °C; Rows of trees = 21-23 °C	41.0 - 42.0 °C	Vegetation 6% Buildings 24% Impermeable surface 62%